Examining negative modulators of glutamatergic receptors as anti-cancer agents in glioblastomas

Julia Spagnolello

A thesis submitted for the Master of Philosophy at

Cardiff University

06 February 2025

Acknowledgments:

I would like to thank Dr. Siebzehnrubl and Prof. Ward for setting up this project and for their excellent and kind supervision. I would also like to thank Dorit and Ayesha for their friendly guidance and assistance whenever I needed it. Lastly, a big thank you goes to every member of the ESCRI community for making this year so great and to my friends and family for the much needed moral support throughout.

Abstract:

Glioblastoma (GBM) is an aggressive brain tumour, representing approximately 50% of all primary brain malignancies. The median survival for GBM patients is 20 months, with less than 10% surviving beyond 5 years post-diagnosis. Currently, there are no FDA-approved targeted therapies for GBM. Recent studies have highlighted the crucial role of glutamate signalling in GBM tumour growth and migration, with functional neurogliomal synapses forming and firing glutamate between neurons and GBM cells. Moreover, preliminary data show that glutamatergic antagonists inhibit tumour progression. Therefore, this study investigates the potential of glutamatergic receptor modulators as novel therapeutic agents for GBM.

Using patient-derived GBM cell lines (U3042, U3019 and L2) we identified the ionotropic glutamate receptors and their subunit compositions that are overexpressed in GBM. Here, qPCR and western blot analyses revealed that AMPA receptors were the most highly expressed, followed by Kainate and NMDA receptors, with U3042 exhibiting the highest levels of expression. Notably, GRIA2, GRIA3, and GRIK3 subunits were found to be particularly enriched in GBM cells compared to normal human astrocytes. To then assess the proliferative effects of glutamate, cell proliferation was measured using cell-titre glow and Ki-67 staining assays. Here, U3042 cells exhibited a significant proliferative response to 500 μM glutamate, while U3019 cells did not. Interestingly, in this study treatment with glutamatergic antagonists did not reduce proliferation in these cell lines. Additionally, the impact of glutamate on intracellular calcium fluctuations was explored. Here, glutamate at 500 μM significantly enhanced calcium signalling, with similar effects observed using s-AMPA and kainic acid, two glutamatergic specific compounds. Lastly, the addition of Perampanel and UBP-302, two glutamatergic antagonists targeting AMPA and Kainate respectively, significantly decreased these calcium fluctuations.

These results suggest that glutamate, via the AMPA and Kainate receptor subunits, may promote GBM cell proliferation through the influx of intracellular calcium. Therefore, targeting these glutamatergic pathways with negative modulators holds promise as a novel therapeutic strategy for treating GBM.

Table of Contents

List of Tables:

List of Figures:

Abbreviations:

CNS Central Nervous System

CL Classical

CNQX Cyanquixaline (6-cyano-7-nitroquinoxaline-2,3-dione)

ECM Extra cellular matrix

EAAT2 Excitatory amino acid transporter 2

EPSC Excitatory post synaptic currents

ER Endoplasmic reticulum

GBM Glioblastoma

L2 GBM Line 2

MES Mesenchymal

NSC Neuronal stem cells

PL Pro-neural

SVZ Sub-ventricular zone

TME Tumour microenvironment

NHA Normal human astrocytes

Chapter 1: Introduction

Cancer is a disease characterised by uncontrollable cell proliferation, and arises due to an accumulation of genetic changes or the inheritance of a genetic mutation (1). Cancer can be subdivided into 5 categories, depending on the cell of origin: Carcinoma, Lymphoma, Leukaemia, Sarcoma, and Central Nervous System (including brain and spinal cord) (2). The majority of primary brain tumours derive from non-neuronal cells in the brain and nervous system termed glial cells and are collectively called gliomas (3). According to the 2021 World Health Organization classification of gliomas, there are three main types which are classified according to their cell of origin: oligodendrogliomas, ependymomas and astrocytomas (4).

Astrocytomas are the most common and constitute approximately 60% of all brain tumours. Astrocytomas derive from astrocytes, the most abundant type of glial cell in the central nervous system (CNS) (5). To note, astrocytes play a pivotal role in maintaining a healthy CNS by performing metabolic, structural, homeostatic and neuroprotective functions. Such tasks can be facilitating the formation of synapses, regulating the blood-brain barrier and recycling neurotransmitters (5). Other than their protective function, if dysregulated, they can lead to astrocyte abnormalities such as low grade astrocytomas. Up until recently, glioblastomas (GBM) were considered to be the most aggressive type of astrocytoma (grade 4) and classified according to the presence or absence of the isocitrate dehydrogenase (IDH) mutation (6, 7) (8). However, according to the new 2021 WHO classification gliomas are now classified according to their histological features and molecular features. Therefore, adult-type glioma are subdivided into three distinct categories: isocitrate dehydrogenase (IDH)-mutant astrocytoma; IDH-mutant, 1p/19q-codeleted oligodendroglioma; and IDH wild-type glioblastoma (7, 9) .

Here, IDH-mutant astrocytoma can present as a grade 2 (low grade) or grade 3 and 4 (high grade). Here, low grade tumours are characterised by slow growing, infiltrative, poorly defined tumours whilst also presenting with thickening of the gyri. High grade tumours present a CDKN2A/B homozygous deletion, show microvascular proliferation and present higher levels of necrosis. On the other hand, IDH-mutant, 1p/19q-codeleted oligodendrogliomas are characterised by the loss of short arm chromosome 1 and the long arm of chromosome 19. Once again, these gliomas can be categorised as low or high grade according to their histological characteristics and can be easily identified due to the presence of possible gross calcification (seen following a

radiological image) (7, 9) . Lastly, the IDH wild-type glioblastoma subgroup can be identified by at least one of the following histological or molecular features: microvascular proliferation; necrosis; telomerase reverse transcriptase (TERT) promoter mutation; amplification of the epidermal growth factor receptor (EGFR) gene; and gain of chromosome 7 and loss of chromosome 10 (7, 9) .

1.1 Glioblastoma prevalence and occurrence

Glioblastoma (GBM) is an aggressive tumour, that accounts for 45.6% of primary brain malignancies (6). GBM is classified by the World Health Organisation as a Grade 4 cancer, associated with a poor prognosis and fast onset of symptoms (6) (10). Based on clinicopathologic features, GBM can be subclassed into two categories. Primary GBM is classified as glioblastoma IDH wildtype, which corresponds to the sub-set of patients (approximately 90%) which present no identifiable precursor lesion or mutation. On the other hand, GBM can be IDH mutant which represents the remaining 10% of the GBM population, predominates in younger patients and generally presents a better prognosis (11) (7). To note, the origins of glioblastomas are still not fully resolved, although some studies implicate oligodendrocytes precursors as the cell of origin for GBM (12).

3,200 new patients are diagnosed with GBM each year in the UK, and men and adults of 65+ years are at greater risk of developing this pathology (6). Underlying causes have not yet been identified but exposure to ionizing radiation was determined to be a risk factor after noticing that “Children who receive prophylactic radiation for acute lymphocytic leukaemia may have a 22 times higher risk of developing a CNS malignancy within about 5 to 10 years” (5). Other possible risk factors have been linked to infection with cytomegalovirus and Epstein- Barr virus, and obesity during adolescence (13). Lastly, whilst most GBM are believed to not be genetically linked, GBM appear to be elevated in individuals presenting Neurofibromatosis type 1, Turcot syndrome and Li Fraumeni syndrome, all caused by specific gene mutations (14). Here, the NF1, ACP or MLH1 and TP53 genes are affected, respectively leading to a loss of tumour suppressant or DNA repair proteins heightening the risk of GBM (15)

1.2 The molecular subtypes of glioblastomas

Glioblastoma (GBM) is characterized by pronounced molecular heterogeneity, encompassing diverse genetic, epigenetic, and transcriptomic alterations. Recent research has focused on trying to precisely characterize the different expression patterns with the aim of reaching a more accurate diagnosis for better patient targeted drugs. Following the studies of Phillips, Verhaark, and Wang et al., GBMs are classified into three subgroups: pro-neural (PN), classical (CL) and mesenchymal (MES), on the basis of their transcriptional signatures (16) (17) (18).

Key molecular features of the Proneural glioblastoma subtype include elevated expression of DLL3, PDGFRA, OLIG2, SOX family members, DCX, ASCL1, and TCF4. Here, there is also a loss of PTEN expression and significant activation of the notch pathway. Lastly, a higher brain volume of infiltrative peripheral edema can be observed and elevated levels of creatine and homocysteine are key hallmarks. Furthermore, patients suffering from a PN GBM have a better prognosis and have been shown to respond to current treatment. To note, this tumour subclass is more common in younger patients and most secondary GBMs and >75% of low grade and grade 3 gliomas are of this class (16) (19).

On the other hand, the CL subtype is more aggressive and presents the amplification of EGFR and chromosome 7, the loss of chromosome 10 and 95% exhibit CDKN2A homozygous deletion (17). There is also a high expression of Notch and Sonic hedgehog pathway-linked genes. This subtype displays high cellular density and necrosis (19).

Lastly, MES-GBM subtype is characterized by a dominant *NF1* gene mutation; NF-κB and AKT pathway activation, resulting in high angiogenesis and cell necrosis (19). This subtype also shows elevated expression of VEGF and PECAM1. In contrast with the other two subtypes, MES-GBM have the highest content of immune cells and have a significant higher glycolytic activity, making them an important hallmark. To note, this subtype is the most common, present in 49% of all GBMs (16) (19).

More recently, single cell RNA sequencing has revolutionised GBM classification and has allowed for the comprehensive characterisation of healthy and malignant tissue (20). Using RNA sequencing it was shown that malignant GBM cells exist in 4 different cellular states: (i) Neuronal progenitor-like (ii) Oligodendrocyte-progenitor-like (iii) Astrocyte-like and (iv) Mesenchymal like states, each associated with various copy number amplifications of EGFR, CDK4 and PDGFRA loci as illustrated in *figure 1.1*. To note, each GBM sample was shown to contain cells in multiple states and also present great plasticity between states highlighting that "each tumour is unique and the diversity within a tumour is driven by a combination of factors – genetic, epigenetic and microenvironmental"(20).

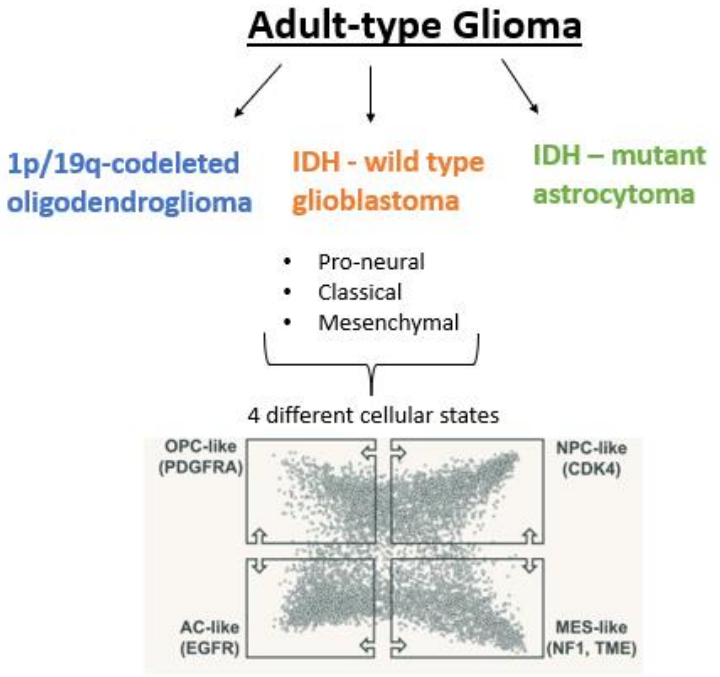

Figure 1.1: The molecular subtypes of Glioblastoma : adult-type glioma can be either IDH-wildtype glioblastoma, 1p/19q-codelted oligodendroglioma or IDH-mutant astrocytoma. Here, IDH-wildtype glioblastoma can exhibit significant molecular heterogeneity and can exist in 4 different cellular states (i) Neuronal progenitor-like (ii) Oligodendrocyte progenitor-like (iii) Astrocyte-like and (iv) Mesenchymal-like, with each state characterised by the expression of CDK4, PDGFRA, EGFR and NF1, respectively.

Figure adapted from Neftel et al., 2019

1.3 Glioblastoma treatment regime

GBM is associated with a devastatingly poor prognosis, the average survival rate of GBM patients is between 15 -17 months with therapy, and less than 10% of patients live past 5 years following diagnosis and care (21). GBM is an incurable disease, and patients live their last few years experiencing debilitating symptoms such as headaches, cognitive impairments and can also experience seizures as seen in 20-40% of patients (10). Currently, the standard treatment entails surgery followed by fractioned radiation and/or oncological chemotherapy. Surgery is the initial therapeutic approach with the hopes to remove as much of the tumour as possible to delay clinical worsening. Because the tumour is capable of infiltrating within healthy brain tissue, it is often impossible to undergo gross total resection. Here, the main goal is to resect as much of the tumour whilst conserving as much brain activity as possible(22). Any remaining tumour is then targeted with chemotherapy and the doses prescribed are according to the results of the EORTC 26981 phase III clinical trial (23). Moreover, Radiotherapy, which uses powerful x-rays, gamma rays or protons can also target and destroy the remaining tumour cells. Here, recommended treatment dose is 60-65 Gy delivered in 1.8-2.0 Gy fractions (24). To note, a randomised phase III clinical trial showed that the addition of temozolomide to radiotherapy improved median survival and 2-year survival compared to postoperative radiotherapy alone (25). Other than not being curative, these treatment regimens come with significant side effects some including fatigue, hair loss and vomiting occur (26) (27).

Regardless of this treatment regime, the presence of single GBM malignant cells that have been displaced from the primary tumour is still likely. To note, these present the ability to self-renew and proliferate and can lead to tumour recurrence. This can be linked to cancer stem cells which are a subpopulation of cells which are present in a quiescent state, yet when stimulated with trophic factors from the TME, are capable of re-entering the cell cycle, favouring migration and initiation of new tumours (28) Moreover, as these remaining cells have already been targeted by chemotherapy, they may have developed favourable mutations to be therapeutic resistant (29). Given the limitations of available/effective treatments, there is a clinical need for novel therapeutic strategies. Unfortunately, this is a hard task due to due to a

lack of control arms, selection bias, small numbers of patients, and disease heterogenicity (22).

1.4 The development of GBM

Cancer stem cells are thought to arise from neural stem cells (NSC) as these undifferentiated cells present self-renewal and differential properties subsequently allowing them to give rise to neurons, astrocytes and oligodendrocyte precursor cells when appropriately stimulated (30). These properties allow NSC to undergo multiple rounds of cellular division which ensures appropriate conditions for oncogenic mutations to arise as DNA replicative errors can occur (30) (31). Following recent large-scale sequencing analysis, these oncogenic mutations have been linked to alterations in many key genes some including EGFR, PIK3CA and PTEN (31). As these mutations dysregulate key cellular pathways, these newly oncogenic NSC can present uncontrolled proliferation and/or the inactivation of tumour suppressants, both key drivers of cancer formation and progression. As highlighted in the previous section, GBM cells are highly heterogenic and thus present different molecular signatures; not all GBM present the same oncogenic mutation. To note, transgenic mouse models have also been used to confirm this hypothesis. For example, *Bachoo et al.* showed that high-grade gliomas could be generated following the transduction of a Ink4a-Arf$^{-/-}$ mouse NSC, presenting a constitutively active EGFR (32).

Current research suggests that these NSC arise within the sub-ventricular zone (SVZ), a region situated by the lateral ventricles of the forebrain, which hosts wide range of different brain and immune cells as illustrated in *figure 1.2* (33). For this reason, the SVZ is thought to be the initial host of GBM. The term initial is used to highlight that GBM is not confined to the SVZ alone, as it is capable of growing and infiltrating into healthy brain tissue. In order for this to occur, these tumour cells are capable of altering their gene expression and influence their tumour microenvironment (TME). To note, the TME refers to a range of *non-cancerous* cells and supportive factors which surround and interact with the tumour (34). Examples of beneficial alterations for tumour progression listed in a review by So et al (35) include: remodelling of the extra cellular matrix (ECM), increasing calcium influx and increasing glutamate release. The latter has significant implications in GBM progression as GBM create a

positive feedback loop by which increased levels of glutamate are present within the TME, which in turn is re-utilised by nearby GBM cells to activate their ionotropic glutamate receptors (3).

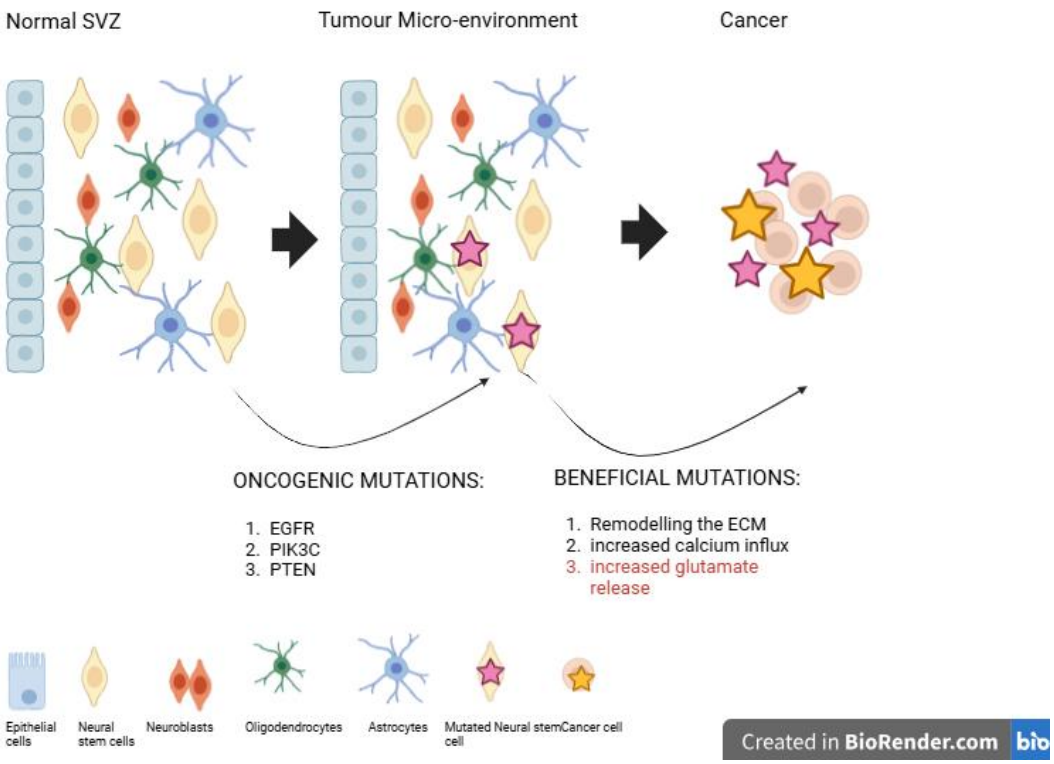

Figure 1.2: Schematic representation of the origin of cancer stem cells. The SVZ is comprised of Epithelial cells, Neural stem cells, Neuroblasts, Oligodendrocytes and Astrocytes. Following cellular division and differentiation, NSC can become mutated and present oncogenic properties such as an increase in EGFR and PIK3C and a decrease or malfunction of PTEN. Following further cell cycles, other DNA errors can be introduced leading to tumour migratory mutations such as an increase in extracellular integrins and an increase in calcium and ionotropic glutamate receptors.

1.5 Glutamate ionotropic receptor subtypes and mechanism of action

Glutamate is the main excitatory neurotransmitter in the central nervous system (36). There are two glutamate receptor families: ionotropic receptors responsible for fast synaptic

transmission and the metabotropic receptors responsible for synaptic transmission and neuronal excitability (37) . In this thesis the metabotropic receptors will not be considered as the focus is on repurposing drugs developed for epileptic and neuropsychiatric disorders, known to target the ionotropic receptor family. The mammalian ionotropic receptor family, encodes 18 different genes that each present an extracellular amino-terminal domain, an extracellular ligand binding domain, a transmembrane domain, and an intracellular carboxyl-terminal domain (38). These genes produce the different subunits required to make up the functional AMPA, Kainate and NMDA channels as illustrated in figure 1.3. Of note, these receptors are expressed within neurons and glia cells, and are regulated by developmental cues and synaptic activity (39) (40) (41).

AMPA receptors are critical for synaptic transmission and plasticity, thus have been identified to play a pivotal role in memory and learning (42). AMPA receptors are heterotetrametric complexes which are composed of various combination of GluA1, GluA2, GluA3 and GluA4 subunits. Each subunit presents an identical membrane topology and core structure but differs within the C-terminal domain. Because of this highly variable region, each subunit undergoes different post-translational modifications and subunit-dependant trafficking (39). Furthermore, more than 99% of GluA2 subunits undergo an RNA modification, within their intracellular re-entrant loop, by which its RNA is edited to replace the Glutamine at position 607 with an Arginine. This RNA editing is caused by adenosine deaminases enzymes (ADAR) which has been shown to be highly expressed and restricted to the neuronal population (Jacobs et al., 2009). This point mutation renders any AMPA receptor containing this subunit calcium impermeable as this bulky ammino-acid now constricts calcium flow though the channel (43). Moreover, because calcium permeable AMPA receptors are very important to CNS function, the GluA2 exit from the endoplasmic reticulum (ER) is highly regulated. Most GluA2 is unassembled retained in the ER, and only leaves when assembled with GluA1 (39).

Kainate receptors also modulate neuronal circuits and synaptic activity, and are strongly expressed during early postnatal life as they are critical for developing the synaptic circuitry (40) (44). These receptors assemble as homotetramer and heterotetramer channels from a pool of five different subunits GluK1-GluK5. Importantly, only the Gluk1-3 subunits can form functional homomeric channels, whilst GluK4 and GluK5 must be present and co-assemble with GluK1-3 as heterotetramers (38) (45) (44).

Lastly, NMDA receptors play a vital role in the development of cortical circuitry, as they mediate activity-dependent plasticity (46). NMDA receptors are tetrameric complexes typically composed of two GluN1 subunits and two GluN2 or GluN3. To note, for this receptor to be functional it requires 2 GluN1 subunits, which present glutamate binding domains. Furthermore, either GluN2 or GluN3 must be present as they contain glycine binding subunits, and glycine is a vital NMDA co-agonist (47).

Briefly, the first step towards glutamate receptor activation is glutamate binding to the extracellular ligand binding domain, thus causing the channel to undergo a conformational change allowing it to open (38). Once opened, calcium and sodium enter the cell leading to membrane depolarisation. In turn, this activates the MAPK and PI3K pathways, as intracellular calcium is capable of activating CAMKII and receptor tyrosine kinases which, following various signalling cascades detailed in figure 1.4, contribute to cellular growth, proliferation and survival (48) (35) (49).

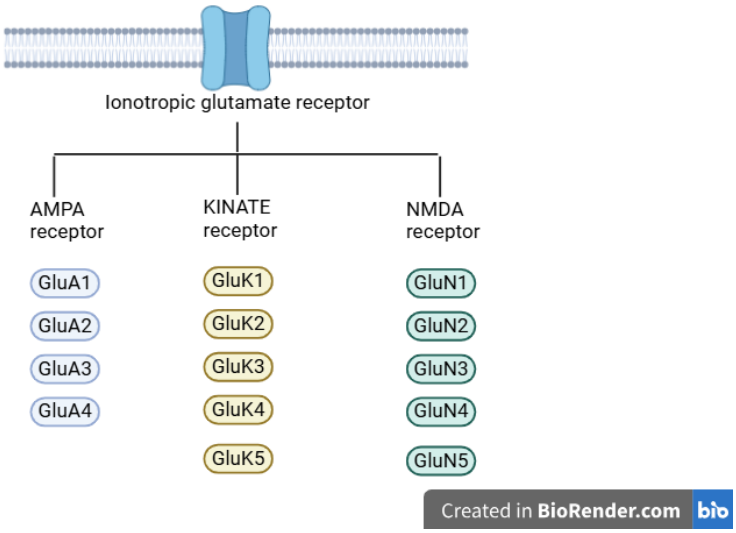

Figure 1.3: Schematic representation of ionotropic glutamate receptors. Ionotropic glutamate receptors can be subdivided into three different families, each presenting various different subunits.

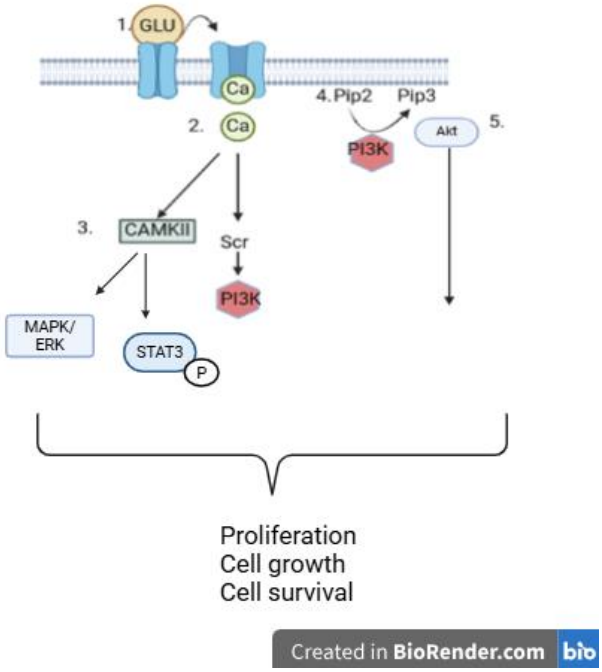

Figure1. 4: Schematic representation of the pathways activated following glutamate-ion channel activation. (1) Extracellular glutamate binds to the receptors LBD, which causes a conformational change allowing the receptors channel to go from gated to open. (2)Once open, extracellular calcium enters the receptors channel and ends up in the gliomas intracellular space. (3) High levels of intracellular calcium activates calmodium which activates CAMKII, which in turn can phosphorylate Ras leading to the activation of the MAPK/ERK pathway whilst also leading to STAT3 phosphorylation which is capable of supporting pro-survival genes. Lastly, CAMKII is also capable of activating SCR, which activates PI3K. (4) PI3K is then recruited to the plasma membrane where it phosphorylates Pip2 converting it to Pip3. (5) newly phosphorylated Pip3 allows for AKT and PDK1 to be recruited to the plasma membrane and activated. Together, all these tyrosine kinase receptors allow for proliferation, cellular growth and survival to occur.

1.6 The links between glutamate and GBM progression

As discussed above, glutamate plays a key role in cellular growth and proliferation. For this reason, GBM promotes increased interactions with this neurotransmitter in order to grow and invade nearby tissues. One way this is achieved is by increasing the amount of glutamate

present within the extracellular space by modulating the expression of glutamate transporters and the exchangers. A paper by de *Groot et al (50)* identified that gliomas lack the excitatory amino acid transporter 2 (EAAT2) transporter compared to healthy astrocytes causing reduced glutamate re-uptake, while a paper by *Ye and Sontheimer (51)* identified the over expression of system X^c , a cystine-glutamate antiporter. To note, under normal conditions, system X^c does not account for a significant change in extracellular glutamate release as extracellular cystine levels are relatively low and glutamate release is counteracted by its re-uptake by EAAT2. As tumorigenic conditions cause increased oxidative stress, extracellular cystine levels are significantly increased causing a shift in this exchange: more cystine enters the cells causing a higher secretion of glutamate into the extracellular space (52). Together, these two phenomena serve as a dual purpose in GBM biology as the increased level of extracellular glutamate causes excitotoxicity within the TME and can activate the ionotropic receptors of nearby glioma cells.

Excitotoxicity can be defined as cell death of neurons resulting from the toxic actions of excitatory neurotransmitters (53). To note, this phenomenon can also affect other cells within the CNS such as glial cells (54). Excitotoxicity plays a vital role in generating space for tumour expansion as the cranium consists of 85% of brain tissue with the remaining 15% filled with cerebrospinal fluid (3). Excessive exposure to glutamate can also cause cell death within the TME clearing space for GBM to migrate more easily. This phenomenon is further reinforced as excessive glutamate uptake causes high intracellular calcium levels which can disrupt the cell's mitochondria leading to high levels of reactive oxygen species being released and the activation of apoptotic pathways (55). Moreover, high levels of extracellular glutamate can also benefit GBM progression as other GBM surrounding cells will use it as an agonist to activate its ionotropic receptors as previously discussed.

A recent paper by *Venkataramani et al* (56) has highlighted another way by which GBM can manipulate the use of glutamate firing to promote its growth and survival. The main concepts their research highlights are that neurons are capable of forming functional synaptic connections with GBM cells and that these neurogliomal synapses produce postsynaptic currents that are mediated by glutamate receptors. This was determined as their excitatory post synaptic currents present amplitudes, rise times and decay times consistent with glutamatergic pre-established values and cease to function following the addition of an

ionotropic glutamatergic antagonist. They also show that glutamate output is related to tumour progression as conceptualised in *figure 1.5*. Here glutamate firing led to an increase in GBM intracellular calcium, promoting cellular proliferation and migration. Further investigation also showed that when these neurogliomal synapses were treated with an AMPA receptor antagonist, the glioma cells grew significantly slower than the control glioma cells (56).

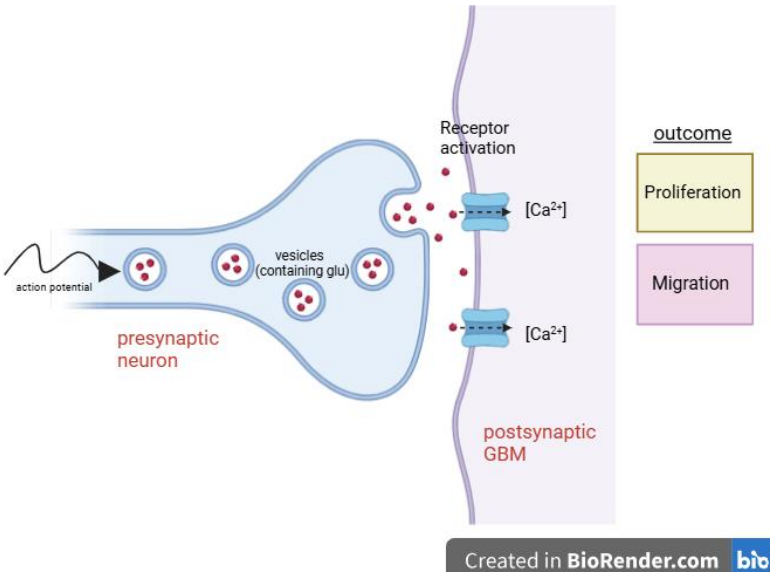

Neurogliomal synapse

Figure 1. 5: A schematic illustration of the neurogliomal synapses and its role in GBM progression (Fig. adapted from Venkataramani 2019). Neurons and GBM cells can form neurogliomal synapses which

following neuron stimulation, glutamate containing vesicles can fuse with the neuron's plasma membrane and release glutamate in the synaptic cleft. Here, this glutamate can bind and activate the glutamatergic ion receptors present on the postsynaptic GBM cell. Intracellular calcium enters the cell and proliferation and migration can occur.

1.7 The role of calcium in GBM progression

Calcium is a secondary messenger which underlies a variety of key cellular functions such as excitability, contractility, exocytosis and differentiation (57). Accumulating evidence also demonstrates that calcium plays a pivotal role in tumour growth (58) (57). As briefly discussed and illustrated in *figure 1.3,* extracellular calcium can enter the cells via the glutamatergic ion receptors and lead to proliferation, cell growth and proliferation. In line with this, a study by *Ishiuchi et al* clearly demonstrated that calcium permeability is critical for tumour migration as the absence of calcium influx caused GBM cells to stop migrating and induce apoptosis (48).

It is imperative to highlight that glutamatergic receptors are not the only ones which allow calcium to enter and allow the GBM cells to grow. Others include plasma membrane channels such as voltage-gated calcium channels, transient receptor potential channels and mechanosensitive Piezo channels. A review by *Azab et al.* highlights that calcium channels and their downstream binding protein (calmodulin) have a wide range of effects on GBM growth such as cellular growth, invasiveness and cellular volume changes (57).

1.8 Pharmacological targeting of glutamatergic receptors

As described above glutamate can activate glutamatergic ion receptors by binding to the ligand binding site and causing a conformational change. Glutamatergic antagonists are capable of counteracting this activation by either directly binding to its ligand binding domain and outcompeting glutamate, or by binding to an allosteric site on the receptor thus changing the conformation of the receptor, inhibiting glutamate binding. These antagonists are classified as competitive and non-competitive, respectively. There are currently a wide range of

commercially available glutamatergic receptor antagonists but the ones used in this study were CNQX, Perampanel, UBP-302 and Ketamine, which as illustrated in *figure* 1.6, target specific glutamatergic receptor subtypes. As there is increasing evidence to suggest that glutamate plays a key role in tumour progression CNQX and Perampanel were specifically chosen as initial studies have shown they are able to reduce GBM cell proliferation (56). On the other hand, an educated guess made us choose UBP-302 and Ketamine as they are the most effective receptor antagonist for the Kainate and NMDA receptor, respectively.

Briefly, CNQX is a competitive antagonist for the AMPA and Kainate receptor as it binds to the glutamate-binding site of these receptors, preventing glutamate from activating them while also acting as a non-competitive antagonist for NMDA as it binds at the glycine modulatory site (Tocris Bioscience). Perampanel is a non-competitive antagonist to the AMPA receptor, and preclinical studies found that this compound was capable of preventing seizures by lowering the neuronal excitability (59, 60). To note, this compound was approved by the European Medical Agency in 2012 and has since been on the market as an anti-epileptic drug. UBP-302, on the other hand is a Kainate receptor non-competitive antagonist which antagonises GluK1 subunit-containing KA receptors at low concentrations but can antagonise other KA subunits utilising a higher dose (61). Lastly, Ketamine is a non-competitive antagonist to the NMDA receptor which works by an open channel block mechanism (62).

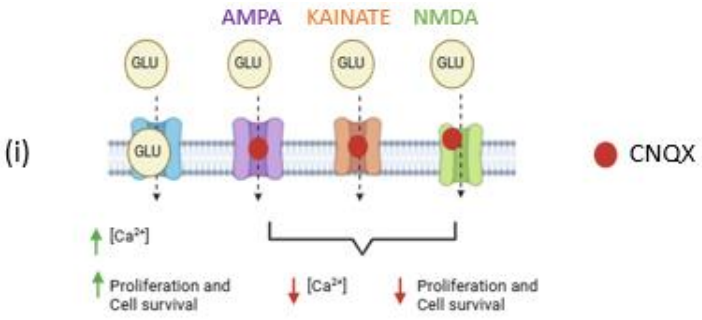

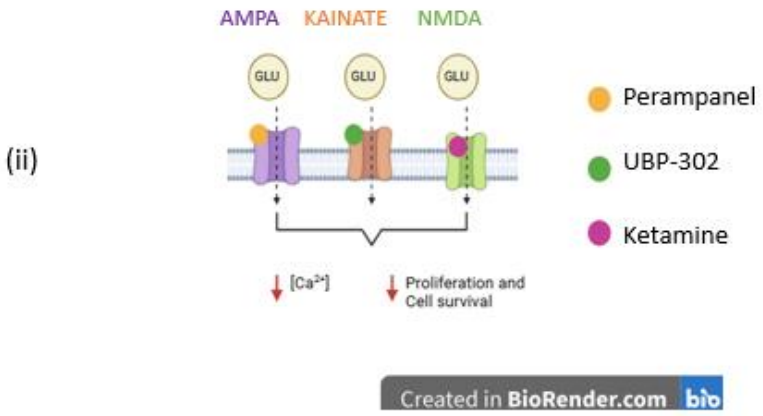

Figure 1.6: Ionotropic glutamate receptor antagonist. (i) in the absence of CNQX, glutamate can enter the GBM cell via the glutamatergic ion receptor thus leading to increased intracellular calcium, proliferation and cell survival. In the presence of CNQX, the entry of glutamate is inhibited leading to a significant reduction in intracellular calcium, proliferation and cell survival. To note, for both AMPA and Kainate, CNQX binds in the active site, while for NMDA it bind in the allosteric site. (ii) Perampanel, UBP-302 and Ketamine bind to their specific glutamatergic ion receptor. Perampanel and UBP-302 bind to the allosteric site of AMPA and Kainate, respectively. Ketamine binds to NMDA within its active site, through an open channel mechanism.

1.9 Hypothesis and aims of project

In light of glutamate's key role in promoting GBM progression, a potential therapeutic avenue is to inhibit the activation of glutamatergic ionotropic receptors. For this reason, the hypothesis of this study is: **negative modulators of glutamatergic receptors can be used as anti-cancer agents in GBM.** Therefore, this study will seek to examine whether these allosteric modulators will reduce glioblastoma cellular proliferation and Ca^{2+} signalling. The main aims of this study, which will be divided into thesis chapters are therefore to:

1. Establish which ionotropic receptors and combinations of subunits are present in GBM. This will be performed using qPCR with receptor subunit-specific primers and on 3 different patient-derived GBM lines.

2. **Establish whether changes in cellular proliferation are observed in GBM cell lines following stimulation with glutamate (agonist) and whether this change can be counteracted by using anti-glutamatergic drugs (antagonist).** This will be performed by initially establishing whether glutamate promotes proliferation in GBM cells. This data will be gathered using cell growth and proliferation assays. In the instance glutamate causes a change, proliferation will be then monitored with the addition of anti-glutamatergic drugs (CNQX, Perampanel, UBP-302 and Ketamine which target the glutamatergic receptor, as detailed in section 5) to determine whether blocking these ionotropic receptors present therapeutic value.

3. Establish whether an increase in intracellular calcium influx is observed in GBM lines following glutamate stimulation and whether this change can be counteracted by using anti-glutamatergic drugs. This will be performed by initially establishing whether glutamate promotes increased calcium fluctuations in GBM cells, and thus generating a secondary message which will go on and activate the PI3K and MAPK kinase pathways, leading to proliferation and cell survival. This data will be gathered by performing calcium on GBM cells in the presence of glutamate. In the instance glutamate causes a change, intracellular calcium will be then monitored with the addition of anti-glutamatergic drugs to determine whether blocking these ionotropic receptors decreases calcium entry.

Chapter 2: Methods

2.1 Reagents list

Reagents and concentrations	Source
U4 Cell Culture Media 500ml:	
- 250ml DMEM/F-12 (1:1) (1X) + GlutaMAX	Gibco 105665-042
- Neurobasal Medium (1X)	Gibco 21103-049
- 1ml MycoZap Plus-CL	Lonza VZA-2011
- 500uL Transferin-Putrescince Sodium Selenite	Sigma T8158, Sigma P5780, Sigma S5261
- 500uL Insulin	Sigma I5500

- 500uL Progesterone	Sigma P8783
Glutamate Free Cell Culture Media 500uL: - 250ml DMEM/F-12 (1:1) (1X) - Neurobasal Medium (1X) - 1ml MycoZap Plus-CL - 500uL Transferin-Putrescince Sodium Selenite - 500uL Insulin - 500uL Progesterone	 Gibco 21331-020 Gibco 21103-049 Lonza VZA-2011 Sigma T8158, Sigma P5780, Sigma S5261 Sigma I5500 Sigma P8783
N2 Cell Culture Media 500uL N2: - Neurobasal Medium (1X) - 1ml MycoZap Plus-CL - 500uL Transferin-Putrescince Sodium Selenite - 500uL Insulin - 500uL Progesterone	 Gibco 21103-049 Lonza VZA-2011 Sigma T8158, Sigma P5780, Sigma S5261 Sigma I5500 Sigma P8783
Astrocyte Media : Astrocyte Medium	 AM, Cat.#1801
Growth Factor Supplements - EGF (20ng/ml) - Thermostable FGF2 G3 (3 ng/ml)	 Peprotech AF-100-15-1mg Qkine Qk053-0100
Acutase	Peprotech AF rhEGF AF-100-15
Poly-Ornithine (10ug/ml)	Sigma P3655
Laminin (5ug/ml)	Gibco 23017-15
Geltrex	Fisher Scientific 12053569
Quick Start Bradford Protein Assay	BioRad 500-0203
Quick Start Bradfrod 1x Dye Reagents	Bio-Rad 5000205
Qiagen RNeasy Mini Kit	Qiagen 74104
Qunatitech Kit Qiagen Reverse Transcription	Qiagen 205311

Takyon Low ROX SYBR Master Mix Blue Dttp qPCR Mix	EurogentecUF-LSMT-B0701
Taq Recombinant DNA PCR Mix	Thermo Scientific EPO402
Hoechst (used 1:1000, dilution)	Thermo Sceintific 62249
CellTiter-Glo Luminescent Cell Viability Assay	Promega G7572
Cal-520	AAT Bioquest: Biomol ABD-21130
l-glutamate	Tocris 0218
(s)-AMPA	Biotechne 0254/1
Kainic Acid	Biotechne 7065/1
NMDA	Tocris 0114
CNQX	Abcam ab120044-10mg
Perampanel	Clinisciences AOB887762-5
UBP-302	Biosciences 24309-1mg-CAY
Ketamine	Sigma K2753
10 x RIPA	Cell signaling 9806
Protease inhibitor (PIC1)	Sigma P8340
Phosphatase inhibitor cocktail 2 (PIC2)	Sigma P5726
Phosphatase inhibitor cocktail 3 (PIC3)	Sigma P0044
PMSF 0.1M	Fluka 93482

2.2 In-vitro culture of cell lines

In this experiment, three different human patient-derived GBM cell lines (U3019, U3042 and hGBM Line 2) and one Normal Human Astrocytes cell line were used and cultured. The U3019 cell line was derived from a 82 year old female, which presented a proneuronal GBM subtype from the Uppsala University Hospital. The U3042 cell line was derived from a 67 year old male, which presented a classical GBM subtype and was also collected at the Uppsala University Hospital. Human GBM Line 2 were isolated from GBM patient biopsies and obtained from Dr Brent Reynolds laboratory at the University of Florida McKnight Brain Institute. Lastly, Normal Human Astrocytes were

derived from human brain (cerebral cortex), commercially available from ScienCell, Catalog#1800.

Each cell line was grown in T75 flasks and incubated in their respective growth media (detailed in table 1.1) at 37 °C and 5% $C0_2$ until they reached 80% confluency. Media was replaced every 7 days with the addition of growth factors. Once spheres reached their appropriate size, they were passaged as previously described (28). The spheres were collected and centrifuged at 300 xg at room temperature (RT) for 5 min. The supernatant was then removed and the pellet was re-suspended using 300uL of Accumax in order for the spheres to enzymatically disassociate and left for 4 min at 37°C. Following, these cells were pipetted thoroughly 40 times to break up the spheres and then washed with 5ml PBS and centrifuged. The cell pellet obtained was then resuspended in 1ml of U4 and plated into a new T75 flask. U3019, U3042 and L2 were plated at a density of 50,000 - cells per ml of media. Whilst Normal Human Astrocytes (NHA) were plated at a density of 5,000 cells per ml of media.

For experiments that required adherent cells, single cells were plated on a tissue cultured 96 well plate coated with 10ug/ml Poly-L-Ornithine and 10ug/ml Laminin (diluted in water and PBS, respectively) or using Geltrex matrix using the thin gel method. Sufficient Poly-L-Ornithine was added to the well and left to dry at room temperature (RT) overnight. The following morning, 3 washes with water were performed prior to the addition of Laminin. Following, the plate was left to incubate at 37 °C and 5% $C0_2$ for 2h, prior to seeding the cells. On the other hand, Geltrex was thawed on ice, and diluted 1:100 in cold medium. Sufficient Geltrex (final concentration 130-150 ug/ml) was added to coat the well and left to incubate for at least 1h at 37°C and 5% $C0_2$. 30 min prior to seeding the cells on this newly formed basement membrane, the plate was left at RT.

Please note all cell lines used here are patient derived samples, and thus cell line authentication was not performed. This is because these cells are not expected to drift from their original DNA compared to commercially available lines. Furthermore, to make sure the cells used in this project were clear of mycoplasma, every 5 passages the cells were tested for it using the MP0035-1KT LookOut mycoplasma PCR Detection

Kit, as per manufactures instructions. Lastly, all cell lines used in these experiments did not exceed a passage number of 25.

Cell Line	Feeding Media
U-lines (U3019 and U3042)	U4 Media + EFH
L2	N2 Media + EFH
Normal Human Astrocytes	Astrocyte Media

Table 2.1: Cell specific feeding media

2.3 Determining which ionotropic receptors are present in GBM

2.3.1 RNA extraction and cDNA synthesis

In order to extract RNA, single cells were plated on Poly-L-Ornithine and Laminin coated 6-well plates and left to grow up to confluency. Once confluent the cells lysates were collected using Qiagen RNeasy Mini Kit, as per the handbook protocol using RNeasy spin columns and RNase free water. The RNA yield was then quantified utilising the Nanodrop Spectrophotometer (Thermo Fisher Scientific ND200). To convert this RNA into cDNA, Reverse Transcription was carried out using the Quantititech Kit from Qiagen on a total of 1ug RNA.

Prior to qPCR experiments, the quality of the RNA was measured using the NanoDrop spectrophotometer. Here, the A260/A280 and A260/A30 ratio were assessed and all RNA values were ~2.0, indicating pure RNA free from organic solvents, carbohydrates or residual salt.

2.3.2 Quantitative Polymerase Chain Reaction (qPCR)

A list of validated primers used to determine the expression levels of glutamatergic receptors subtypes can be found in *table* 2.3.2

IDT qPCR Primers	Primer Assay ID	Primer sequence
GRIA1	Hs.PT.58.15517507	5'-CTTAATCGAGTTCTGCTACAAATCC-3' 5'-GTATGGCTTCGTTGATGGATTG-3'
GRIA2	Hs.PT.58.39732953	5'-GAACATTAGACTCTGGCTCCA-3' 5'CGTAGTCCTCACAAACACAGA-3'
GRIA3	Hs.PT.58.19733939	5'-GGTCATTCTCACGGAGGATTC-3' 5'-GTGGTGTTCTGGTTGGTGTT-3'
GRIA4	Hs.PT.58.3139260	5'-CAACATTGAGACAGCCAACAG-3' 5'-CCGACCTCTTATCATAGAGTCCA-3'
GRIK1	Hs.PT.58.15458669	5'-TGCTATCCTCCCTCAGACC-3' 5'-GTGACTGCAAACTTGAAAGCTA-3'
GRIK2	Hs.PT.58.3109772	5'-TAGTTTCTGGTTTGGAGTTGGA-3' 5'-CAAATGCCTCCCACTATCCT-3'
GRIK3	Hs.PT.58.19469239	5'-GTGTCCGTGTGCTACCAG-3' 5'-TCCAGTTAATCCTTCCCATTGAG-3'
GRIK4 forwards	-	5'-AATTCCAACTACGCCTTCCTC-3'
GRIK4 reverse	-	5'-TCAAACTCGTCCCGGAAAAC-5'
GRIK5	Hs.PT.58.39107351	5'CCTCAAGTCCTTCAACTACCC-3' 5'-TCCAACATCCTCACTGACAG-3'
GRIN1	Hs.PT.58.39141804	5'-CTCCTGGAAGATTCAGCTCAA-3' 5'-GTGGATGGCTAACTAGGATGG-3'
GRIN2C	Hs.PT.58.41037260	5'-CTGATGCCACGTTCCCTATG-3' 5'-GAAGAGCGAGGTGAGCAAC-3'
GRIN3A	Hs.PT.58.39634235	5'-ACCAGAACTTGCTCTCATTCC-3' 5'-CTCTGAAAGTGGTATTGGCTAGA-3'
GusB	Hs.PT.58v.27737538	

Table 2.3.2: List of validated qPCR primers

The primers listed above were reconstituted to 10uM in milliQ water and the cDNA generated (section 2.3.1) was diluted 1:10 also utilising milliQ water. RT-qPCR was carried out on a 384-well plate utilising Takyon Low ROX SYBR Master Mix Blue dTTP

mix. Each reaction was made up of 5 µL of Takyon master mix, 0.3 µL of Primer (10uM), 1 µL of cDNA (1:10 diluted) and 3.7 µL of H_20 to make a total volume of 10 µL. Each sample was run in triplicates and placed in the Applied Biosystems QuantStudio 7 Flex Real-Time PCR System (40 PCR cycles: 3min hold at 95°C, then 10sec at 95°C activation and denaturation, followed by 45sec at 58°C for primer annealing). To calculate the delta Ct value of each gene, the Ct value of each triplicate was averaged and subtracted by the average Ct value of GusB (the housekeeping gene).

2.3.3 Z-score collection

The HGCC is a biobank of well-characterised GBM cell lines which derive from GBM patient samples. Currently this biobank holds 48 lines, including U3019 and U3042. Using this website the expression z-score of each ionotropic glutamate receptor subunit was extracted. This z-score is a statistical measure that describes how many standard deviations a raw score is from the population mean. To note, here the population mean is all the cell lines present in the HGCC biobank.

2.3.4 Comparative gene expression analysis

In order to determine GBM specific glutamatergic receptor subunits a ΔΔCt value was calculated using the Ct values of GBM lines vs HAD.

"ΔCt(GBM) – ΔCt(HAD) = ΔΔCt"

2^(-ΔΔCt) × 100 = % expression of GBM subunits relative to HAD

2.3.5 Preparation of protein lysates

In order to collect the cells protein lysates, the cells were passaged as described in section 2.1. Instead of plating the re-suspended single cells in a new T75, the cells were placed in a 1.5ml tube and centrifuged at 300g at 4°C for a total of 5min. Afterwards, the supernatant was removed and the Eppendorf containing the cell pellet was placed on dry ice for instant freezing and stored at -80°C.

To then generate the protein lysates, the pellet was re-suspended in 100uL of cold RIPA buffer (for 10ml RIPA buffer, 9ml of h_20, 1ml of 10x RIPA, 100uL of PMSF and 100uL of PIC1, PIC2 and PIC3 were added together). This was left to incubate for 30 minutes, with a 10-second vortex every 10 minutes. Following, this solution was centrifuged at max speed at 4°C for a total of 30min, and the supernatant containing the proteins was collected in a new Eppendorf tube, previously cooled down on ice.

2.3.6 Quick Start Bradford Protein Assay

To measure the protein concentration, a Bradford assay was performed according to the manufacturer's instructions. Here, 5uL of each pre-made protein standard (1-7, Bio-Rad), sample lysate (diluted 1:10, and 1:40) and blank (lysis buffer alone) were added into different wells of a 96 well plate with 250uL of Quick Start Bradford (1x) Dye Reagent (Bio-Rad) in duplicates (Table 2.3). This mixture was incubated for 5min at RT in the dark. Following, the absorbance of each well was analysed using the CLARIOstar microplate reader (BMG Labtech) measured at a wavelength of 595 nm. The absorbance value of each standard was plotted to obtain a standard curve, which was used to calculate the final concentration of each sample.

Standard/Sample	Volume (uL)	Bradford Reagent volume (uL)	Concentration (ug/mL)
Blank	5	250	0
Standard 1	5	250	125
Standard 2	5	250	250
Standard 3	5	250	500
Standard 4	5	250	750
Standard 5	5	250	1000
Standard 6	5	250	1500
Standard 7	5	250	2000
And Sample	5 (of 1:10 and	250	-

	1:40 dilution)		

Table 2.3.6: Standard concertation used for Bradford assay

2.3.7 Western blot

Between 10-15 µg of protein sample, depending on primary antibody specificity, were mixed with an equal volume of Laemmli (2x) sample buffer (Merk). Afterward, the samples were placed at 95°C for 5 minutes in order to denature the protein, and then immediately placed on ice for a minimum of 2 minutes. A mini-Protean TGX Precast Gel Bis-Tris 10% gradient gel (Bio-Rad) was placed into a loading cassette and the gel combs were carefully removed. This was then positioned in an electrophoresis tank and filled with (1x) Tris-Glycine SDS running buffer (Bio-Rad). 5µL of protein ladder was loaded into the first well of the gel, followed by 10µL of denatured protein samples in the subsequent wells. Following loading, the SDS-PAGE gel was run for 30min at 200 V.

The separated proteins were then transferred onto a 0.2µm PVDF membrane (Bio-Rad) using a semi-dry transfer method, utilising the Mini Trans-Blot Turbo Transfer System (Bio-Rad). Prior to transfer, the PVDF membrane was activated in methanol for 1 min and then placed in the trans-blot turbo (1x) transfer buffer (Bio-Rad) to stop this reaction. Moreover, 2 stacks of filter paper were also pre-soaked using transfer blot buffer. For transfer to occur, a sandwich stack was created by placing one of the pre-soaked stacks into the transfer cassette, followed by the activated PVDF membrane, the SDS-PAGE gel and lastly the other paper stack. The cassette was then run for 7 minutes at 2.5 A and 20 V.

2.3.8 Protein blotting and visualisation

Following protein transfer, the PVDF membrane was blocked with 5% skimmed dry milk for 1h at RT. Following, the membrane was probed with primary antibodies (Table 2.3.7), appropriately diluted according to its manufacturing instructions in 2.5% skimmed dry milk overnight at 4 °C. The following morning, the membrane was washed again 3 times with TBS-T (0.1% Tween-TBS) for 5 minutes each and then probed again with secondary antibodies for 1h at RT. Following, another 3 washes were performed with TBS-T and lastly, the membrane was

incubated with Clarity Western Enhanced Chemiluminescence (ECL) substrate. The chemiluminescent signal produced was detected using the ChemiDoc MP imaging system (Bio-Rad).

Primary Antibodies	Source	Dilution
GRIA1	Cell Signaling 13185T	1:1,000
GRIA2	Cell Signaling 13607T	1:1,000
GRIA3	Cell Signaling 4676T	1:1,000
GRIK1	Thermo Fisher 25779-1-AP	1:1,000
GRIK2	Synaptic Systems 180 003	1:1,000
GRIK3	Synaptic Systems 180 203	1:1,000
GAPDH	EnCor 2572289	1:10,000

Secondary Antibody	Source	Dilution
Anti–rabbit HRP-linked	Cell Signaling	1:3K

Table 2.3.7: Specific Glutamatergic receptor subunit antibodies

2.4 Investigating the role of glutamate (agonist and antagonist) using proliferation assays

2.4.1 Agonist treatment

U3019 and U3042 were plated on pre-coated Poly-L-Ornithine and laminin 96-well plates (CELLSTAR 655180) at a seeding density of 12,000 and 17,000 cells/well in a total volume of 150µL glutamate free media. Following plating, the cells were left to incubate at 37°C and 5% $C0_2$ in the Incucyte machine (S3 Essen Bioscience), where images were taken every 12h. The next day, the cells were treated with glutamate-free media, 0.5µM, 5µM ,50µM and 500µM glutamate, in triplicates. Treatment was repeated every 24h for a total of 4 days.

To note, the highest concentration of glutamate used (500uM) was chosen as “In-situ glutamate levels found to be in the 100-500uM range in GBM patients (63)”.

2.4.2 Antagonist treatment

U3019 and U3042 were prepared and treated as detailed above (section 2.4.1), with the addition of glutamatergic receptor antagonists. Here, 20μM of CNQX, 10 μM Perampanel, 5 μM UBP-302, 20μM Ketamine and their respective vehicles were also added. Here, CNQX and Ketamine were reconstituted in molecular grade cell culture H_20, whilst Perampanel and UBP-302 were reconstituted in DMSO. To note, these concentrations were chosen as they are the antagonists EC_{50} for these GBM lines. An example of this treatment is shown in Table 2.4.2.

Veh	Veh	Veh	Veh + Antagonist	Veh + Antagonist	Veh + Antagonist
0.5 Glu	0.5 Glu	0.5 Glu	0.5 Glu + Antagonist	0.5 Glu + Antagonist	0.5 Glu + Antagonist
5 Glu	5 Glu	5 Glu	5 Glu + Antagonist	5 Glu + Antagonist	5 Glu + Antagonist
50 Glu	50 Glu	50 Glu	50 Glu + Antagonist	50 Glu + Antagonist	50 Glu + Antagonist
500 Glu	500 Glu	500 Glu	500 Glu + Antagonist	500 Glu + Antagonist	500 Glu + Antagonist

Table 2.4.2: Example treatment layout

2.4.3 Incucyte Analysis

During the 4-day experiment, the treated cells were imaged every 12h, at 20x magnification by the Incucyte S3 Essen Bioscience. Here, bright field images of 4 selected sections of any well containing cells were taken. The acquired images were then processed by the instrument using Incucyte AI confluence analysis to determine the presence of cells in each section, shown as a mask (Fig. 2.4.3). This mask image allowed the Incucyte software to determine the cell's area coverage throughout each individual well. To note, as each condition was performed in triplicates, the Incucyte AI analysis software grouped same treated wells together, and their final area coverage

was divided by their area coverage at 24h. This value was then normalised to the vehicle (glutamate-free media) and plotted using GraphPad Prism software.

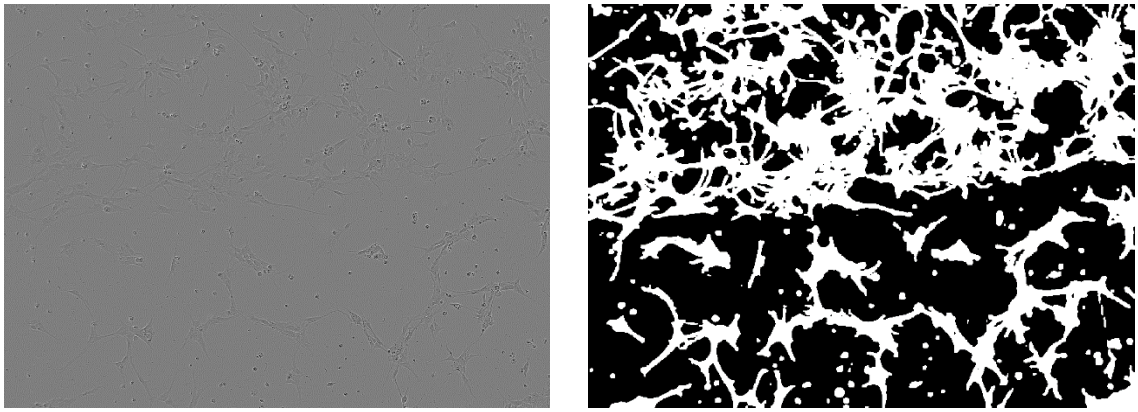

(a) (b)

Figure 2.4.3: U3019 Plated on Poly-O/Laminin and placed in the Incucyte machine (a) 10x bright field image (b) Incucyte AI analysis MASK

2.4.4 Cell Titre Glow Assay

To determine the number of viable cells in culture, U3019 and U3042 were taken out of the Incucyte, after the completion of 4 day imaging, and a Cell-Titre Glo assay was conducted according to manufacturer's instructions. Here, a volume of CellTitre-Glo reagent equal to the volume of cell culture media present in each well was added to each well. This content was mixed for 2min on a shaker, and then left to incubate at RT for a following 10min to stabilise the luminescent signal. Following, the luminescence produced was quantified using the CLARIOStar microplate reader (BMG Labtech), with a wave length of 560 nm.

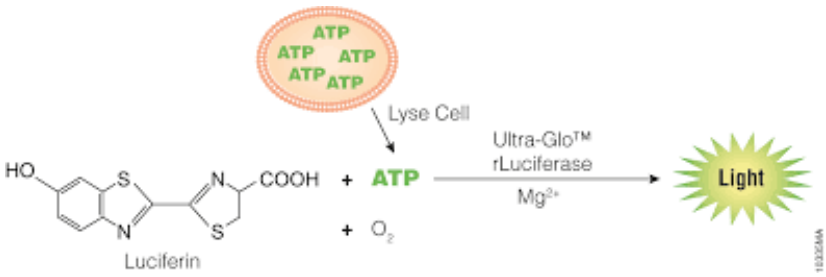

Figure 2.4.4: Luciferase is capable of catalysing the mono-oxygenation of luciferin in the presence of Mg^{2+}, ATP and Oxygen. This is a direct readout of ATP present in cell and thus is used to determine the number of viable cells in culture.

2.4.5 Ki-67 Staining

U3019 and U3042 were plated with a seeding density of 12,000 and 17,000 x well on a Poly-L Ornithine and Laminin coated glass bottom 96-well plate. The cells were treated every 24h with 50uM and 500uM glutamate and on day 4, the cells were fixed with 100ul of 4% paraformaldehyde for a total of 15min at room RT. Following, the cells were washed twice with PBS-T (1X PBS + 0.1% Triton X-100) for 5 minutes at RT. Subsequently, the cells were blocked using FBS+T and left incubating for 1h at RT. The primary antibody was then appropriately diluted (1:500) in FBS+T and then added and left to incubate overnight at 4°C on a shaker (Table 2.4.5). The following day, 5 washes were then performed with PBS+T for 5 minutes each, followed by the addition of the secondary antibody, appropriately diluted (1:100) in FBS+T. After a 3h incubation period, a subsequent 5 washes were performed using PBS+T. Nuclear staining was then achieved by adding Hoechst at appropriate concentration (1:500) in the first 1x PBS-T wash. Here, Hoechst was left to incubate for 10 minutes at RT. Lastly, PBS-T was replaced by PBS and then plate was wrapped in parafilm and placed in the cold room (4 degrees) for storage.

Antibody	**Dilution**	**Company**
Ki67 primary	1:1000	Universal Biologicals
Alexa Fluor 594 Anti-chicken	1:500	Stratech

Table 2.4.5: Antibodies used for KI-67 staining.

2.4.6 Imaging and analysis

Immunofluorescent images were taken on the Opera Phenix High-Content Imager (PerkinElmer) with a 20x water immersion objective. Two different channels representing the

nuclei and KI-67 were acquired simultaneously on a multicamera system in confocal mode (Channel 405 for Hoechst and Channel 594 for Alexa 594, ki-67 staining). To note, 3 different focal points per well were imaged and analysed using the Harmony software. Analysis took place by setting up some parameters as detailed in figure 2.4.5.

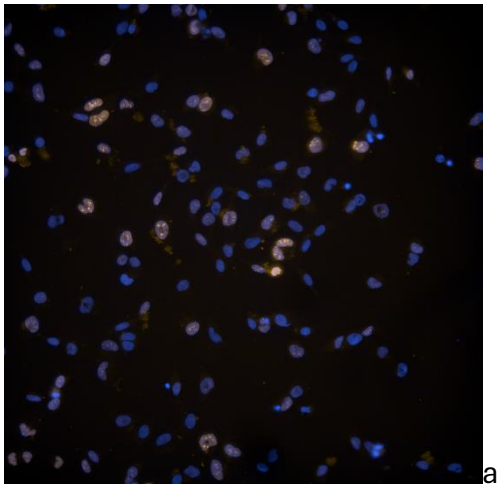
a)Raw immunofluorescence picture

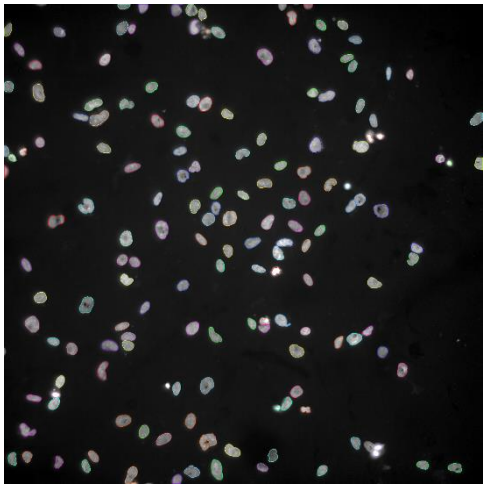
b)Find nuclei

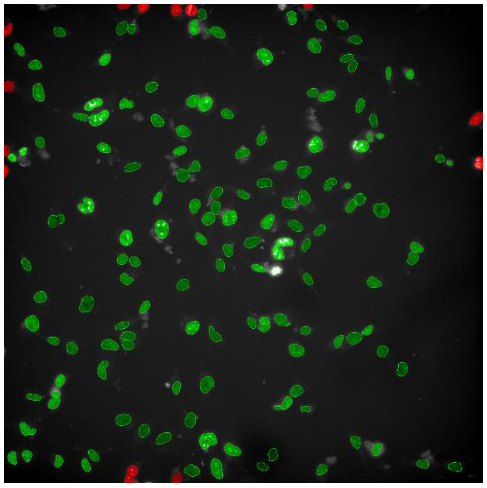
c)Select population

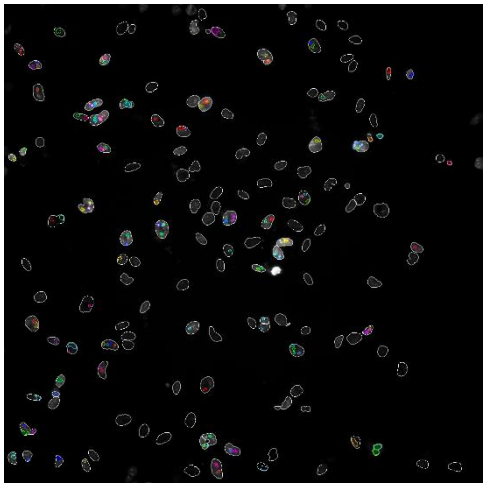
d) Find spots

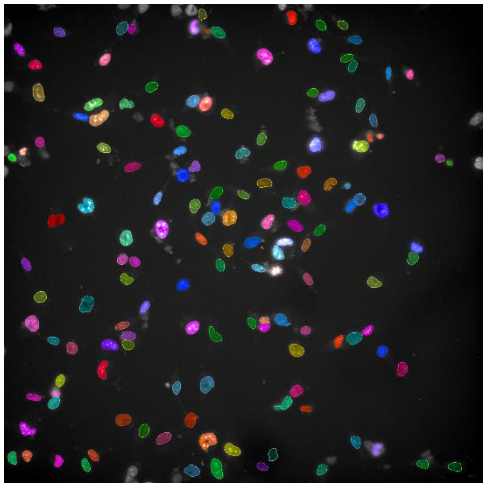
e) Define Population

Figure 2.4.5 Harmony analysis: Image (a) was analysed for the % of Ki-67 positive cells by initially finding the nuclei (b). Here the DAPI channel was selected and software method used is C. Following, the nuclei was selected to discard the border objects (C). This population was

then initially selected for Ki-67 spots (D), achieved by selecting the Alexa 594 channel within the defined nuclei population using the software's method A. This population was further selected and filtered using nuclei selected as my population and filter by property as the method, with number of sports greater than 1 as my parameter. Lastly, as shown in E, the population results gets defined as total number of spots **(D)**/total number of cells **(C)** X100.

2.5 intracellular calcium influx analysis

2.5.1 Cellular preparation

For intracellular calcium imaging, U3042 cells were seeded at 35,000 cells/well into a glass bottom PhenoPlate 96-well microplate (6005430). After a 36h incubation period, the cells were treated with 1uM Cal-520, AM (AAT Bioquest: Biomol ABD-21130) for 30min in the incubator. Afterwards the staining solution was replaced with fresh glutamate free media, and left to incubate for another 30min, prior to imaging.

2.5.2 Image acquisition

The assay plate was transferred to a pre-equilibrated temperature and $C0_2$ Opera Phenix Plus system. Images were acquired in non-confocal mode using a 20x water immersion objective, using the FITC channel. Images were taken in two subsequential steps: firstly, a 1min baseline was taken, with an image taken every 9 sec. Following this baseline, the machine allowed a rest for drug treatment to occur, by which the plate was ejected from the machine. Following the addition of vehicle or agonist +/- antagonist, fast kinetic image acquisition occurred every 4sec for a total of 9min and 5 focal points per well were imaged at the same time. To note, intracellular calcium was monitored as its release within the cells enhanced the fluorescence signal.

2.5.3 Analysis

The acquired images were then analysed using Java image processing program (Image J). The images corresponding to each focal point were imported as a sequence, and the first image

was analysed using the analyse particle function to detect nuclei using the following parameters: pixel units between 50-infinity, showing overlay and selecting clear results, exclude edges and add to manager. Following, the multi-measure function was applied and a table with the mean fluorescence intensity of each individual cell at every time point was produced. The acquired table was then analysed using a custom R-script which calculated the change in intracellular Ca^{2+} for each cell based on the change in fluorescence between time points (Ca^{2+} spikes) using dF/F_0, which corresponds to the calcium fluorescence at time point X – the calcium fluorescence at baseline over the average calcium fluorescence at time point 0. To note, time point 0 corresponds to the average of all time points before glutamatergic agonist was added. Any dF/F_0 values greater than 0.5 were considered as calcium spikes.

This data is then presented in two ways. Firstly, each cellular calcium spike per well is graphed up over time to give a comprehensive overview of how each cells responds. Secondly, all calcium spikes per condition are combined in a bar graph to give an overview analysis.

2.6 Statistical Analysis

2.6.1 Kruskal-Wallis One-Way ANOVA

Graph pad prism was used to perform a one-way Anova between the various different conditions. Following, a multiple comparison was also performed comparing all samples to the vehicle. Significance was observed when $p \leq 0.05$

2.6.2 T-test

Graph pad prism was used to perform a t-test between two different conditions. Here, significance was observed when $p \leq 0.05$

Chapter 3: Determine which ionotropic receptors and combinations of subunits are present in GBM

3.1Gene expression analysis of Ionotropic receptors and combination of subunits in GBM cells relative to their HGCC Z-score

There are three different families of glutamatergic ligand-gated ion channels (AMPA, NMDA and Kainate), each presenting different types of specific subunit combinations (38). Currently, there is limited insight into which ionotropic glutamatergic receptors are present in GBM, and whether this is distinctive from other normal astrocytic cells. A NGS experiment led by *Venkatramani et al*. identified that AMPA is the most robustly expressed glutamatergic receptor followed by Kainate and NMDA in single GBM cells. To confirm and expand on this, qPCR experiments on 2 different GBM lines (U3019 and U3042) were performed utilising primers for each individual subunit. Moreover, the subunit expression levels were also compared with its relative Z score, a statistical measurement derived from GBM patient samples, found on the HGCC website. It is key to highlight that this comparison is only used in order to gain some insights into their glutamatergic composition and that caution must be taken as this set of data comes across different technological platforms.

The receptor subunit expression of U3019 follows a similar pattern to its HGCC derived Z-score as the genes which present a low (-) delta Ct value show a low Z score (Fig. 3.1a). This pattern is disrupted for GRIK1, GRIK5 and its NMDA receptors subunits as their Z score should be a much lower score to correctly recapitulate their Ct value. The receptor subunit expression of U3042 also follows a similar pattern to its HGCC derived Z-score as the genes which present a higher Ct value (value closer to 0) is recapitulated with a high Z score value (Fig. 3.1b). Once again there is an exception to this pattern as GRIK4, GRIK5 and GRIN2C. To assess whether there was a correlation between the z-score and the -dt CT values a correlation analysis was performed and a negative correlation was found for U3019 whilst a moderate correlation was shown for U3042 (Supplementary F1).

(a)

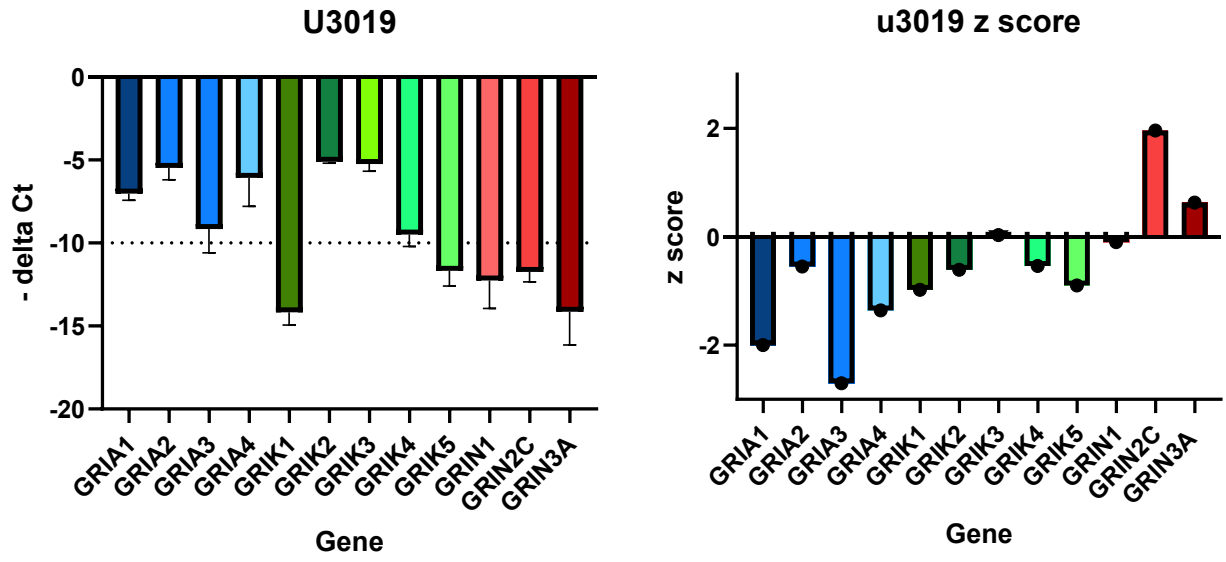

(b)

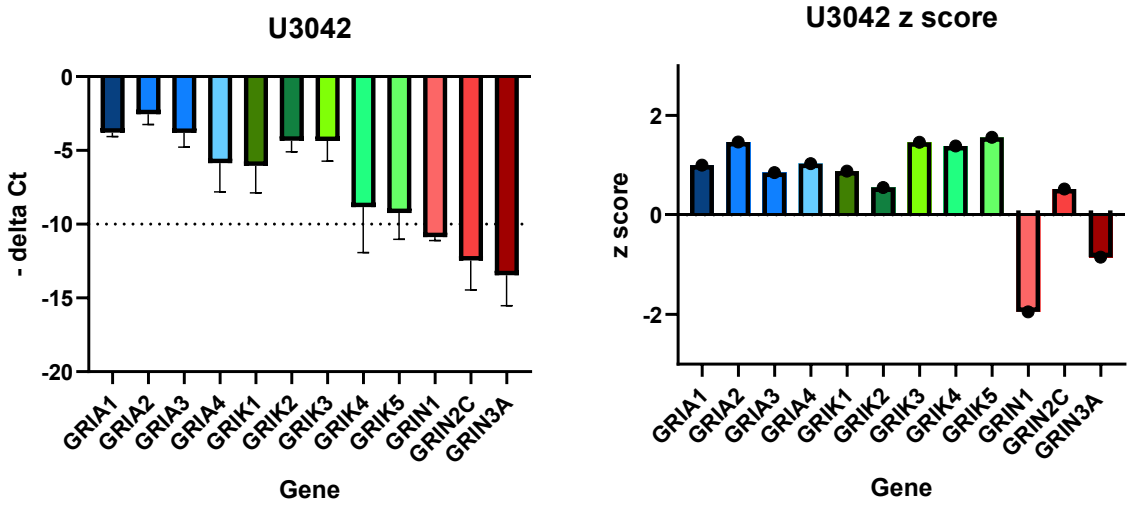

Figure 3.1: The delta Ct values of Glutamatergic gene expression compared to the genes' HGSS derived Z-score. The delta Ct values were calculated via qPCR using specific glutamatergic receptor subunit primers on 3 subsequent passages of (a) U3019 and (b) u3042 cDNA, using GusB as the reference gene. This experiment was performed using three technical repeats each, graph plotted as – Ct value mean + SD. The Z scores for each subunits were extracted from the HGSS website.

This data shows that U3019 and U3042 present a different receptor subunit expression, and that this expression is in line with the Z-score reported by the Human Glioblastoma Cell Culture Resource.

3.2 Gene expression analysis of ionotropic receptors and combinations of subunits in GBM cells

In order to compare the different receptor subunit expression across the three different glutamatergic receptor families, these delta Ct values collected where grouped accordingly. Moreover, their expression was also compared to the hGBM Line 2 (L2).

Fig.3.2a shows the (-) delta Ct values of all AMPA receptor subunits in the L2, U3019 and U3042 cell lines. When examining the L2 AMPA receptor profile, GRIA1 and GRIA3 show the highest delta Ct value with values of -5.67 and -2.69 respectively, indicating these are the most expressed AMPA receptors within that cell line. GRIA2 on the other hand is the least expressed within the L2 cell line with a value of -13.40. Of note, this value is the lowest seen across all cell lines (U3019 and U3042). Looking at the expression levels of AMPA subunits in U3019, these receptor subunits present a relatively similar expression with the delta Ct values ranging from -5.13 to -8.42, representing GRIA2 (most expressed) and GRIA3 (least expressed) respectively. GRIA2 is also the most expressed in U3042 with a delta Ct value of -2.54, which the highest expressed receptor subunit across all lines.

When focusing on the Kainate receptor subunits (Fig. 3.2b), each cell line presents a similar pattern. They all express GRIK2 and GRIK3 at similar level, as their delta Ct values all fall within -4.12 and -6. Moreover, to the exception of GRIK1 for U3019, GRIK4 and GRIK5 are the lowest subunits expressed in each cell line. Lastly, Fig. 3.2c depicts the expression levels for the NMDA receptor subunit. Here, each gene is expressed at a similar level within its cell line with delta Ct values ranging between -7.2 to -8.34 for L2, -11.74 to -12.77 for U3019 and -10.88 to -12.44 for U3042.

(a)

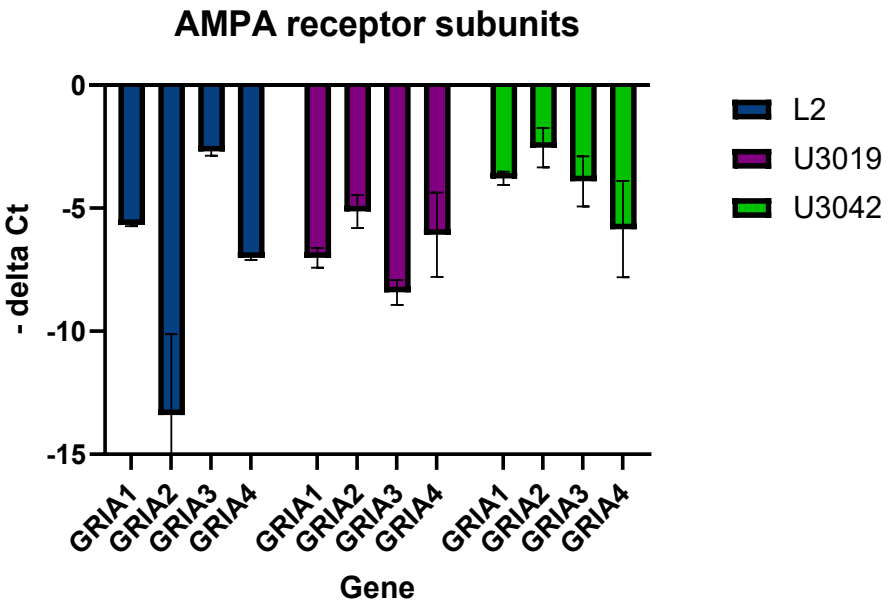
AMPA receptor subunits
0
-5
-10
-15
- delta Ct
GRIA1
GRIA2
GRIA3
GRIA4
GRIA1
GRIA2
GRIA3
GRIA4
GRIA1
GRIA2
GRIA3
GRIA4
Gene
L2
U3019
U3042

(b)

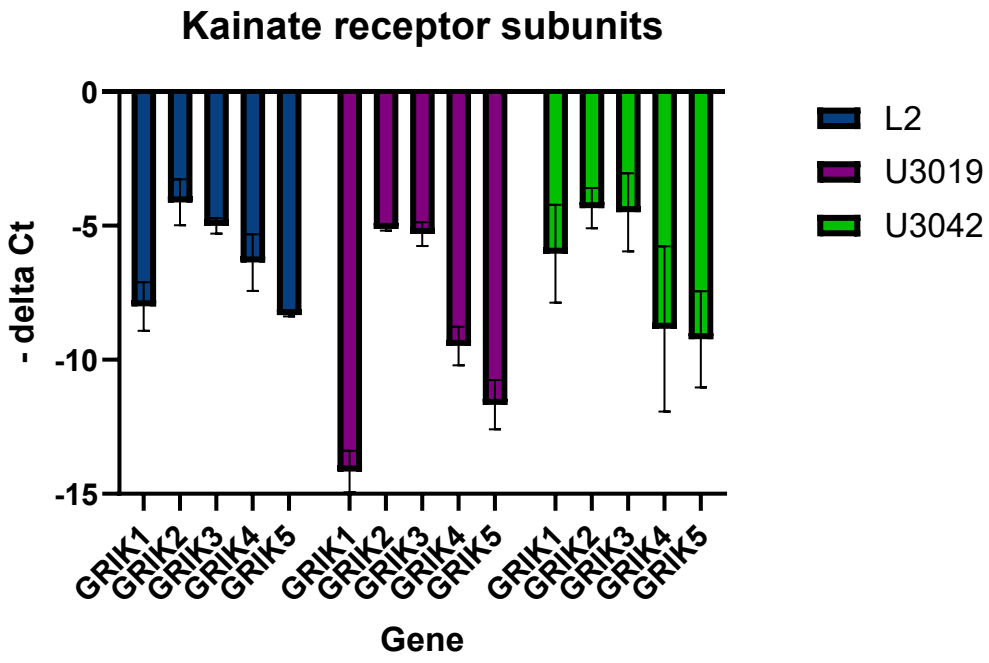
Kainate receptor subunits
0
-5
-10
-15
- delta Ct
GRIK1
GRIK2
GRIK3
GRIK4
GRIK5
GRIK1
GRIK2
GRIK3
GRIK4
GRIK5
GRIK1
GRIK2
GRIK3
GRIK4
GRIK5
Gene
L2
U3019
U3042

(c)

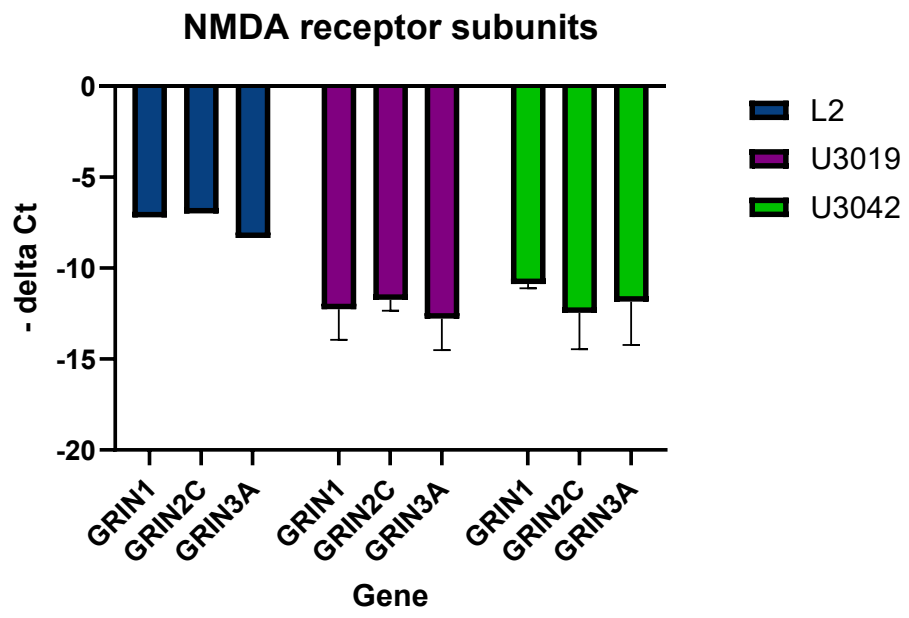

Figure 3.2: qPCR analysis comparing the expression level of (a)AMPA, (b)Kainate and (c) NMDA subunits. This experiment was performed using validated GRIA1-4, GRIK1-5 and GRIN1,2C and 3A primers on the cDNA of L2, U3019 and U3042 lines, from three different passages. This experiment was performed using three technical repeats each, graph plotted as – Ct value mean + SD (n=3).

This data shows that L2, U3019 and U3042 present different receptor subunit expression for all three glutamatergic receptors. This said, U3042 presents the highest receptor expression for the AMPA and Kainate subunits, with the exception of GRIK4 and GRIK5. Moreover, all three cell lines present low expression levels of NMDA receptor subunits.

3.3 Gene expression analysis of Ionotropic receptors and combinations of subunits in normal human astrocytes

As GBM is an aggressive astrocytoma, to determine whether U3019 and U3042 present a different glutamatergic receptor pattern to astrocytes, a qPCR experiment was performed using normal human astrocytes (NHA) cDNA.

Fig. 3.3 shows that GRIA is the most expressed glutamatergic receptor subunit within Human derived Astrocytes, with a delta Ct value of -4.75. Looking at the Kainate subunits, GRIK2 and

GRIK5 are also highly expressed with a delta Ct value of -5.23 and -6.19, respectively, whilst GRIK4 is the least expressed subunit with a delta Ct value of -12.28. Lastly, the NMDA receptors are the least expressed receptor subunit family, with GRIN1, GRIN2C and GRIN3A presenting values between -10.58 and -11.63.

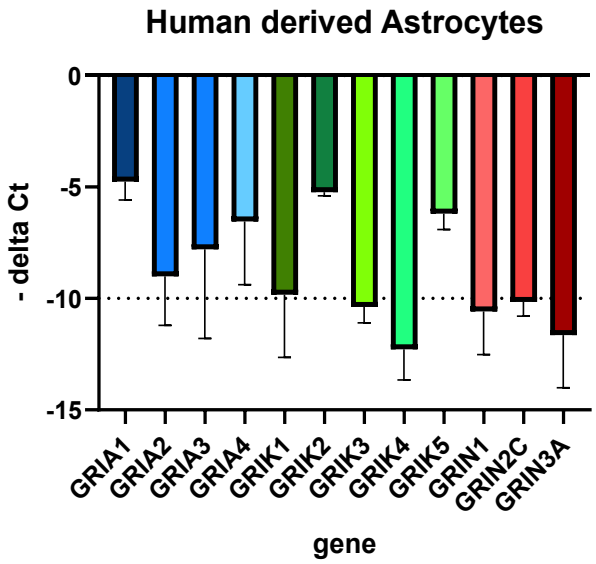

Figure 3.3. The delta Ct values of Glutamatergic gene expression. The delta Ct values were calculated via qPCR using specific glutamatergic receptor subunit primers on normal human astrocytes cDNA using GusB as a reference gene. This experiment was performed using three technical repeats each, Graph plotted as mean – delta Ct (n=3)

This data shows that the AMPA receptor subunit GRIA1 and the Kainate receptor subunits GRIK2 and GRIK5 are the most highly expressed subunits in NHA.

3.4 Comparative gene expression analysis of ionotropic receptors and combinations of subunits in GBM cells and normal human astrocytes

To determine whether any of these glutamatergic receptor subunits are GBM specific, a ddCt value was calculated using the Ct values of my GBM lines vs HDA.

As seen in Fig. 3.4, the receptor expression profile for U3019, U3042, and L2 is different to the one for NHA. For instance, all glutamatergic receptor subunits are expressed at a much higher

level in U3019, U3042 and L2 compared to NHA, specifically GRIA2 for U3019 and U3042 and GRIK3 AND GRIK4 for all three lines.

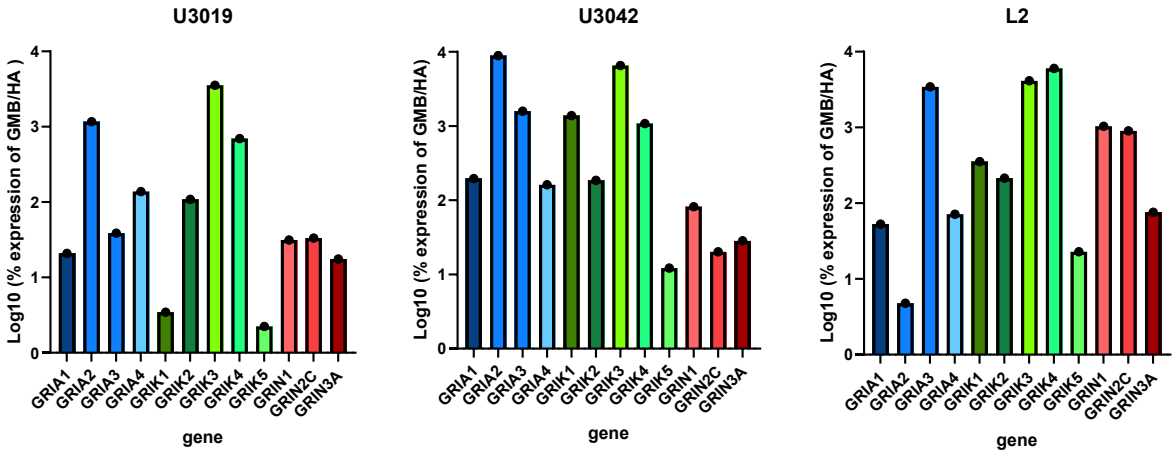

Figure 3.4: Percentage expression of GBM glutamatergic subunit compared to normal human Astrocytes. The expression levels of GBM glutamatergic receptor subunits was compared to the expression of NHA by performing a ($2^{-ddCT} x\ 100$) calculation. This value was then converted to its log10 value.

This data shows that GRIA2, GRIA3, GRIK3 and GRIK4 are expressed at a much higher level compared to NHA in GBM cell lines and thus can be considered GBM specific receptor subunits.

3.5 Expression analysis of GRIA1-3 and GRIK1-3 proteins in GBM cells and normal human astrocytes

Having shown that the AMPA and Kainate receptors are the most highly expressed receptor subunits in all three cell lines and that they are GBM specific following qPCR experiments, a western blot experiment was performed to confirm this using GRIA1-3 and GRIK1-3 receptor subunit antibodies. It is key to note that here the western blots are all cut so all glutamatergic

receptor subunits below 55kDA in size are not shown. This is because within each sample lane, both the receptor and GAPDH were probed.

Fig. 3.5 shows that AMPA1 is detected in all 4 cell types, and at multiple different molecular weights. At approximately 180 kDa a faint band can be shown for NHA, U3019 and L2. On the other hand U3042 shows a more intense band. At approximately 60 kDa, a strong band can be seen for U3042 and U3019, whilst L2 show a much fainter one. AMPA2 on the other hand a protein band can also be seen in L2, and two bands can be seen corresponding to 175 and 100 kDa in size. AMPA3 is also not seen in Astrocytes, whilst U3042 presents 2 bands corresponding to 175 and 100 kDa in size. U3019 and L2 show only a faint band of 175 kDa in size.

Fig. 3.6 shows that GRIK1 is strongly present in U3042 as it shows the highest band signal. Astrocytes, U3019 and L2 show this protein too, although at a much lower level. U3042 also presents GRIK2 the highest, followed by L2, U3019 and Astrocytes, with a molecular weight of 100 kDa. Here, we can also see a band of approximately 60 kDa for the 3 GBM lines. Looking as the western blot for GRIK3, multiple bands be observed. At approximately 100k Da in size, U3042 presents the strongest band, followed by 2 faint bands for U3019 and L2. Bands for all 4 samples can be seen at approximately 210 and 75Kda.

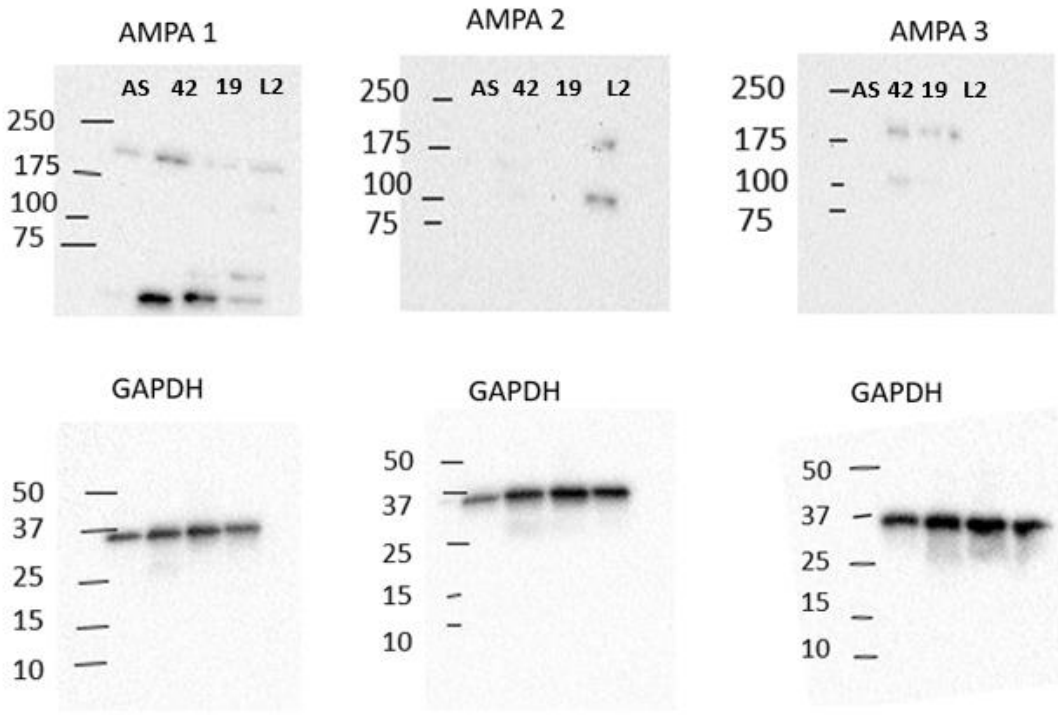

Figure 3.5: GRIA1,GRIA2 and GRIA3 expression in Astrocytes, U3042, U3019 and L2 by western blot (n=1). Astrocyte, U3042, U3019 and L2 cells were collected and their protein lysates were extracted. 15ug of their lysate was run on an SDS-page gel and then transferred on a PVDF membrane. Following transfer, the membrane was cut accordingly and probed with GRIA1-3 and GAPDH primary antibodies. Here shown is the chemo luminescent signal produced which correlated to the quantity of protein present (n=1)

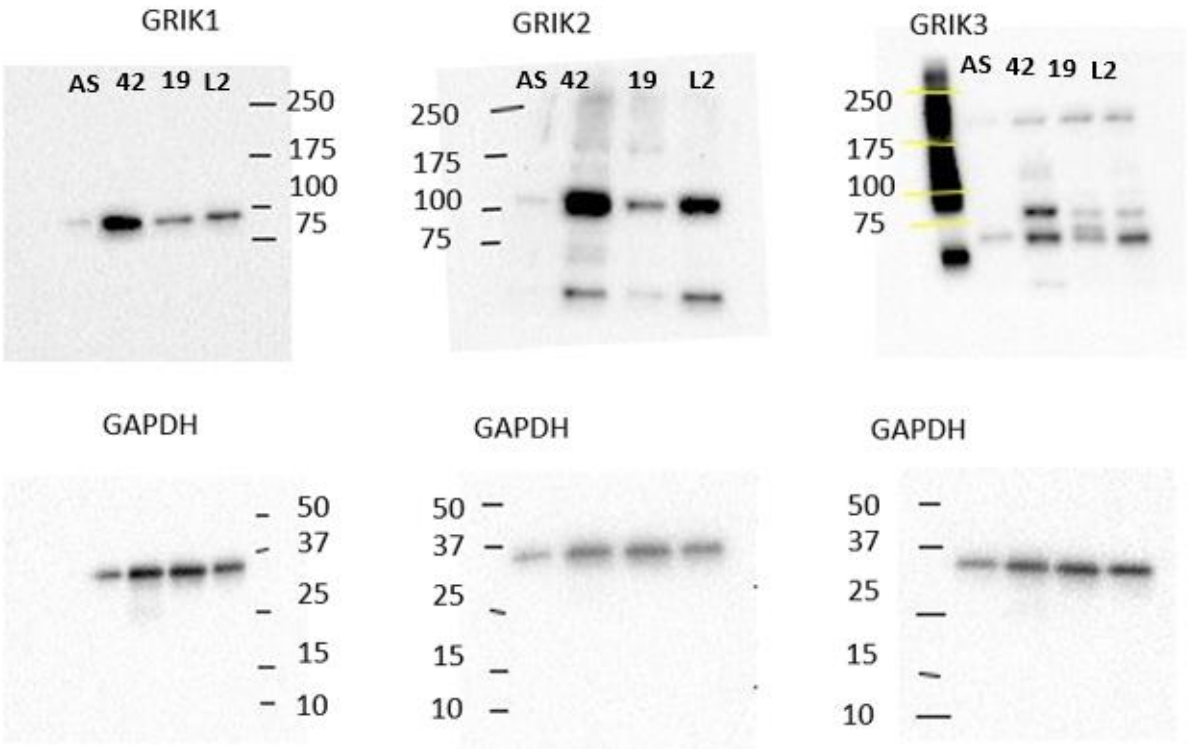

Figure 3.6: GRIK1,GRIK2 and GRIK3 expression in Astrocytes, U3042, U3019 and L2 by western blot. *Astrocyte, U3042, U3019 and L2 cells were collected and their protein lysates were extracted. Their lysate was run on an SDS-page gel and then transferred on a* PVDF membrane. Following transfer, the membrane was cut accordingly and probed with GRIK1-3 and GAPDH primary antibodies. Here shown is the chemo luminescent signal produced which correlated to the quantity of protein present (n=1)

This data shows that GRIA1 is expressed in all four cell lines, whilst AMPA 2 is only expressed in L2 and AMPA3 only in GBM lines. The western blots for GRIK1, GRIK2 and GRIK3 all show that GBM cells express these proteins at a higher level than astrocytes.

Conclusion:

In this section the expression levels glutamatergic receptor subunits were analysed in 3 GBM lines U3019, U3042, L2 and also in normal human astrocytes in order to determine whether there is any GBM specific receptor subunit preference. The initial qPCR results identified that U3042 expresses the AMPA and Kainate receptor subunits at a higher level to U3019, L2 and NHA. This data also reviled that NMDA subunits are hardly expressed in U3019 and U3042. Moreover, by then calculating the percentage expression of GBM glutamatergic subunit compared to normal human Astrocytes, GRIA2, GRIA3 and GRIK3 were determined as GBM favourable receptor subunits. This statement is confirmed following western blot analysis. Here the expression analysis of GRIA2, GRIA3 and GRIK1-3 was heightened in my GBM lines compered to normal human astrocytes.

Chapter 4: Identify the role of glutamatergic receptor modulators in GBM cell lines, using cell proliferation assays

4.1Cell titre glow assays show Glutamate Increases cellular proliferation in GBM

In order to identify the proliferative role of glutamate in the U3019 and U3042 GBM cell lines, their responsiveness to 0.5, 5 ,50 and 500uM of glutamate was monitored by performing Cell Proliferation assays. To note U3042 was chosen because it presented the highest glutamatergic receptor profile and U3019 was chosen over L2 due to its ability of growing adherently (an important property for calcium imaging, see chapter 5), and because it required the same growth media as U3042, thus getting rid of possible variants. Here, brightfield microscopy using the Incucyte S3 (Essen Bioscience) was used to visually assess the cells growth rate in real-time. Although potential limitations such as cellular spreading and uneven cellular growth could skew the end point result, proliferation rates were obtained by measuring well confluency over time. In addition, following this 4-day experiment, a CellTiter-Glo® Luminescent Cell Viability Assay was performed to determine the number of metabolically active cells. Here, we can assume that the number of metabolically active cells is directly proportional to the number of cells present in culture. Therefore, an increase in the number of metabolically active cells correlates to an increase in cellular proliferation.

Fig. 4.1a shows that the levels of area coverage for U3019 (coloured in purple) and U3042 (coloured in green) do not change when treated with different glutamate concentrations. Here, even when treated with 500uM of glutamate the area coverage does not change compared to the glutamate-free medium (U4).

Fig. 4.1b depicts the mean growth slope of U3019 and U3042 following glutamate treatment, used as an indicator of growth speed. To note, slope is calculated by taking the final area coverage and subtracting it by the 24h time point coverage. When treated with various concentrations of glutamate, both U3019 and U3042 do not statistically increase their mean growth rate. This said, when the U3042 are treated with the two highest glutamate concentrations, their slope does increase compared to the glutamate-free medium, as their present values of 2.58 and 2.3, respectively.

Fig. 4.1c shows the levels of luminescence present in each cell following glutamate treatment. Here, the levels of luminescence following treatment in U3019 do not change compared to the glutamate-free medium condition. On the other hand, a change in luminescence is observed for U3042. Here, significance is observed when the cells are

treated with 50uM and 500uM of glutamate as their values increase from 1 to 1.19 and 1.29, respectively.

(a)

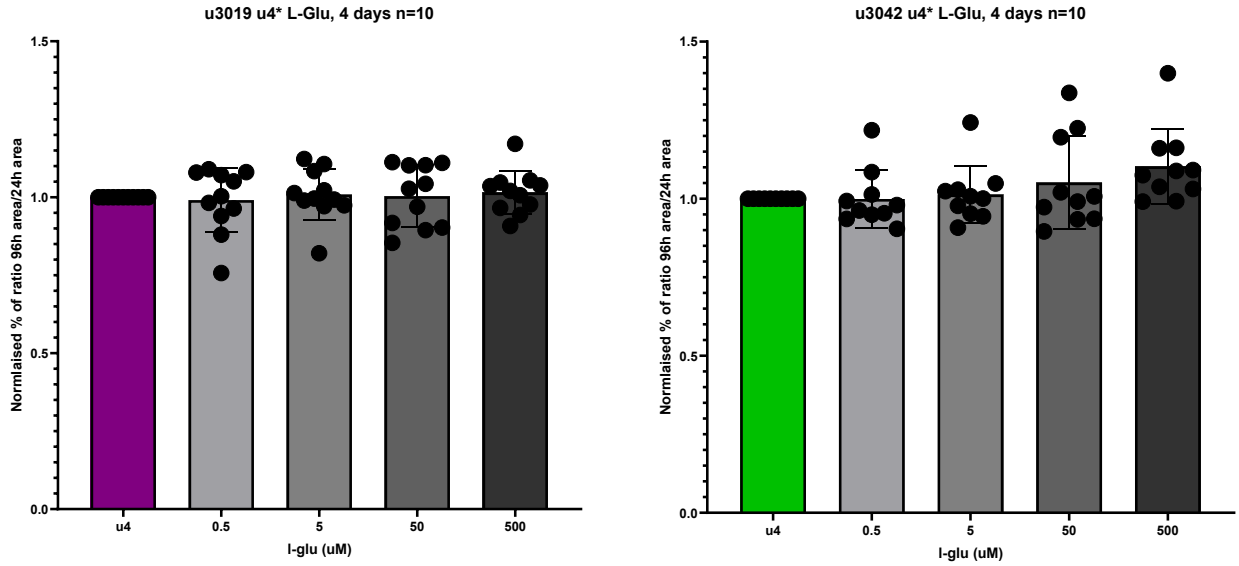

(b)

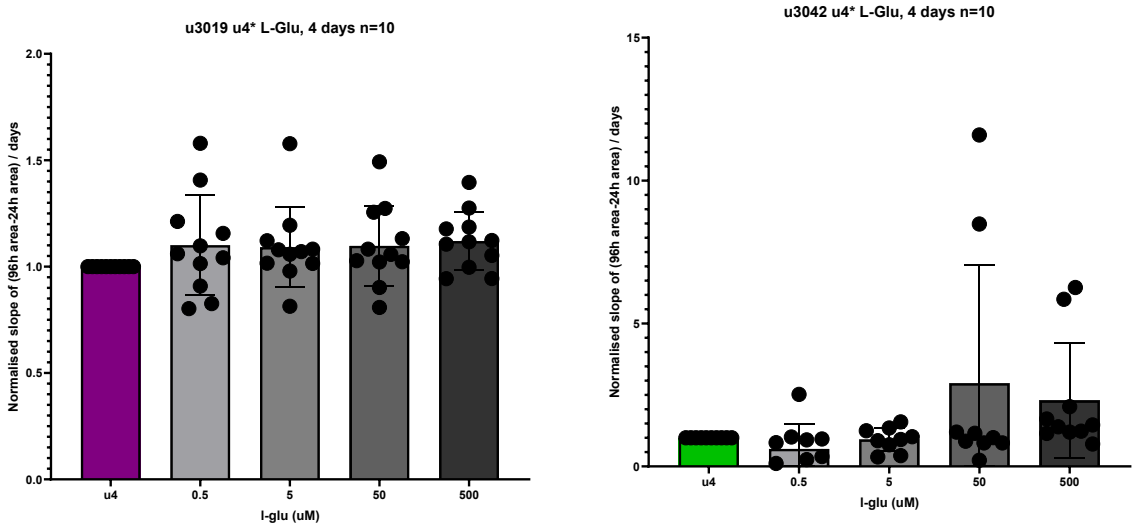

(c)

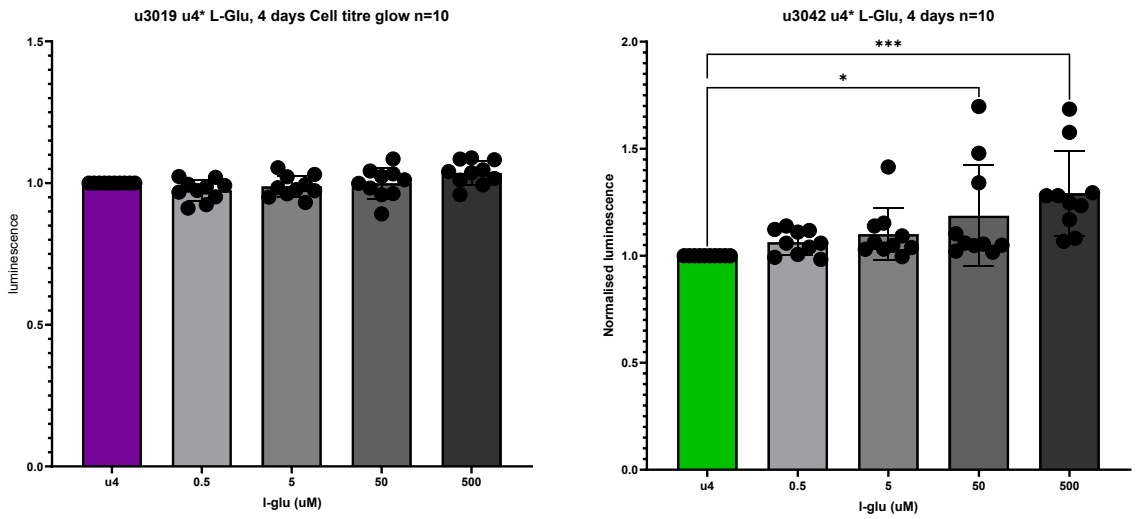

Figure 4.1: Glutamate dose-response curve on U3019 and U3042 analysed using (A)Incucyte area (B) Incucyte slopes and (C) Cell titre glow. U3019 and U3042 were plated on laminin in a 96 well plate with a starting seeding density of 12k/well and 17k/well, respectively, in U4 feeding media lacking glutamate and growth factors. Following plating, they were placed in the incucyte for image capture every 12h for a total of 4 days. Cells were treated with the 0.5, 5, 50 and 500 μM Glutamate concentrations every 24h. Following 4days, a cell titre glow assay was performed. (a) Shows the mean total area coverage at 96h over the mean area coverage at 24h. (b) Shows the mean area coverage slopes per each condition calculated using the final area coverage – the 24h coverage over 4 days. (c) Shows the mean luminescence readout per condition, normalised to the vehicle. Each experiment was performed using an N=3 and all graphs plotted as mean + SD. Statistical analysis was performed using a 1-way ANOVA (p≤0.05).

This data shows that U3019 does not respond to glutamate whilst U3042 increases its metabolic profile following the addition of 50 and 500uM glutamate. This positive response can be attributed to the receptor expression profile of this cell line. Previous experiments have highlighted that U3042 has a higher AMPA and Kainate receptor expression compared to U3019.

4.2 Ki-67 staining shows glutamate increases GBM cell proliferation

As confluency measurements did not yield significant results in either cell line (Fig. 2.1a) but a trend to increased proliferation was observed when performing cell titre glow analysis on the U3042 GBM cell line (Fig. 4.1c), Ki-67 staining was chosen as another end-point. Ki-67 was chosen as a potentially more sensitive method for quantifying proliferation as it is a generic proliferation marker which gives us insight into whether the cells are diving or not. Moreover, as only 50 and 500uM glutamate caused an increase in GBM proliferation (Fig 4.1c), I choose to perform the following experiments focusing on these two concentrations.

When treating U3019 with 50 and 500uM glutamate, the number of Ki-67 positive stained cells do not increase compared to the glutamate-free media treated ones. Here, the cells present a similar red intensity signal across all 3 images (Fig. 4.2.1a). This is recapitulated in Fig 4.2.1b, as the calculated % of Ki-67 positive cells is not statistically different in the three different conditions. On the other hand, when treating U3042 with 50 and 500uM glutamate, a visual increase in the number of Ki-67 stained cells is observed as the red intensity signal is stronger compared to the glutamate-free medium ones (Fig 4.2.2a). This increase is only statistically significant when the cells are treated with 500uM glutamate, following analysis (Fig 4.2.2b).

U3019 Results:

(a)

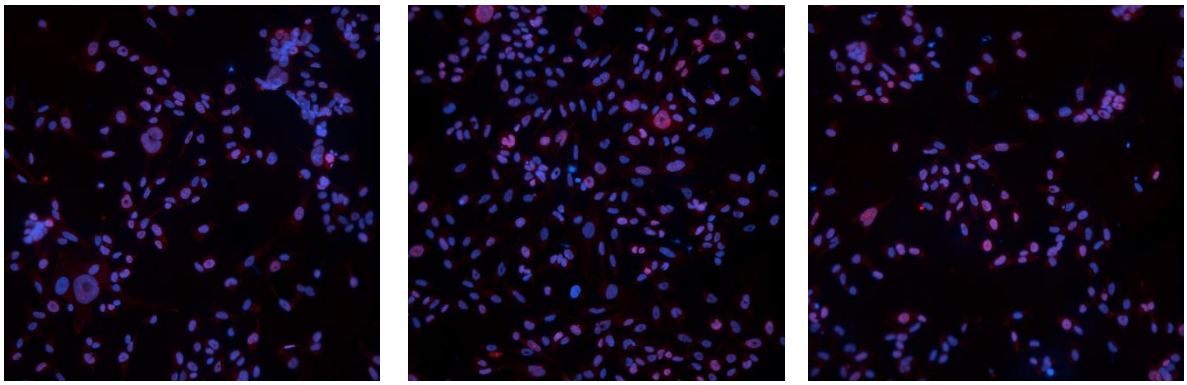

Glutamate-free medium N=1 50 µM Glutamate N=1 500 µM Glutamate N=1

(b)

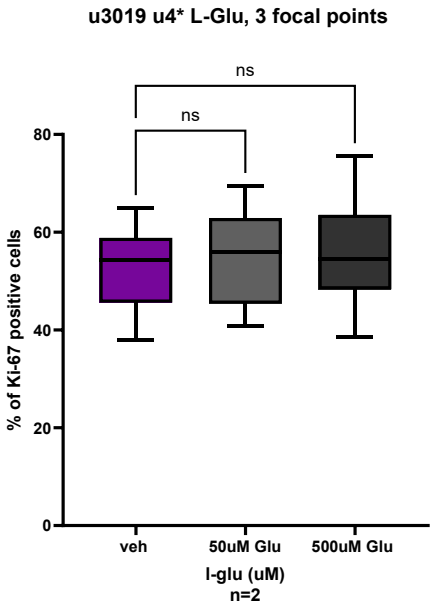

Figure 4.2.1: Percentage of KI-67 positive cells following glutamate treatment. U3019 cells were plated on laminin in a 96 well plate with a starting seeding density of 12k/well, in U4 feeding media lacking glutamate and growth factors. Cells were treated with 50 and 500 µM Glutamate concentrations every 24h for a total of 4 days. On day 4, the cells were fixed with 4% Formaldehyde and stained for Ki-67 and DAPI. (a) Visual representation of DAPI (blue) and ki-67 staining (red) Imaged on the Opera Pheonix, 20x Air. (b) Percentage of KI-67 positive cells analysed using the Opera Phoenix Analysis function. 3 focal points per well were imaged. Data plotted as mean + SD (n=2)

U3042 Results:

(a)

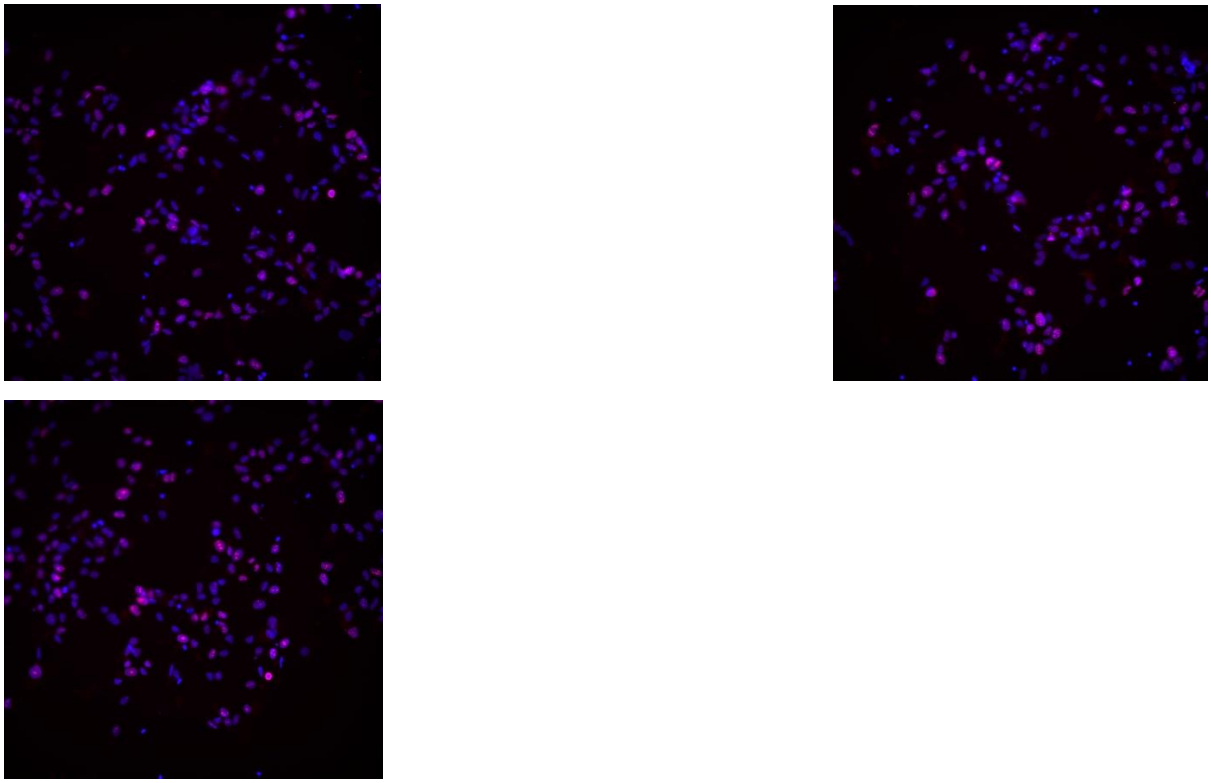

Glutamate-free medium N=1 50 µM Glutamate N=1 500 µM Glutamate N=1

(b)

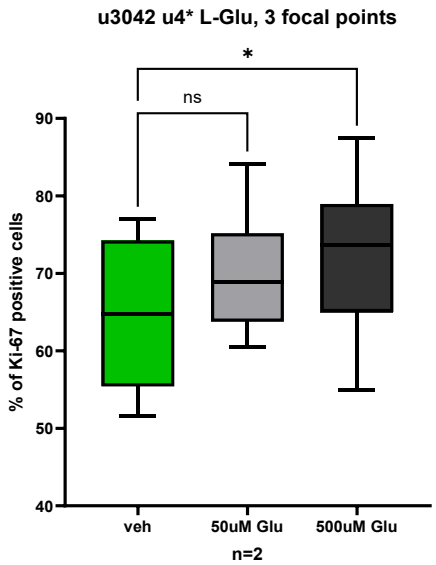

Figure 4.2.2: Percentage of KI-67 positive cells following glutamate treatment. U3042 cells were plated on laminin in a 96 well plate with a starting seeding density of 17k/well, in U4 feeding media lacking glutamate and growth factors. Cells were treated with 50 and 500 µM

Glutamate concentrations every 24h for a total of 4 days. On day 4, the cells were fixed with 4% Formaldehyde and stained for Ki-67 and DAPI. (a) Visual representation of DAPI (blue) and ki-67 staining (red) Imaged on the Opera Pheonix, 20x Air. (b) Percentage of KI-67 positive cells analysed using the Opera Phoenix Analysis function. 3 focal points per well were imaged. Data plotted as mean + SD (n=2).

This data shows that U3019 does not increase the number of Ki-67 positive cells following glutamate treatment. On the other hand, 500uM glutamate causes an increase in the number of Ki-67 positive U3042 cells. Again, this positive response can be attributed to the receptor expression profile of this cell line. Previous experiments have highlighted that U3042 has a higher AMPA and Kainate receptor expression compared to U3019. Moreover, a response to 500uM only can be linked to the fact that "in-situ glutamate levels are found to be in the 100-500uM range in GBM patients" (63).

4.3 Ki-67 staining reveals anti-glutamatergic receptor modulators do not decrease cellular proliferation in GBM cell lines

Having established that glutamate increases proliferation in the U3042 cell line, the next step in this project was to try and determine whether antagonists to the ionotropic glutamate receptors counteract this effect. This was addressed by performing the previously validated Ki-67 staining experiments with the addition of antagonists to the glutamatergic ion channels using their EC_{50} concentration + 10 fold higher/lower.

When U3042 were treated with 500uM Glutamate and 200uM CNQX, a general competitive glutamatergic antagonist, the % of Ki-67 positive cells increased compared to the glutamate only treated cells. When treated with 20 and 2uM of CNQX, the % of Ki-67 staining was the same as for glutamate treated only (Fig. 4.3a). When the cells were treated with various concentrations of Perampanel and UBP-302 which target the AMPA and Kainate receptor respectively (Fig 4.3b,c), the % of Ki-67 positive cells did not change compared to the glutamate only treated cell. To note, 10 fold higher than the EC_{50} for Perampanel is not shown as that concentration causes the cells to undergo cell death.

Results:

(a) 500uM Glutamate + CNQX

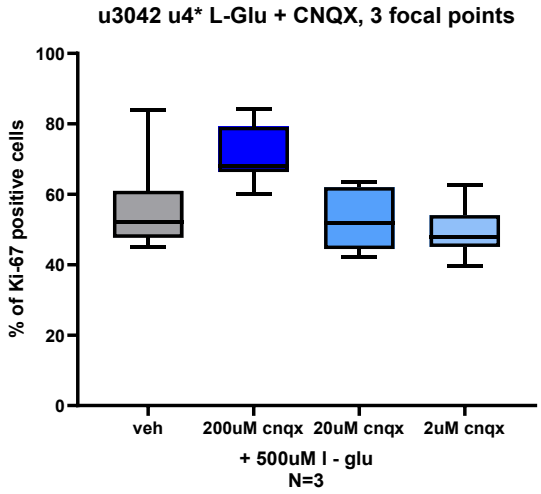

(b) 500uM Glutamate + Perampanel

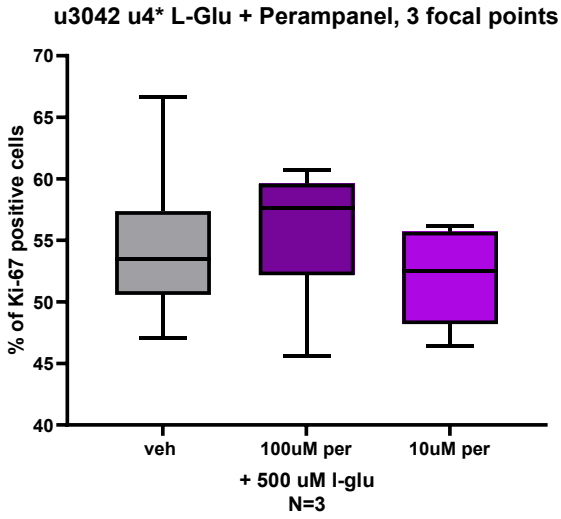

(c) 500uM Glutamate + UBP-302

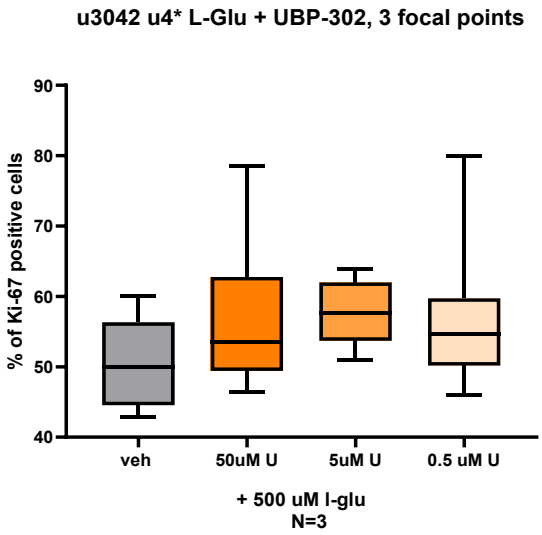

Figure 4.3: *Percentage of KI-67 positive cells following glutamate +/- antagonist treatment. U3042's were plated on laminin in a 96 well plate with a starting seeding density of 17k/well in U4 feeding media lacking glutamate and growth factors. Following plating, they were placed in the incubator. Cells were treated with 500 μM Glutamate and (a) 2, 20 and 200 μM CNQX, (b) 1, 10 and 100 μM Perampanel, (c) 0.5, 5 and 50 μM UBP-302. On day 4, the cells were fixed with 4% Formaldehyde and stained for Ki-67 and DAPI and imaged on the Opera Pheonix, 20x Air. The images were then analysed using the Opera Phoenix Analysis function. 3 focal points per well were imaged. Data plotted as mean + SD (n=1).*

This data shows that CNQX, Perampanel and UBP-302 does not decrease the number of Ki-67 positive cells compared to glutamate only treated cells.

Disclaimer, these results were obtained using the wrong concentration of KI-67 primary antibody (1:1000 rather than 1:10000). This was only realised towards the end of this project so I only had time to repeat this using the antagonists EC_{50} value.

4.4 New Ki-67 staining confirms anti-glutamatergic receptor modulators do not decrease cellular proliferation in GBM cell lines

When U3042 was treated with 500uM Glutamate and 20uM CNQX, 10uM Perampanel, 5uM UBP-302 and 20uM Ketamine, no cellular proliferation decrease was observed compared to both the vehicle and 500uM glutamate (Fig.4.4)

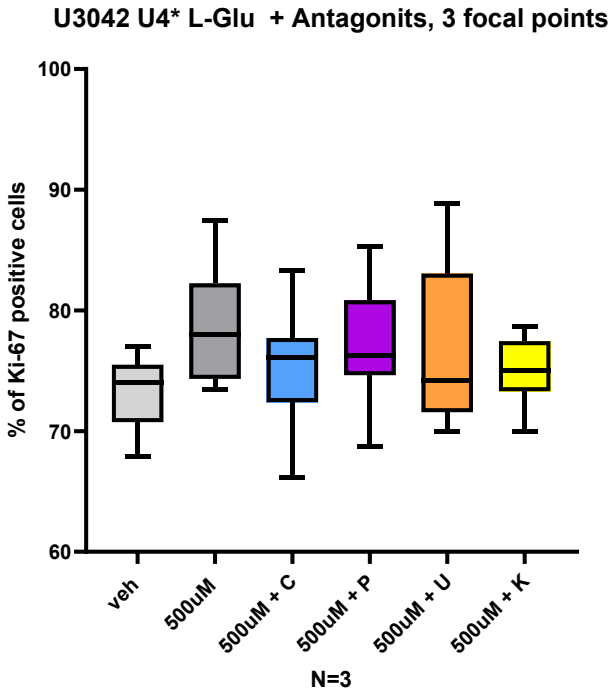

Figure 4.4: *Percentage of KI-67 positive cells following glutamate +/- antagonist treatment. U3042's were plated on laminin in a 96 well plate with a starting seeding density of 17k/well in U4 feeding media lacking glutamate and growth factors. Following plating, they were placed in the incubator. Cells were treated with 500 μM Glutamate and 20 μM CNQX, 10 μM Perampanel, 5 μM UBP-302 and 20μM Ketamine. On day 4, the cells were fixed with 4% Formaldehyde and stained for Ki-67 and DAPI and imaged on the Opera Phenix, 20x water immersion lens. The images were then analysed using the Opera Phenix Analysis function. 3 focal points per well were imaged. Data plotted as mean + SD (n=1).*

This data shows that anti-glutamatergic receptor modulators do not decrease cellular proliferation in U3042 cell lines.

Conclusion:

In this section the proliferative effects of glutamate were assessed by performing Incucyte, cell titre glow and KI-67 staining experiments on U3019 and U3042. These results identified glutamate as an important promoter of proliferation in U3042 as treatment with 500uM glutamate caused an increase in luminescence (cell titre glow end point) and % of KI-67 positive cells. On the other hand, U3019 was shown to not respond to glutamate. This is consistent with what shown in chapter 1, which identified a significantly different glutamatergic receptor expression between these two Uppsala lines, with U3042 presenting higher expression of AMPA and Kainate receptor subunits.

However, having identified glutamate as a promoter of proliferation I then tried to inhibit glutamate's effect by targeting the different glutamatergic receptors with antagonists CNQX, Perampanel and UBP-302. My results showed that U3042 did not show any decrease in proliferation following antagonist treatment.

Chapter 5: Establish whether an increase in calcium fluctuation is observed in GBM lines following glutamate stimulation

5.1 Investigating whether glutamate increases calcium influx

As the effects of glutamate on cell proliferation were limited, a different and more direct readout was chosen. Here, intracellular calcium was analysed to determine whether glutamate affects the cell at a molecular level.

Calcium is a secondary messenger which is implicated in a variety of different cellular processes including proliferation and apoptosis (64). To monitor if there are any changes in intracellular calcium flux following the addition of 500uM glutamate, we used a calcium sensitive dye (Cal-520), to perform live cell imaging of Ca^{2+} transients on the Opera Phenix imaging system. The acquired images were then processed using image J, which calculated the fluorescent intensity per cell at each time point. Following, an intracellular calcium spike was calculated using dF/F_0, which corresponds to the calcium fluorescence at time point X – the calcium fluorescence at baseline over the average calcium fluorescence at time point 0.

Anytime a cell increases intracellular calcium, the spike will show a value greater than 0. To note, the average calcium fluorescence at time point 0 was used in order to normalised each calcium spike. Furthermore, in this chapter there is variability across calcium spike experiments which is due to the fact that each experiment was performed on different U3042 plated wells and one needs to account for cell distribution and variety of processes formed.

Fig. 5.1a shows the normalised calcium spikes present in each cell following the addition of vehicle. Here, the calcium spikes are in the -0.5 and 1 range, to the exception of 3 peaks in well 3 at time point 180-200s. On the other hand, with the addition of 500uM glu (Fig. 5.1b), the calcium spikes can reach a maximum of 2.4. Here, well 1 and 2 show an increase in calcium spikes as soon as glutamate is added (60 seconds) which lasts up to 300 and 120 seconds, respectively. On the other hand, the calcium spike profile for well 3 shows that 2 cells present a continuous spike following the addition of glutamate until 300 seconds. Glutamate's ability to increase intracellular calcium spikes can be conceptually recapitulated in Fig. 5.1(c) where the number of cells which presented a calcium spike per condition is plotted. Here, an increase in calcium spikes is seen following the addition of 500uM Glutamate.

Results

(a) Vehicle

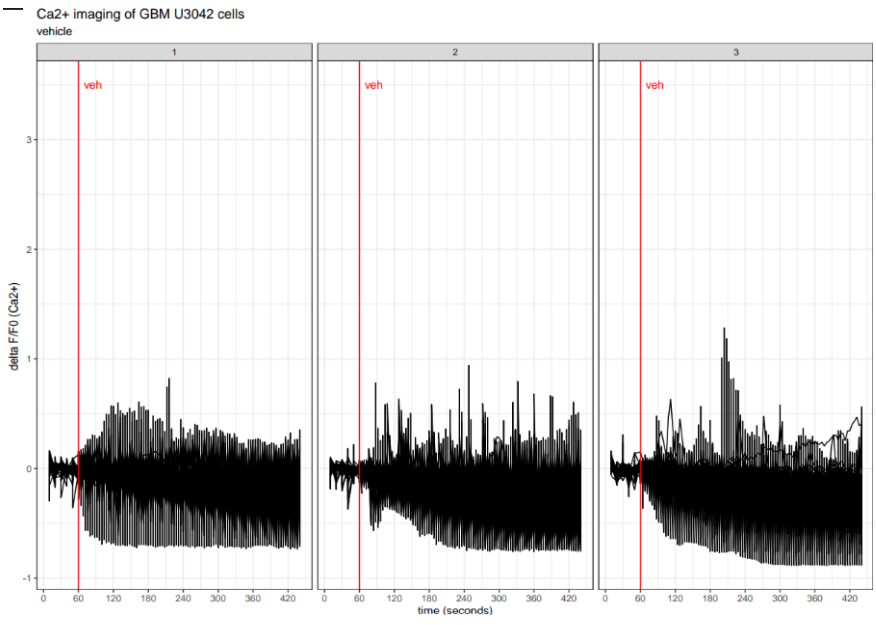

(b) Glutamate 500uM

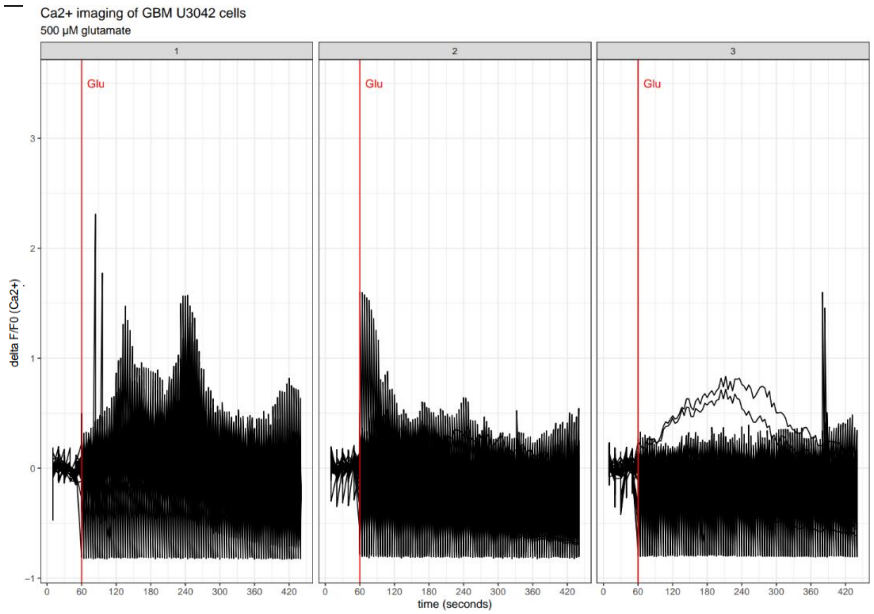

(c) calcium spikes per condition

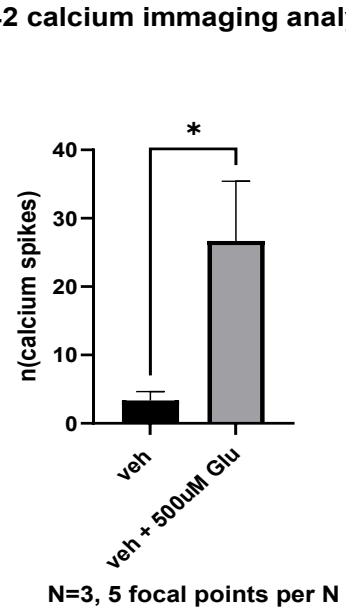

Figure 5.1: Number of normalised calcium spikes occurring in u3042 cells following vehicle and 500uM l-glutamate treatment. U3042 cells were plated on Geltrex in a 96 well plate with a starting seeding density of 40k/well, in U4 feeding media lacking glutamate and

growth factors. Following a 48h incubation period, the cells were stained with 1uM of cal-502. Following a 30min staining, the cells were placed within the opera phoenix and a baseline image was taken every 10s for the first 1min. The cells were then treated with (a) Vehicle and (b) 500 μM l-glutamate, and images were taken every 5s for a total of 5minutes. 5 focal points per well were imaged and each graphed. To note, each graph represents a separate well and each line represents a cell (c) The total number of calcium spikes per focal point were grouped per their appropriate condition. Statistical analysis was performed using an unpaired t-test ($p \leq 0.05$).Graph plotted as total number of spikes + SEM (N=3).

Data generated by me, graphs were created by Dr. Florian Siebzehnrubl

This data shows that following the addition of 500uM glutamate there is an increase in intracellular calcium compared to when treated with vehicle, glutamate free media.

5.2 Investigating which glutamatergic agonist increases calcium influx

Having established that 500uM of glutamate causes and increase in calcium flux compared to its vehicle, more specific glutamatergic agonists (AMPA, Kainic acid and NMDA) were tested using this assay in order to identify which glutamatergic receptor is most functionally active and therefore make a better therapeutic target.

5.2.1 AMPA

To test the AMPA receptor activity, a specific agonist for the AMPA receptor was used (S-AMPA). Here, 3 different concentrations of S-AMPA were used (using its EC_{50} concentration + 10-fold higher/lower), and their calcium spike profile was compared against the one of 500uM glutamate.

Fig. 5.2.1(a) shows the normalised calcium spikes present in each cell following the addition of glutamate. Here a strong increase in calcium spikes can be observed in well 2 and 3, where

the spike values reach 2.5 and 5.5 respectively. In all three wells, an instant increase in spike value is show at time point 60s which corresponds to the addition of glutamate.

Following the addition of 2uM of AMPA, Figure 5.2.1(b), the calcium spikes do not exceed a value of 1.4 and the spikes are not at their highest value straight after AMPA addition, this occurs between time point 120sec and 300sec. When adding 20uM (Fig. 5.2.1(c)), the calcium spike reaches a maximum of 4 and 5, for well 1 and 2 respectively. For well 2, the calcium spikes progressively increase following the addition of AMPA up until time point 300sec and then plateau. On the other hand well 3 does not have the same calcium trend, here, the values hover around 1. Lastly, Fig. 5.2.1(d) shows that well 1 and 2 do not respond to 200uM of AMPA, as the calcium spikes shown have a value lower than 1, similar to the baseline values. On the other hand, well 3 shows progressively increasing calcium spikes following AMPA, reaching a value of 3.

All this can be conceptually recapitulated in Fig. 5.2.1(e) where the number of cells which presented a calcium spike per condition was plotted. Here, 500uM glutamate causes the highest number of calcium spikes and the addition of increasing concentrations of AMPA correlated to an increase in calcium spikes. To note, the addition of 2uM AMPA is the only concentration which causes a significant decrease in calcium spikes compared to 500uM Glutamate.

Results

(a) glutamate 500uM

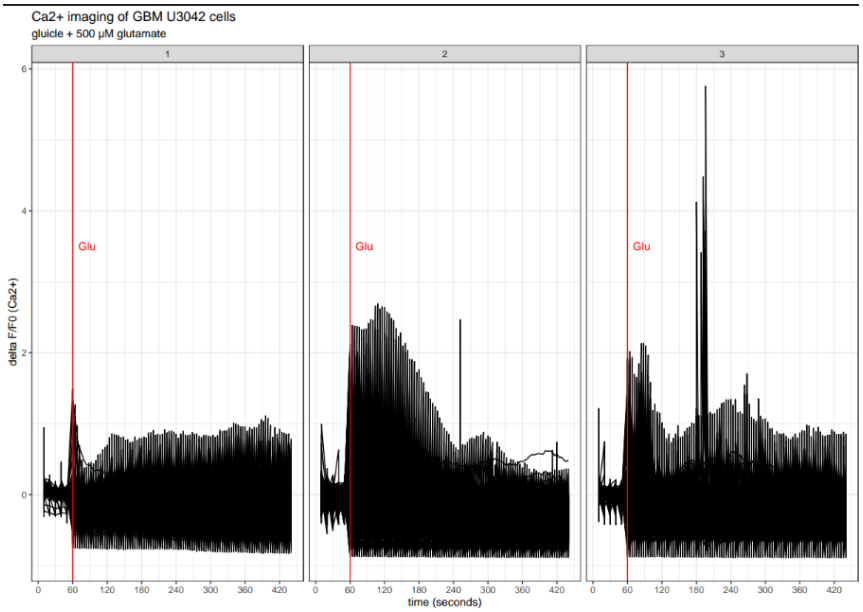

(b) AMPA 2uM

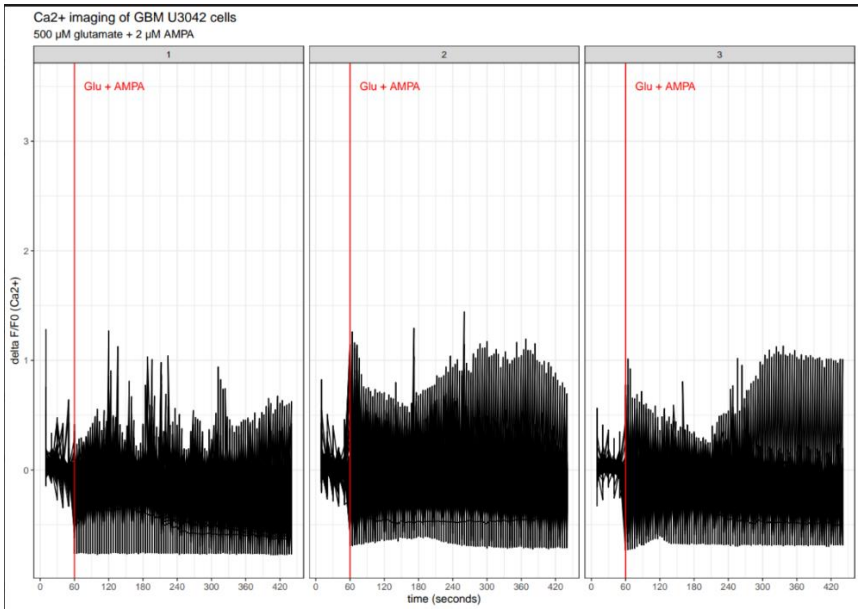

(c) AMPA 20uM

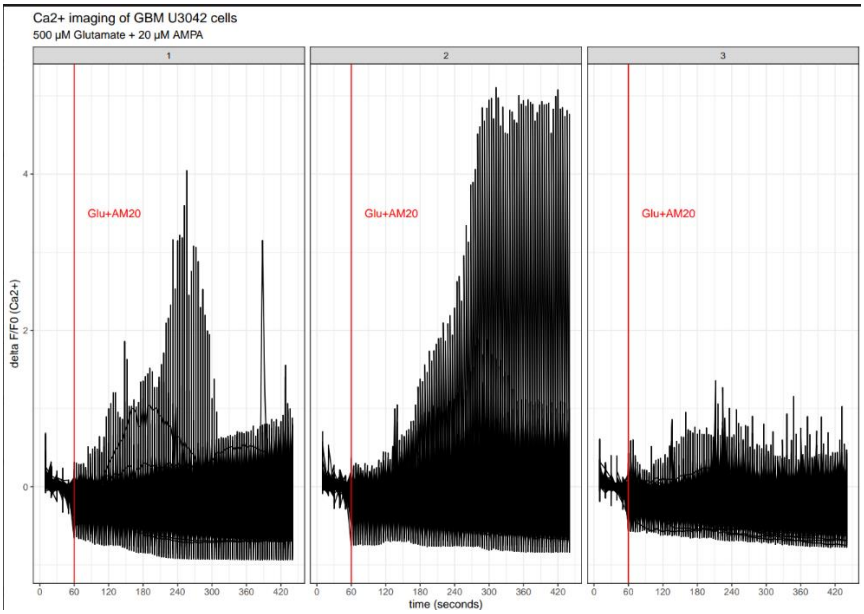

(d) AMPA 200uM

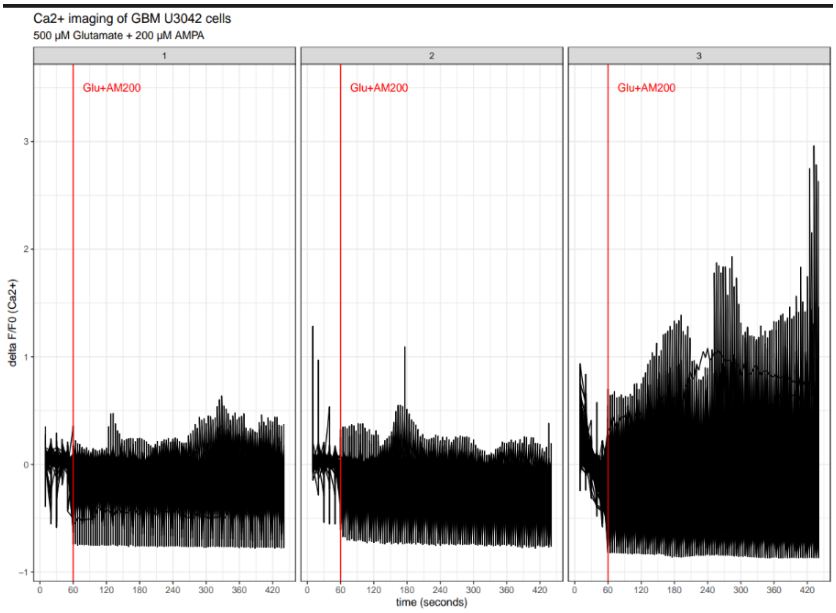

(e) calcium spikes per condition

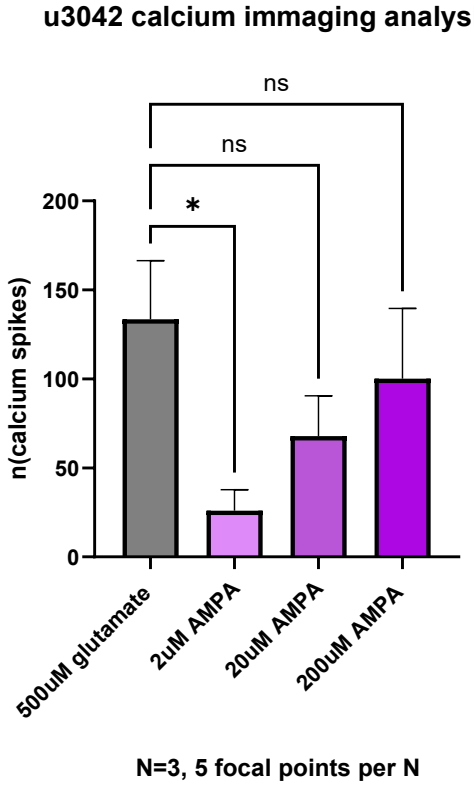

Figure 5.2.1: Number of normalised calcium spikes occurring in u3042 cells following 500uM l-glutamate and AMPA treatment. U3042 cells were plated on Geltrex in a 96 well plate with a starting seeding density of 40k/well, in U4 feeding media lacking glutamate and growth factors. Following a 48h incubation period, the cells were stained with 1uM of cal-502. Following a 30min staining, the cells were placed within the opera phoenix and a baseline image was taken every 10s for the first 1min. The cells were then treated with (a) 500uM glutamate (b) 2uM s-AMPA, (c) 20uM s-AMPA, (d) 200uM s-AMPA, and images were taken every 5s for a total of 5minutes. 5 focal points per well were imaged and each graphed. To note, each graph represents a separate well and each line represents a cell. (e) The total number of calcium spikes per focal point were grouped per their appropriate condition. Graph plotted as mean + SEM. Statistical analysis was performed using a 1-way non-parametric ANOVA ($p \leq 0.05$). Graph plotted as total number of spikes per well + SEM (N=3).

Data generated by me, graphs were created by Dr. Florian Siebzehnrubl

This data shows that S-AMPA can cause the same intracellular calcium influx as 500uM glutamate, when 20 and 200uM are used. When the cells are treated with 2uM of AMPA, the calcium response is significantly weaker.

5.2.2 Kainic acid

To test the Kiante receptor activity, a specific agonist for this receptor was used. Here, 3 different concentrations of Kainic acid were used, and their calcium spike profile was compared against the one of 500uM glutamate.

Fig. 5.2.2(a) shows the normalised calcium spikes present in each cell following the addition of glutamate. Here a weak increase in calcium spikes can be observed in well 1 and well 3, where the spike values reach a max value of 1.5. On the other hand, well 2 did not responds to glutamate stimulation as the calcium spike reported is similar to the baseline.

Fig.5.2.2(b) shows that 5uM Kainic acid does not cause an increase in calcium spikes. This is because in all three well, following stimulation the spike value is lower than 1. Fig.5.2.2(c) reports what seen with 5uM kainic. On the other hand, when the cells are treated with 500uM Kainic acid Fig.5.2.2(d), the cells responded and an increase in intracellular spikes is shown as the values reported are between 1 and 2.5. Lastly, all this can be conceptually recapitulated in Fig. 5.2.2(e) where the number of cells which presented a calcium spike per condition was plotted. Here, no significance was observed conditions.

<u>Results:</u>

(a) 500uM glutamate

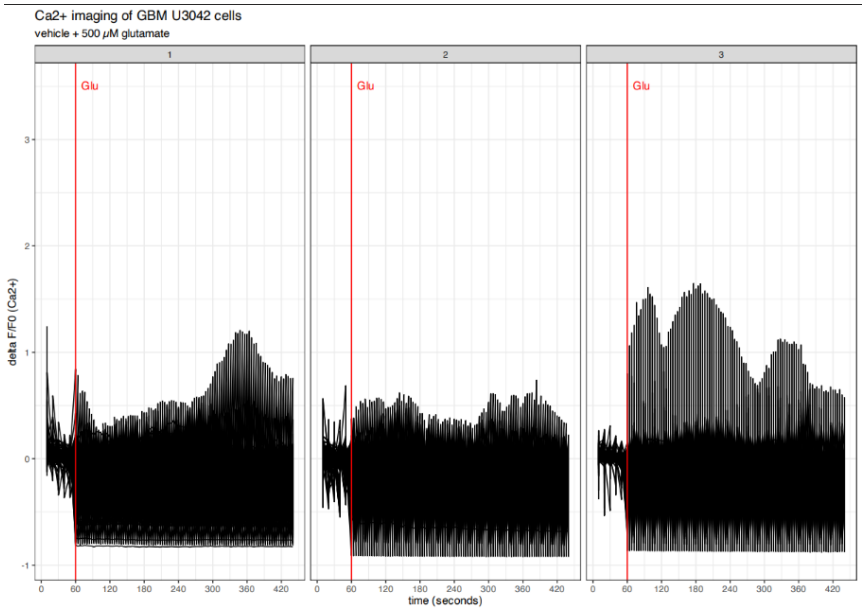

(b) 5uM Kainic acid

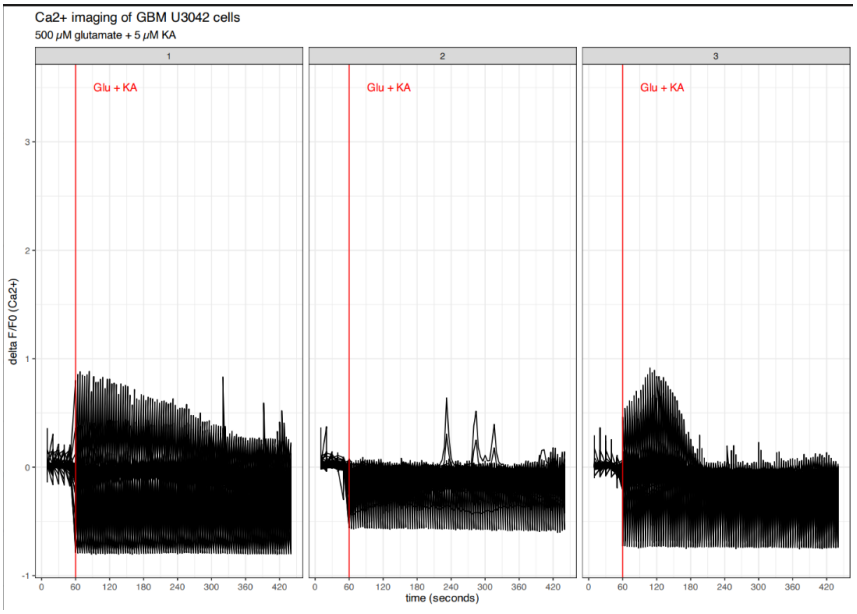

(c) 50uM Kainic acid

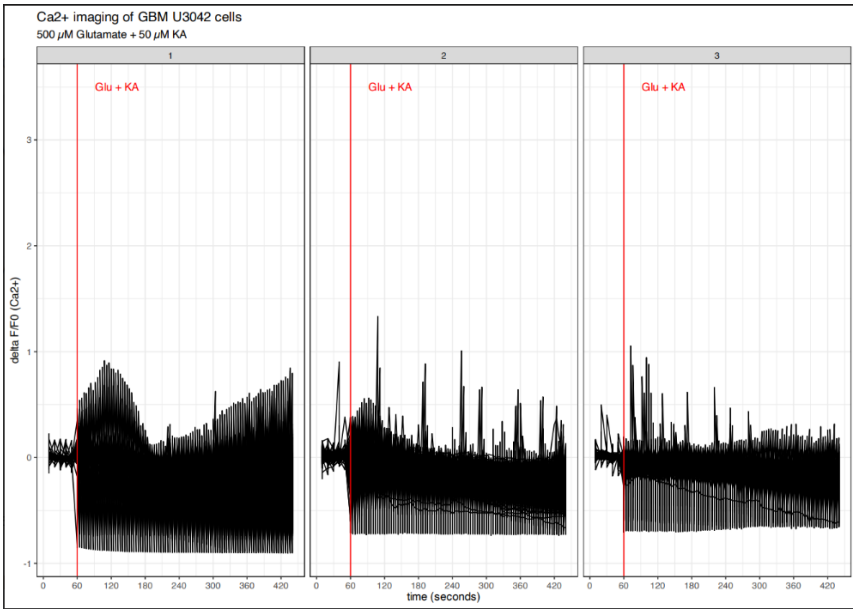

(d) 500uM Kainic acid

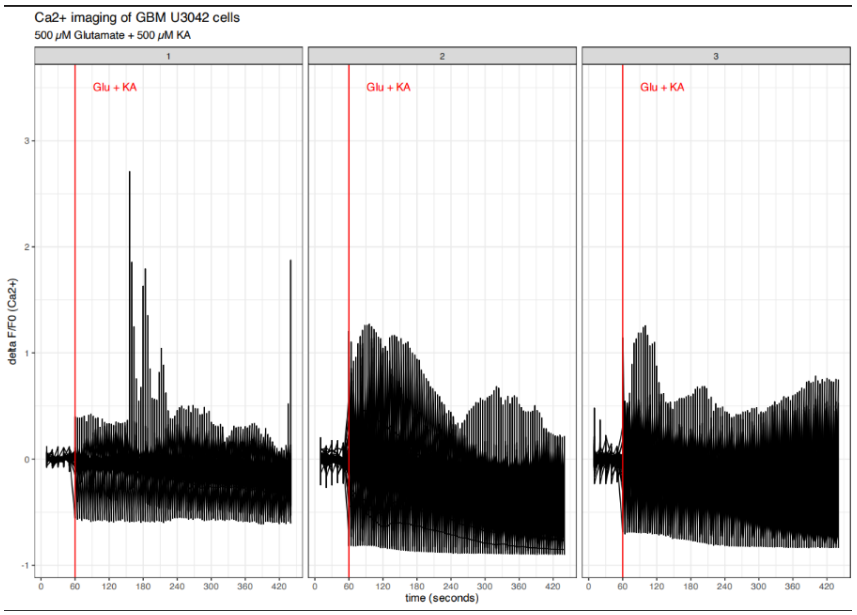

(e) Calcium spikes per condition

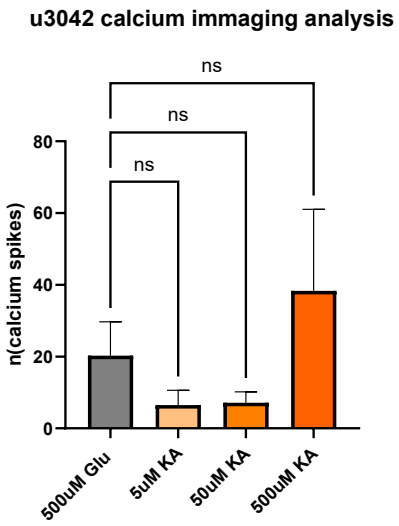

Figure 5.2.2: Number of normalised calcium spikes occurring in u3042 cells following 500uM l-glutamate and Kainic acid treatment U3042 cells were plated on Geltrex in a 96 well plate with a starting seeding density of 40k/well, in U4 feeding media lacking glutamate and growth factors. Following a 48h incubation period, the cells were stained with 1uM of cal-502. Following a 30min staining, the cells were placed within the opera phoenix and a baseline image was taken every 10s for the first 1min. The cells were then treated with (a) 500uM glutamate (b) 5uM KA, (c) 50 uM KA, (d) 500uM KA, and images were taken every 5s for a total of 5minutes. 5 focal points per well were imaged and each graphed. To note, each graph represents a separate well and each line represents a cell. (e) The total number of calcium spikes per focal point were grouped per their appropriate condition. Graph plotted as mean + SEM. Statistical analysis was performed using a 1-way non-parametric ANOVA (p≤0.05). Graph plotted as total number of spikes per well + SEM (N=3).

Data generated by me, graphs were created by Dr. Florian Siebzehnrubl

This data shows Kainic acid presents the ability to induce intracellular calcium fluctuations to the same extent as 500uM Glutamate.

5.2.3 NMDA

To test the NMDA receptor activity, a specific agonist for this receptor was used. Here, 3 different concentrations of NMDA were used, and their calcium spike profile was compared against the one of 500uM glutamate.

Fig. 5.2.3.1(a) shows the normalised calcium spikes present in each cell following the addition of glutamate. Here a weak increase in calcium spikes can be observed in well 1, where the spike values reach a max value of 3. Here, the calcium spikes increase following the addition of glutamate. On the other hand, well 2 did not responds to glutamate stimulation in the same way as the calcium spike reported are much lower, approximately 1.

Figure 5.2.3(b) shows the normalised calcium spikes present in each cell following the addition of 50uM NMDA. Here, well 1 shows a distinctive phenomenon, with calcium spikes generated at random time points throughout the 9 minutes. To note, no calcium spikes are present up until 1 min following NMDA stimulation. Although well 2 presents a much lower calcium spike activity to well 1, it presents a similar waiting period of spike post NMDA activation.

Figure 5.2.3(c) shows that there is a difference between the number of spikes generated with 500uM Glu compared to 50uM NMDA. Significance cannot be determined due to lack of repeats.

<u>Results:</u>

(a) 500uM glutamate

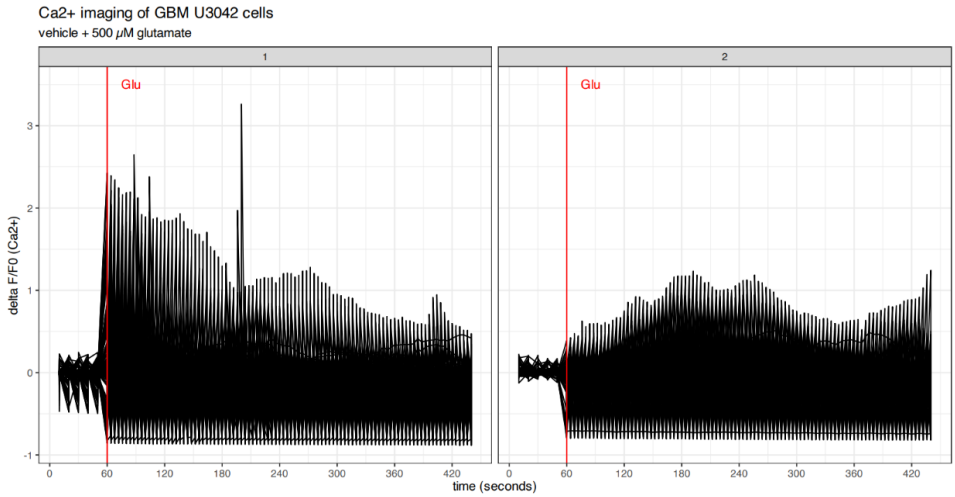

(b) 50uM NMDA

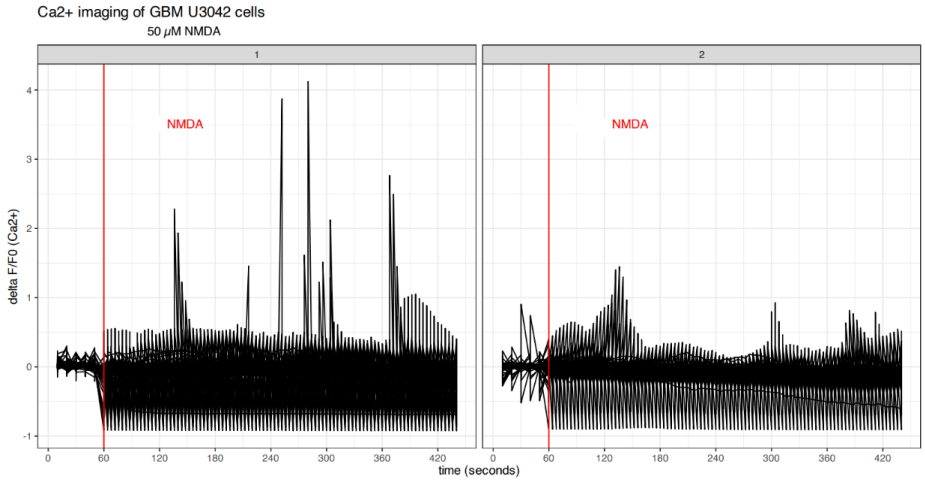

(c) Calcium spikes per condition

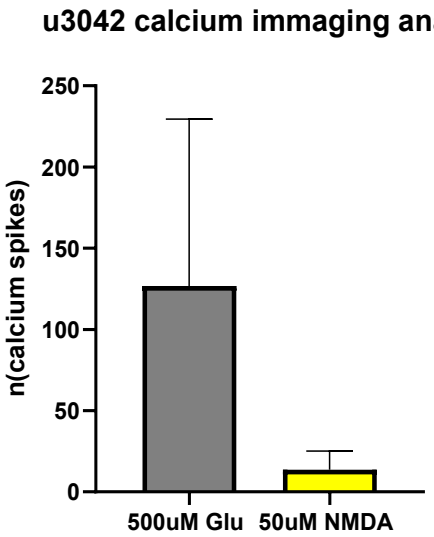

Figure 5.2.3: Number of normalised calcium spikes occurring in u3042 cells following 500uM l-glutamate and NMDA treatment U3042 cells were plated on Geltrex in a 96 well plate with a starting seeding density of 40k/well, in U4 feeding media lacking glutamate and growth factors. Following a 48h incubation period, the cells were stained with 1uM of cal-502. Following a 30min staining, the cells were placed within the opera phoenix and a baseline image was taken every 10s for the first 1min. The cells were then treated with (a) 500uM glutamate (b)50uM NMDA, and images were taken every 5s for a total of 5minutes. 5 focal points per well were imaged and each graphed. To note, each graph represents a separate well and each line represents a cell. (e) The total number of calcium spikes per focal point were grouped per their appropriate condition. Graph plotted as total number of spikes per well + SEM (N=2).

Data generated by me, graphs were created by Dr. Florian Siebzehnrubl

This data suggests NMDA does not presents the ability to induce intracellular calcium fluctuations to the same extent as 500uM Glutamate.

5.3 Investigating whether anti-glutamatergic drugs counteract calcium influx

Having identified that both AMPA and Kainic acid is capable of activating the glutamatergic receptor to the same extent of 500uM glutamate, the next step was to determine which specific glutamatergic receptor antagonists counteracts this effect.

Fig. 3.3.1a shows the normalised calcium spikes present in each cell following the addition of 500uM glutamate. Here, the calcium spikes increase following the addition of glutamate, reaching a max value of 3 and 8, for well 1, 2 and 3, respectively. Following the addition of 20uM CNQX, the glutamate response is significantly dampened (Fig. 3.3.1b). This is because, the calcium spike values are all bellow the value of 1, to the exception of well 3, where the value following treatment reaches 1.5. Following the addition of 10uM Perampanel, the glutamate response is also significantly dampened (Fig. 3.3.1c). Here too, the calcium spike values are all bellow the value of 1, to the exception of well 3, where the value following treatment reaches 3.5. The calcium spike profile following the addition of UBP-302 shows that intracellular calcium spikes occur, especially in well 1 and 2, where their value reach 2 (Fig.3.3.1d). Lastly, figure 3.3.1e shows that Ketamine does not counteract the calcium spikes generated by 500uM of glutamate. This is because these cells show high calcium spikes reaching values of 3.

All this can be conceptually recapitulated in figure 3.3(f) where the number of cells which presented a calcium spike per condition was plotted. Here, 500uM glutamate causes the highest number of calcium spikes and that the addition of CNQX and Perampanel glutamatergic antagonists cause a significant decrease in intracellular calcium. UBP-302 also causes a significant decrease in intracellular calcium spike, although to a lower degree than CNQX and Perampanel. On the other hand, Ketamine does not inhibit glutamate effects, as its calcium spike profile is shown to be similar to the glutamate only profile, and determined as non-significant.

Results

(a) 500uM Glutamate

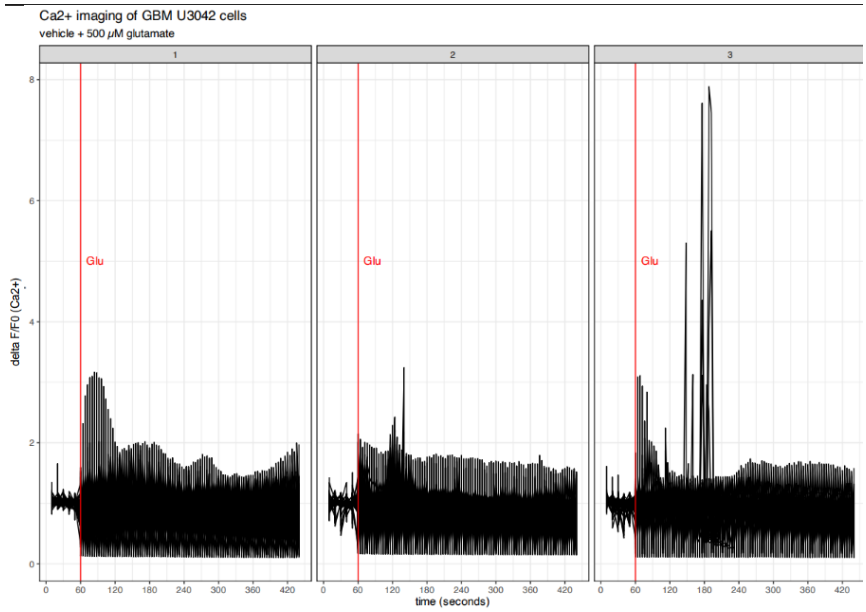

(b) 20uM CNQX

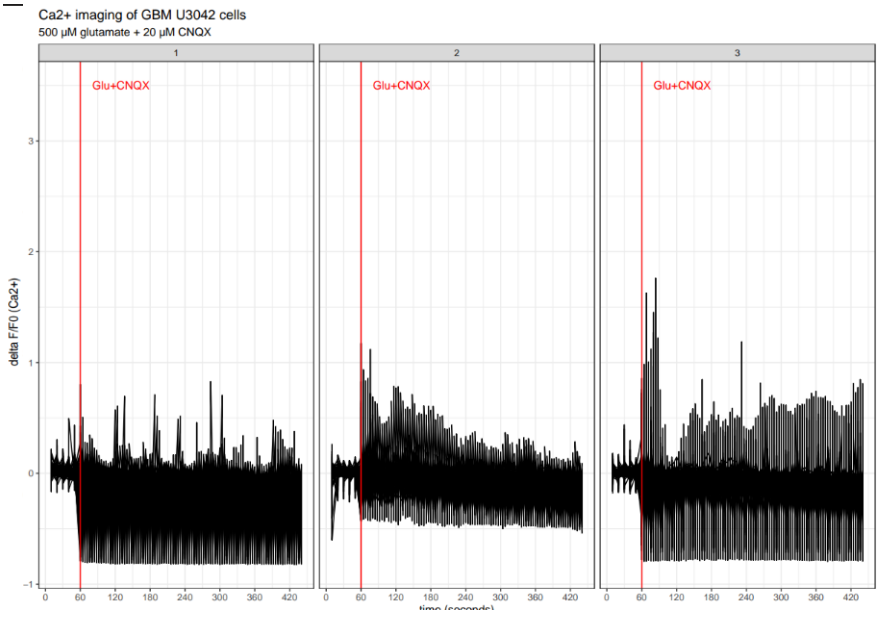

(c) 10uM Perampanel

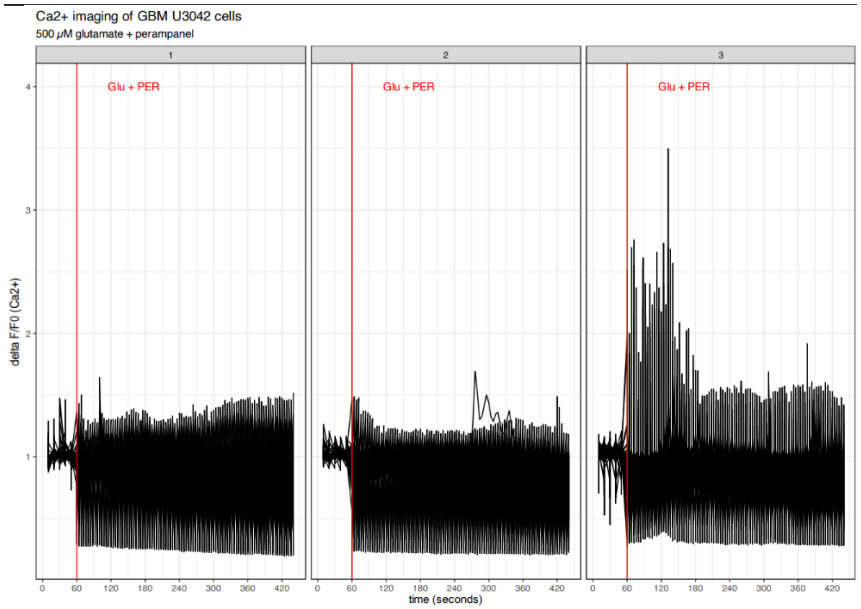

(d) 5uM UBP-302

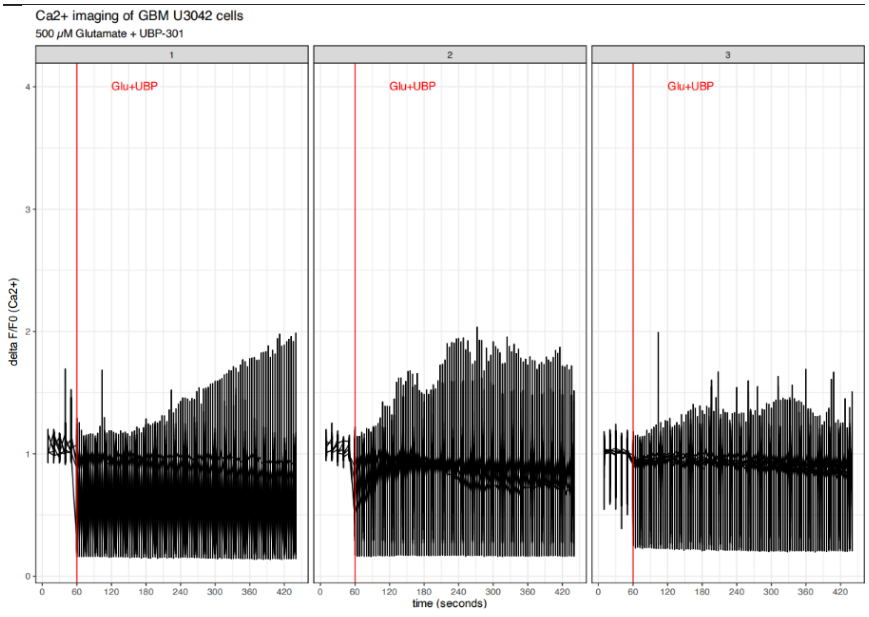

(e) 20uM Ketamine

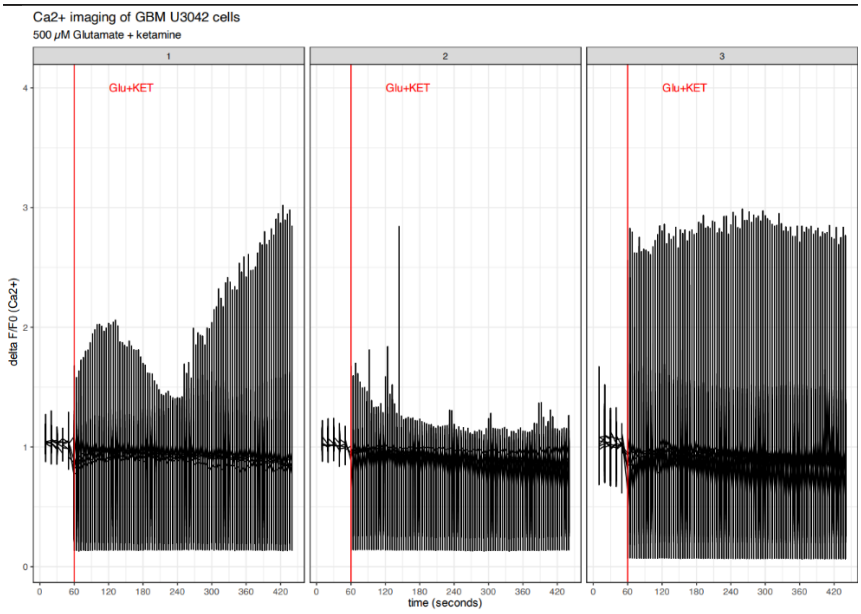

(f) Calcium spikes per condition

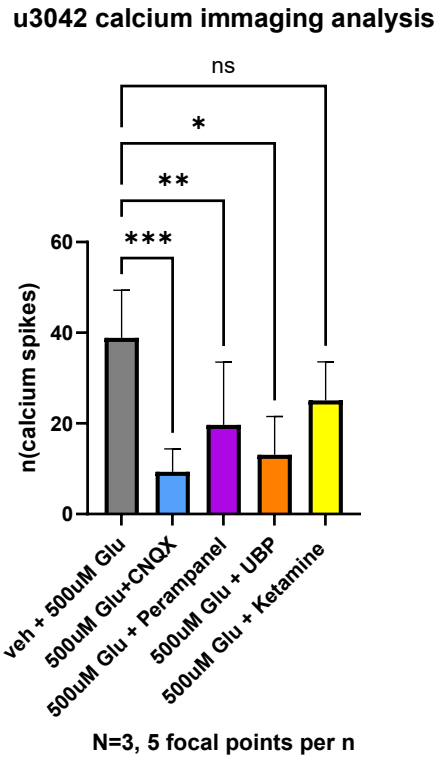

Figure 5.3.1: Number of normalised calcium spikes occurring in u3042 cells following 500uM l-glutamate treatment in the presence of glutamatergic antagonists. U3042 cells

were plated on Geltrex in a 96 well plate with a starting seeding density of 40k/well, in U4 feeding media lacking glutamate and growth factors. Following a 48h incubation period, the cells were stained with 1uM of cal-502. Following a 30min staining, the cells were placed within the opera phoenix and a baseline image was taken every 10s for the first 1min. The cells were then treated with (a) Vehicle + 500 μM l-glutamate (b) 20uM CNQX +500 μM l-glutamate (c) 10uM Perampanel 500 μM l-glutamate (d) 5μM UBP-302 + 500 μM l-glutamate and (e) 20uM Ketamine + 500 μM l-glutamate, and images were taken every 4s for a total of 5minutes. 5 focal points per well were imaged and each graphed. To note, each graph represents a separate well and each line represents a cell (f) The total number of calcium spikes per focal point were grouped per their appropriate condition. Graph plotted as total number of spikes per well + SEM. Statistical analysis was performed using a 1-way non-parametric ANOVA ($p \leq 0.05$) (N=3).

Data generated by me, graphs were created by Dr. Florian Siebzehnrubl

This data shows that CNQX is capable of significantly reducing the number of calcium spikes generated following the addition of 500uM glutamate. This decrease is also seen following the addition of Perampanel and UBP-302. On the other hand, Ketamine does not reduce the number of calcium spikes causes by glutamate.

Conclusion:

As only U3042 was shown to responded to 500uM of glutamate previously, this is the only cell line that was used in this chapter. Here, intracellular calcium flux was chosen as the experimental end-point and was shown to be significantly increased following glutamate treatment compared to glutamate-free media. Moreover, when treating the cells with S-AMPA and Kainic acid, the intracellular calcium flux was of comparable values to when treated with glutamate, suggesting that glutamate responds by activating the AMPA and Kainate receptor. This is consistent with what seen in chapter 1 as U3042 expressed AMPA and Kainate subunits at high values. This is also consistent with the data acquired following treatment with glutamate + antagonist, as Perampanel (a specific AMPA blocker) and UBP-302 (a specific Kainic acid blocker) caused the most significant intracellular calcium decrease to the exception of CNQX, with targets all three glutamatergic receptors. NMDA on the other hand does not generate the same number of calcium spikes causes by glutamate, which once again is in line with what observed following qPCR analysis. In line with this, Ketamine (a NMDA blocker) did not inhibit the calcium influx generated by glutamate.

This preliminary data suggests that CNQX Perampanel and UBP-302 are involved in supressing glutamate's calcium signal in U3042 and that novel therapeutics could target the glutamatergic pathway using these antagonists. It is pivotal to note that this effect has only been tested on U3042 and needs to be explored in other GBM lines which present high glutamatergic receptors. Furthermore, this experimental method is 2D, future experiments should involve the use of organoids or be performed in-vivo.

Chapter 6: Discussion

Glioblastoma is an aggressive brain tumour which affects around 3,200 new patients each year in the UK (7) (6). Despite this, there are no FDA approved targeted therapeutics for GBM. Recent studies have highlighted a new role for glutamate in the proliferation and migration of this disease (56) (52). For this reason, this study focused on elucidating the molecular and functional role of glutamate in GBM progression and determine whether glutamatergic ionotropic receptors make good therapeutic targets. Furthermore, this study also investigated whether negative allosteric modulators of glutamatergic ionotropic receptors could be used to inhibit cancer progression.

The current literature surrounding the glutamatergic receptor expression in GBM is limited and is mostly based on the RNA-seq data acquired in single GBM cells. Here, *Venkataramani et al* showed that AMPARs were the most robustly expressed receptors with GRIA2 and GRIA3 being most highly expressed, followed by Kainate being expressed at approximately half the rate of AMPAR and lastly NMDA, which are barely expressed (56). In line with this, a GBM single-cell transcriptomic study by *Venkatesh et al* also reviled that NMDA receptor subunits are not highly expressed compared to the GRIA and GRIK subunits (65). Moreover, by exploring the glutamatergic receptor

expression in GBM following RT-PCR, *Stepulak et al*, showed that U87-MG and U343 (two glioma cell lines) presented all three ionotropic receptors. Contrastingly, this data revealed that U343 expresses the NMDA receptor subunits at a higher level to AMPAR (66).

To further contribute to the GBM glutamatergic receptor expression knowledge, this study involved performing qPCR on the mRNA of 3 distinct GBM cell lines: U3019, U3042 and L2. These cell lines were chosen as they were readily available in the lab and are derived from GBM patients. U3042 and U3019 were also chosen on the basis of their glutamatergic receptor subunit Z-score, found utilizing the human glioblastoma cell culture resource (HGCC, biobank) with the intent of having a highly receptor expressing cell line (U3042) and a lesser expressing one to use as a negative control (U3019). Following qPCR, a distinct expression pattern for each 3 cell lines was observed with AMPA receptor subunits being most readily expressed across all lines, heightened for U3042. This data also reviled that GRIA2 is the most expressed receptor subunit for both U3019 and U3042, which contradicts what observed by *S. Ishiuchi et al.* as GRIA1 and GRIA4 were shown to be expressed at a higher rate than GRIA2 in their primary GBM cell cultured lines (48). Furthermore, other studies have also reported GRIA2 being poorly represented, an expected result as GRIA2 is calcium im-permeable thus making it an unfavourable tumour promoting property (63).

This current study results also reveals high receptor expression for the Kainate subunits in L2 and U3042, compared to U3019 and reviles that all cell lines presented a low expression of NMDA receptor subunits. To note, all three cell lines express the GRIK2 and GRIK3 receptor subunits at the same levels and at a higher level compared to GRIK1,4 and 5. This heightened expression for GRIK2 and 3 is also observed by *Venkatesh et al (65).* To the best of my knowledge reasons regarding this have yet not been explored, but according to this data they may present some viable tumour promoting properties.

As GBM is an astrocytoma, this study focused on comparing the receptor subunit expression of the three GBM lines to the level of normal human astrocytes. To note, it is reported that astrocytes present glutamatergic receptor subunits with different expression patterns depending on the developmental stage they are in and in which

brain region they reside (67) (68). Cerebral cortical human derived Astrocytes have been shown to present high expression levels of GluA2 (GRIA2), with GRIA1 and GRIA4 transcripts being present a significantly lower level (69). The Kainate receptor is less studied in astrocytes, yet the rodent cortex was shown to express the GRIK2 and GRIK4 subunits at higher levels than the rest (67).Lastly, the presence of NMDA receptors in human primary astrocytes was confirmed by *Ming-Chak Lee et al*. as their qPCR analysis reviled that both adult and fatal human primary astrocytes express GluN1, Glun2A-D and GluN3A-B (70).

In this current study, all glutamatergic receptor subunits were expressed in normal human astrocytes. By then comparing the gene expression analysis of ionotropic receptors between HA and GBM, the data reviled that most receptor subunits were expressed at a higher level in GBM. This suggests that the tumour alters its receptor expression to enhance growth and migration through glutamate activation. Moreover, GRIA2/3 and GRIK3/4 were significantly higher expressed in both U3019 and U3042 GBM, compared to NHA, thus making these receptor subunits a potential therapeutic target. In agreement with increased GRIA2/3, *Piao et al*. showed that there is direct correlation between the expression of AMPARs and the level of GBM cell migration both *in-vivo* and *in-vitro* (71)

Lastly, to verify these qPCR results, expression analysis of GRIA1-3 and GRIK1-3 proteins were carried out in both the GBM lines and in NHA. This data shows that AMPA1 is expressed in all the different cell lines with a visually different intensity. Here, U3042 presents the strongest band whilst U3019 shows the lowest, which nicely recapitulates what shown in the previous qPCR data. On the other hand, AMPA2 is only shown to be present in L2, contradicting what previously shown via qPCR. To note, as both U3019 and U3042 were shown to lack the expression of this receptor subunit, it presents favourable tumour progression properties as GluA2 is calcium impermeable (43). The expression levels of AMPA3 also recapitulates what previously observed in the qPCR data as all three GBM lines expressed that protein whilst NHA does not. By then focusing on the expression levels of GRIK1-3 we can see that the tumour cell lines present a higher intensity band for each protein compared to NHA. Once again, this

aligns with the qPCR data collected in this study confirming that GRIK1-3 are expressed at a higher level in U3019, U3042 and L2 GBM lines compared to NHA.

It is important to note that all the glutamatergic receptor proteins probed for in this study present a molecular weight of approximately 100 kDA. This does not align with the western blots for GRIA1-3, and only partially aligns the other three GRIK proteins. A range of bands of different molecular weights can be observed, which can be related to post translational modifications (PTM). An example of PTM is phosphorylation and it presents a molecular weight of 94 kDA. As GRIA1-3 are shown to present a molecular weight of approximately 190 kDa in my western blots, this hypothesis fits nicely. Moreover, the literature reports on the phosphorylation of AMPA subunits once activated (72). To verify this, an experiment can be repeated using phospho-specific antibodies to detect this. Alternatively phosphatases can be added to the sample prior to loading in order to cleave the phosphate group. Looking at GRIK2 and 3, one can also observe multiple bands indicating that various different PTM might have occurred.

Although this study shows that AMPA and Kainate receptors are more highly present in GBM compared to NHA, it is key to point out the limitations surrounding these results. In regards to the qPCR data, the primers used were commercially available and may not pick up every single receptor subunit isoform present or could have led to non-specific amplification. In addition, qPCR measures the gene expression by quantifying the levels of mRNA present in the sample, and as shown in this experiment does not truly recapitulate with protein expression. On the other hand, western blots present the issue of antibody leading to nonspecific binding, thus showing a false positive.

Having determined a different expression of glutamatergic receptors for U3019, U3042 and L2, the next step in this current project was to determine whether their expression levels correlate with distinctive molecular and functional GBM progression properties. This was examined as glutamate receptor activation is known to activate the PI3K and MAPK pathways in order to lead to cellular proliferation (73). In line with this, S. Ishiuchi et al, showed that GBM cultured cells over-expressing calcium permeable AMPAs often were found as elongated fusiform cells presenting long processes, and were capable of proliferating a at high rate than GBM cells overexpressing calcium impermeable AMPAR. This proliferative phenomenon was then validated by KI-67 staining which confirmed

that GBM cells overexpressing calcium permeable AMPAR had a significantly higher % of KI-67 positive cells compared to GluR2 over-expressing GBM cells (74). Moreover, the role of ionotropic glutamate receptors in tumour progression is also studied by *Venkatramani et al*. Here, they observe that glutamate output is related to tumour progression and migration, and that the use of glutamatergic antagonist CNQX is capable of allowing S24 glioma cells to grow at a more slower rate (56).

In this current study, it was determined that only U3042 was capable of promoting tumour proliferation following stimulation with glutamate following Cell titre glow and Ki-67 experiments, which was expected the qPCR and western blot data showed higher levels of glutamatergic receptors compared to U3019. To note, although experiments were performed with a range of different glutamate concentrations, U3042 only responded to 500uM, which is in line with the levels of glutamate in the brain present in GBM patients (63). Moreover, this data also aligns with what shown *Venkataramani et al* as 500uM glutamate causes a luminescence increase on S24 monoculture (56). Furthermore, this proliferative effect shown in U3042 following Cell-titre glow was confirmed and enhanced when staining the cells for Ki-67, a general proliferative marker (75).

To note, Cell titre glow reports on the metabolic activity of cells rather than a direct proliferative readout, yet this method is accepted as a mean of studying cellular growth and various studies have previously used it (56) (76) (77). Contrastingly, U3042 did not reveal any cellular growth following 500uM glutamate when using Incucyte imaging software. This said, the data might have been skewed due to a limited area of imaging, glutamate causing a change in cellular spreading rather than growth or by un-even cellular plating. In order to study GBM proliferation using the Incucyte machine, these cells should be fluorescently labelled using GFP, and the fluorescence intensity over time can be monitored. In addition, other general studies to investigate whether proliferation occurs via the direct activation of glutamatergic receptors could involve the usage of sh-RNA to dampen these receptors expressions or performing gene editing techniques such as crisper-cas9 to fully delete the AMPA, Kainic acid and NMDA receptors, as performed by *C. Jiang et al* (78).

Having shown that U3042 responds to 500uM glutamate, the next step was to try and counteract this effect through the addition of specific glutamatergic antagonists. The current literature surrounding this concept has reported both CNQX and Perampanel to present as anti-tumour activity as CNQX was capable of significant decrease in proliferation the GBM cells whilst Perampanel was able to induce apoptosis in GBM lines (56) (79). In this current study following antagonist treatment the cells were stained for Ki-67, and revealed that the percentage of Ki-67 positive cells did not decrease compared to glutamate treatment only. This data suggest that CNQX, Perampanel and UBP-302 at their EC_{50} concentration are ineffective as anti-GBM treatment, contradicting the current literature (56). An explanation as to why an anti-proliferative response was not seen can be linked to the cells being treated as a mono-culture. Previous experiments have shown that for CNQX treatment to show a significant decrease in proliferation the GBM cells must be co-cultured with neurons (56). There is currently no insight into why this is the case, although one could speculate that the neurogliomal synapse is required for the glutamatergic receptors to be expressed on the post synaptic GBM membrane.

As a co-culture model was un-available, I sought to examine the functional aspect of glutamatergic receptor antagonists on U3042, by examining the levels of intracellular calcium flux using the Cal-520 dye. Calcium was chosen as it is an important secondary messenger following glutamatergic receptor activation (67). To note, this assay end point was chosen as several different labs have used it to and reported it to produce viable cell results. For example, *Y. Kudo et al* showed that glutamate was capable of inducing a dose-dependent elevation in intracellular calcium in rat individual hippocampal neurons (80). NMDA and Kainate were also shown to increase intracellular calcium levels, suggesting that all glutamatergic receptor subunits are activated (80) (81).

This current study sought to analyse the intracellular calcium response in U3042 following glutamate stimulation. Here, a significant increase in intracellular calcium influx was observed following the addition of glutamate compared to the vehicle, which is comparable to what know in the literature. To then investigate which specific receptor glutamate acted upon, s-AMPA, kainic acid and NMDA (specific glutamatergic agonists)

were investigated. Here, when treating the cells with 20 and 200uM s-AMPA, no statistically significant change was observed compared to glutamate, thus indicating glutamate activates the AMPA receptor. This observation in supported by the qPCR data showing AMPA receptors are the most robustly expressed. Moreover, aligns with the results of *Ishiuchi et at.,* as they show that the addition of 200uM AMPA (together with 100Um Cyclothiazide) increases intracellular calcium in cultured GBM cells. When treating U3042 with Kainic acid, all three different concentrations did not cause a significant difference compared to 500uM glutamate. This data suggests that Kainic acid also activates the glutamate receptor, although it is key to highlight that the cells were shown to not respond to glutamate as strongly in this experiment as all my other indicating that this experiment should be repeated for a more definitive answer. Moreover, it is imperative to note that the Kainate receptor is not permeable to Ca2+ , its only permeable to Na+ and K+ (67). Because of this, we can hypothesise that the stimulation of Kainic acid might also activate the AMPA receptor, or that an entirely different process is being activated for the observed effect of increased intracellular Ca2+ fluctuations. Unfortunately, due to lack of time in the lab, experiments determining the effect of NMDA on intracellular calcium flux were only performed using its EC50 concentration. This preliminary data reveals that NMDA is not capable of causing calcium spikes, suggesting that the NMDA receptor subunit is not involved in calcium influx. This is in agreement with the qPCR data acquired in this study.

Having determined the role of glutamate, AMPA and Kainic acid in promoting intracellular calcium flux in U3042, the next step was to investigate whether glutamatergic antagonist would counter act this effect. As predicted via the qPCR data, CNQX and Perampanel caused a significant decrease in intracellular calcium flux, as their receptor expression is high. UBP-302 also caused a significant decrease in intracellular calcium influx which raises the question as to whether there is some other molecular interaction occurring at the same time as UBP-302 is a potent and selective antagonist of GluK1.

Lastly, Ketamine did not show any ability in counteracting glutamate's effects. This result is in line with the qPCR studies and literature surrounding GBM cells, indicating that the NMDA receptor is not highly present. Although this study shows glutamate,

AMPA and Kainic acid promoting intracellular calcium flux and glutamatergic antagonists are capable of blocking this at their EC50 concentration, there are a few study limitations that need to be considered. Firstly, in order for these results to be validated, repeats need to be made. Due to lack of time, each calcium experiment was only performed once. Furthermore, this experimental concept should be repeated using patch clamp too see whether glutamate increases the intracellular calcium current and whether the various different antagonists counteract this. Moreover, this study does not account for the calcium that enters via the various transient receptor potential channels and calcium ion exchanger (82). This study also doesn't confirm where this calcium is coming from the extracellular space or is released internally form the ER. In order to test the latter statement, various calcium inhibitors can be used targeting channels present on the plasma membrane and/or the ER.

As glutamate has been shown to play a proliferative role in GBM cells, in order to take this project forwards one could repeat the experiment utilising the glutamatergic antagonists in a co-culture model as per Venkatramani's protocol (56). Furthermore, as these experiments were performed in a 2D culture, they do not fully recapitulate what occurs in patient as these lack physiological complexity and are under artificial culture conditions. This means that 2D models fail to recapitulate the cells TME where complex interplay between extracellular components/immune factors reside whilst also evade any mechanical forces or nutrients strains our cells undergo on a daily basis. Because of this, more suitable model would be a 3D organoid model with GBM cells incorporated into it or take this experiment in-vivo. In the event glutamate antagonists show promising results in all these assays, the antagonists used in this study stand a strong change of being tested clinically and be used in combination of current GBM treatment. To note, here a suitable delivery system (such as a viral vector targeted to GBM specifically) must be considered as glutamate is vital for CNS communications. It is thus imperative these antagonist will only inhibits GMB's signalling.

To conclude, this study has highlighted that U3042 exhibits higher expression of AMPA and Kainate receptor subunits expression compared to U3019 and L2. Furthermore, it highlights that GRIA2/3 and GRIK3/4 are highly expressed GBM receptors compared to astrocytes and thus makes them a potential therapeutic target. Moreover, on a more

functional aspect, this study has highlighted the role of 500uM glutamate in promoting cellular proliferation and calcium fluctuations in U3042. Lastly, we have shown that calcium fluctuations caused by glutamate can be counteracted by antagonists such as CNQX, Perampanel and UBP302. Overall this study has provided an initial insight into the role of glutamate in glioblastoma progression and following further research, I hope these glutamatergic antagonists will make it into the clinic and ameliorate patients' lives.

References:

1. Brown JS, Amend SR, Austin RH, Gatenby RA, Hammarlund EU, Pienta KJ. Updating the Definition of Cancer. Mol Cancer Res. 2023;21(11):1142-7. doi: 10.1158/1541-7786.Mcr-23-0411

2. UK Cr. Types of Cancer. 2024 [accessed. Available from: https://www.cancerresearchuk.org/about-cancer/what-is-cancer/how-cancer-starts/types-of-cancer

3. Sontheimer H. A role for glutamate in growth and invasion of primary brain tumors. Journal of Neurochemistry. 2008;105(2):287-95. Available from: https://onlinelibrary.wiley.com/doi/abs/10.1111/j.1471-4159.2008.05301.xdoi: https://doi.org/10.1111/j.1471-4159.2008.05301.x
4. Mesfin FB, Karsonovich T, Al-Dhahir MA. Gliomas. In: StatPearls. Treasure Island (FL): StatPearls Publishing

5. Kapoor M, Gupta V. Astrocytoma. In: StatPearls. Treasure Island (FL): StatPearls Publishing

6. Wirsching HG, Galanis E, Weller M. Glioblastoma. Handb Clin Neurol. 2016;134:381-97. doi: 10.1016/b978-0-12-802997-8.00023-2
7. Louis DN, Perry A, Wesseling P, Brat DJ, Cree IA, Figarella-Branger D, et al. The 2021 WHO Classification of Tumors of the Central Nervous System: a summary. Neuro Oncol. 2021;23(8):1231-51. doi: 10.1093/neuonc/noab106
8. Brennan C. What is astrocytoma, and how is it different from glioblastoma? 2024 [accessed. Available from: https://www.mdanderson.org/cancerwise/what-is-astrocytoma--and-how-is-it-different-from-glioblastoma.h00-159694389.html
9. Fernandes RT, Teixeira GR, Mamere EC, Bandeira GA, Mamere AE. The 2021 World Health Organization classification of gliomas: an imaging approach. Radiol Bras. 2023;56(3):157-61. doi: 10.1590/0100-3984.2022.0089-en
10. Hanif F, Muzaffar K, Perveen K, Malhi SM, Simjee Sh U. Glioblastoma Multiforme: A Review of its Epidemiology and Pathogenesis through Clinical Presentation and Treatment. Asian Pac J Cancer Prev. 2017;18(1):3-9. doi: 10.22034/apjcp.2017.18.1.3
11. Lan Z, Li X, Zhang X. Glioblastoma: An Update in Pathology, Molecular Mechanisms and Biomarkers. Int J Mol Sci. 2024;25(5). doi: 10.3390/ijms25053040
12. Hide T, Komohara Y, Miyasato Y, Nakamura H, Makino K, Takeya M, et al. Oligodendrocyte Progenitor Cells and Macrophages/Microglia Produce Glioma Stem Cell Niches at the Tumor Border. EBioMedicine. 2018;30:94-104. doi: 10.1016/j.ebiom.2018.02.024
13. Rong L, Li N, Zhang Z. Emerging therapies for glioblastoma: current state and future directions. J Exp Clin Cancer Res. 2022;41(1):142. doi: 10.1186/s13046-022-02349-7
14. Willman M, Willman J, Figg J, Dioso E, Sriram S, Olowofela B, et al. Update for astrocytomas: medical and surgical management considerations. Exploration of Neuroscience. 2023;2(1):1-26. Available from: https://www.explorationpub.com/Journals/en/Article/10069doi: 10.37349/en.2023.00009
15. Plotkin SR, Biegel JA, Malkin D, Martuza R, Evans DG. Familial tumour syndromes: neurofibromatosis, schwannomatosis, rhabdoid tumour predisposition, Li–Fraumeni syndrome, Turcot syndrome, Gorlin syndrome, and Cowden syndrome. In: Batchelor T, Nishikawa R, Tarbell N, Weller M, editors. Oxford Textbook of Neuro-Oncology. Oxford University Press; 2017. p. 0. [accessed 6/3/2025]. Available from: https://doi.org/10.1093/med/9780199651870.003.0015doi: 10.1093/med/9780199651870.003.0015
16. Phillips HS, Kharbanda S, Chen R, Forrest WF, Soriano RH, Wu TD, et al. Molecular subclasses of high-grade glioma predict prognosis, delineate a pattern of disease progression, and resemble stages in neurogenesis. Cancer Cell. 2006;9(3):157-73. doi: 10.1016/j.ccr.2006.02.019
17. Verhaak RG, Hoadley KA, Purdom E, Wang V, Qi Y, Wilkerson MD, et al. Integrated genomic analysis identifies clinically relevant subtypes of glioblastoma characterized by abnormalities in PDGFRA, IDH1, EGFR, and NF1. Cancer Cell. 2010;17(1):98-110. doi: 10.1016/j.ccr.2009.12.020

18. Wang Q, Hu B, Hu X, Kim H, Squatrito M, Scarpace L, et al. Tumor Evolution of Glioma-Intrinsic Gene Expression Subtypes Associates with Immunological Changes in the Microenvironment. Cancer Cell. 2017;32(1):42-56.e6. doi: 10.1016/j.ccell.2017.06.003
19. Xu C, Hou P, Li X, Xiao M, Zhang Z, Li Z, et al. Comprehensive understanding of glioblastoma molecular phenotypes: classification, characteristics, and transition. Cancer Biol Med. 2024;21(5):363-81. doi: 10.20892/j.issn.2095-3941.2023.0510
20. Neftel C, Laffy J, Filbin MG, Hara T, Shore ME, Rahme GJ, et al. An Integrative Model of Cellular States, Plasticity, and Genetics for Glioblastoma. Cell. 2019;178(4):835-49.e21. doi: 10.1016/j.cell.2019.06.024
21. Liebelt BD, Shingu T, Zhou X, Ren J, Shin SA, Hu J. Glioma Stem Cells: Signaling, Microenvironment, and Therapy. Stem Cells Int. 2016;2016:7849890. doi: 10.1155/2016/7849890
22. Vleeschouwer D. In: De Vleeschouwer S, editor. Glioblastoma. Brisbane (AU): Codon Publications

23. Gilbert MR, Wang M, Aldape KD, Stupp R, Hegi ME, Jaeckle KA, et al. Dose-dense temozolomide for newly diagnosed glioblastoma: a randomized phase III clinical trial. J Clin Oncol. 2013;31(32):4085-91. doi: 10.1200/jco.2013.49.6968
24. Radiologists TRCo. Radiotherapy Dose Fraction. 2019;Third Edition. Available from: https://www.rcr.ac.uk/media/fezluddf/rcr-publications_radiotherapy-dose-fractionation-third-edition_march-2019.pdf
25. Stupp R, Hegi ME, Mason WP, van den Bent MJ, Taphoorn MJ, Janzer RC, et al. Effects of radiotherapy with concomitant and adjuvant temozolomide versus radiotherapy alone on survival in glioblastoma in a randomised phase III study: 5-year analysis of the EORTC-NCIC trial. Lancet Oncol. 2009;10(5):459-66. doi: 10.1016/s1470-2045(09)70025-7
26. Badr CE, Silver DJ, Siebzehnrubl FA, Deleyrolle LP. Metabolic heterogeneity and adaptability in brain tumors. Cell Mol Life Sci. 2020;77(24):5101-19. doi: 10.1007/s00018-020-03569-w
27. Kumaria A, Ashkan K. Novel therapeutic strategies in glioma targeting glutamatergic neurotransmission. Brain Res. 2023;1818:148515. doi: 10.1016/j.brainres.2023.148515
28. Siebzehnrubl FA, Silver DJ, Tugertimur B, Deleyrolle LP, Siebzehnrubl D, Sarkisian MR, et al. The ZEB1 pathway links glioblastoma initiation, invasion and chemoresistance. EMBO Mol Med. 2013;5(8):1196-212. doi: 10.1002/emmm.201302827
29. Brandao M, Simon T, Critchley G, Giamas G. Astrocytes, the rising stars of the glioblastoma microenvironment. Glia. 2019;67(5):779-90. doi: 10.1002/glia.23520
30. Kurian KM. The impact of neural stem cell biology on CNS carcinogenesis and tumor types. Patholog Res Int. 2011;2011:685271. doi: 10.4061/2011/685271
31. Kim HJ, Park JW, Lee JH. Genetic Architectures and Cell-of-Origin in Glioblastoma. Front Oncol. 2020;10:615400. doi: 10.3389/fonc.2020.615400
32. Bachoo RM, Maher EA, Ligon KL, Sharpless NE, Chan SS, You MJ, et al. Epidermal growth factor receptor and Ink4a/Arf: convergent mechanisms governing terminal differentiation and transformation along the neural stem cell to astrocyte axis. Cancer Cell. 2002;1(3):269-77. doi: 10.1016/s1535-6108(02)00046-6
33. Altmann C, Keller S, Schmidt MHH. The Role of SVZ Stem Cells in Glioblastoma. Cancers (Basel). 2019;11(4). doi: 10.3390/cancers11040448
34. Mayer S, Milo T, Isaacson A, Halperin C, Miyara S, Stein Y, et al. The tumor microenvironment shows a hierarchy of cell-cell interactions dominated by fibroblasts. Nature Communications. 2023;14(1):5810. Available from: https://doi.org/10.1038/s41467-023-41518-wdoi: 10.1038/s41467-023-41518-w

35. So JS, Kim H, Han KS. Mechanisms of Invasion in Glioblastoma: Extracellular Matrix, Ca(2+) Signaling, and Glutamate. Front Cell Neurosci. 2021;15:663092. doi: 10.3389/fncel.2021.663092
36. Zhou Y, Danbolt NC. Glutamate as a neurotransmitter in the healthy brain. Journal of Neural Transmission. 2014;121(8):799-817. Available from: https://doi.org/10.1007/s00702-014-1180-8doi: 10.1007/s00702-014-1180-8
37. Reiner A, Levitz J. Glutamatergic Signaling in the Central Nervous System: Ionotropic and Metabotropic Receptors in Concert. Neuron. 2018;98(6):1080-98. doi: 10.1016/j.neuron.2018.05.018
38. Traynelis SF, Wollmuth LP, McBain CJ, Menniti FS, Vance KM, Ogden KK, et al. Glutamate receptor ion channels: structure, regulation, and function. Pharmacol Rev. 2010;62(3):405-96. doi: 10.1124/pr.109.002451
39. Henley JM, Wilkinson KA. Synaptic AMPA receptor composition in development, plasticity and disease. Nat Rev Neurosci. 2016;17(6):337-50. doi: 10.1038/nrn.2016.37
40. Lauri SE, Ryazantseva M, Orav E, Vesikansa A, Taira T. Kainate receptors in the developing neuronal networks. Neuropharmacology. 2021;195:108585. doi: 10.1016/j.neuropharm.2021.108585
41. Dzamba D, Honsa P, Anderova M. NMDA Receptors in Glial Cells: Pending Questions. Curr Neuropharmacol. 2013;11(3):250-62. doi: 10.2174/1570159x11311030002
42. Royo M, Escolano BA, Madrigal MP, Jurado S. AMPA Receptor Function in Hypothalamic Synapses. Front Synaptic Neurosci. 2022;14:833449. doi: 10.3389/fnsyn.2022.833449
43. Man HY. GluA2-lacking, calcium-permeable AMPA receptors--inducers of plasticity? Curr Opin Neurobiol. 2011;21(2):291-8. doi: 10.1016/j.conb.2011.01.001
44. Gangwar SP, Yelshanskaya MV, Nadezhdin KD, Yen LY, Newton TP, Aktolun M, et al. Kainate receptor channel opening and gating mechanism. Nature. 2024;630(8017):762-8. Available from: https://doi.org/10.1038/s41586-024-07475-0doi: 10.1038/s41586-024-07475-0
45. Chałupnik P, Szymańska E. Kainate Receptor Antagonists: Recent Advances and Therapeutic Perspective. Int J Mol Sci. 2023;24(3). doi: 10.3390/ijms24031908
46. Rivadulla C, Sharma J, Sur M. Specific roles of NMDA and AMPA receptors in direction-selective and spatial phase-selective responses in visual cortex. J Neurosci. 2001;21(5):1710-9. doi: 10.1523/jneurosci.21-05-01710.2001
47. Yamamoto H, Hagino Y, Kasai S, Ikeda K. Specific Roles of NMDA Receptor Subunits in Mental Disorders. Curr Mol Med. 2015;15(3):193-205. doi: 10.2174/1566524015666150330142807
48. Ishiuchi S, Yoshida Y, Sugawara K, Aihara M, Ohtani T, Watanabe T, et al. Ca2+-permeable AMPA receptors regulate growth of human glioblastoma via Akt activation. J Neurosci. 2007;27(30):7987-8001. doi: 10.1523/jneurosci.2180-07.2007
49. Cipolletta E, Rusciano MR, Maione AS, Santulli G, Sorriento D, Del Giudice C, et al. Targeting the CaMKII/ERK Interaction in the Heart Prevents Cardiac Hypertrophy. PLoS One. 2015;10(6):e0130477. doi: 10.1371/journal.pone.0130477
50. de Groot JF, Liu TJ, Fuller G, Yung WK. The excitatory amino acid transporter-2 induces apoptosis and decreases glioma growth in vitro and in vivo. Cancer Res. 2005;65(5):1934-40. doi: 10.1158/0008-5472.Can-04-3626
51. Ye ZC, Rothstein JD, Sontheimer H. Compromised glutamate transport in human glioma cells: reduction-mislocalization of sodium-dependent glutamate transporters and enhanced activity of cystine-glutamate exchange. J Neurosci. 1999;19(24):10767-77. doi: 10.1523/jneurosci.19-24-10767.1999
52. Sontheimer H. A role for glutamate in growth and invasion of primary brain tumors. J Neurochem. 2008;105(2):287-95. doi: 10.1111/j.1471-4159.2008.05301.x

53. Dong XX, Wang Y, Qin ZH. Molecular mechanisms of excitotoxicity and their relevance to pathogenesis of neurodegenerative diseases. Acta Pharmacol Sin. 2009;30(4):379-87. doi: 10.1038/aps.2009.24
54. Matute C, Alberdi E, Ibarretxe G, Sánchez-Gómez MV. Excitotoxicity in glial cells. Eur J Pharmacol. 2002;447(2-3):239-46. doi: 10.1016/s0014-2999(02)01847-2
55. Boldyrev A, Bulygina E, Makhro A. Glutamate receptors modulate oxidative stress in neuronal cells. A mini-review. Neurotox Res. 2004;6(7-8):581-7. doi: 10.1007/bf03033454
56. Venkataramani V, Tanev DI, Strahle C, Studier-Fischer A, Fankhauser L, Kessler T, et al. Glutamatergic synaptic input to glioma cells drives brain tumour progression. Nature. 2019;573(7775):532-8. doi: 10.1038/s41586-019-1564-x
57. Azab MA, Alomari A, Azzam AY. Featuring how calcium channels and calmodulin affect glioblastoma behavior. A review article. Cancer Treat Res Commun. 2020;25:100255. doi: 10.1016/j.ctarc.2020.100255
58. Ye ZC, Sontheimer H. Glioma cells release excitotoxic concentrations of glutamate. Cancer Res. 1999;59(17):4383-91.
59. Brito da Silva A, Pennifold J, Henley B, Chatterjee K, Bateman D, Whittaker RW, et al. The AMPA receptor antagonist perampanel suppresses epileptic activity in human focal cortical dysplasia. Epilepsia Open. 2022;7(3):488-95. doi: 10.1002/epi4.12549
60. Rogawski MA, Hanada T. Preclinical pharmacology of perampanel, a selective non-competitive AMPA receptor antagonist. Acta Neurol Scand Suppl. 2013(197):19-24. doi: 10.1111/ane.12100
61. Ireland MF, Lenal FC, Lorier AR, Loomes DE, Adachi T, Alvares TS, et al. Distinct receptors underlie glutamatergic signalling in inspiratory rhythm-generating networks and motor output pathways in neonatal rat. J Physiol. 2008;586(9):2357-70. doi: 10.1113/jphysiol.2007.150532
62. MacDonald JF, Miljkovic Z, Pennefather P. Use-dependent block of excitatory amino acid currents in cultured neurons by ketamine. J Neurophysiol. 1987;58(2):251-66. doi: 10.1152/jn.1987.58.2.251
63. Corsi L, Mescola A, Alessandrini A. Glutamate Receptors and Glioblastoma Multiforme: An Old "Route" for New Perspectives. Int J Mol Sci. 2019;20(7). doi: 10.3390/ijms20071796
64. Görlach A, Bertram K, Hudecova S, Krizanova O. Calcium and ROS: A mutual interplay. Redox Biol. 2015;6:260-71. doi: 10.1016/j.redox.2015.08.010
65. Venkatesh HS, Morishita W, Geraghty AC, Silverbush D, Gillespie SM, Arzt M, et al. Electrical and synaptic integration of glioma into neural circuits. Nature. 2019;573(7775):539-45. Available from: https://doi.org/10.1038/s41586-019-1563-ydoi: 10.1038/s41586-019-1563-y
66. Stepulak A, Luksch H, Gebhardt C, Uckermann O, Marzahn J, Sifringer M, et al. Expression of glutamate receptor subunits in human cancers. Histochemistry and Cell Biology. 2009;132(4):435-45. Available from: https://doi.org/10.1007/s00418-009-0613-1doi: 10.1007/s00418-009-0613-1
67. Cuellar-Santoyo AO, Ruiz-Rodríguez VM, Mares-Barbosa TB, Patrón-Soberano A, Howe AG, Portales-Pérez DP, et al. Revealing the contribution of astrocytes to glutamatergic neuronal transmission. Front Cell Neurosci. 2022;16:1037641. doi: 10.3389/fncel.2022.1037641
68. Mölders A, Koch A, Menke R, Klöcker N. Heterogeneity of the astrocytic AMPA-receptor transcriptome. Glia. 2018;66(12):2604-16. doi: 10.1002/glia.23514
69. Ceprian M, Fulton D. Glial Cell AMPA Receptors in Nervous System Health, Injury and Disease. Int J Mol Sci. 2019;20(10). doi: 10.3390/ijms20102450
70. Lee M-C, Ting KK, Adams S, Brew BJ, Chung R, Guillemin GJ. Characterisation of the Expression of NMDA Receptors in Human Astrocytes. PLOS ONE. 2010;5(11):e14123. Available from: https://doi.org/10.1371/journal.pone.0014123doi: 10.1371/journal.pone.0014123

71. Piao Y, Lu L, de Groot J. AMPA receptors promote perivascular glioma invasion via beta1 integrin-dependent adhesion to the extracellular matrix. Neuro Oncol. 2009;11(3):260-73. doi: 10.1215/15228517-2008-094
72. Wang JQ, Guo ML, Jin DZ, Xue B, Fibuch EE, Mao LM. Roles of subunit phosphorylation in regulating glutamate receptor function. Eur J Pharmacol. 2014;728:183-7. doi: 10.1016/j.ejphar.2013.11.019
73. Lange F, Hörnschemeyer J, Kirschstein T. Glutamatergic Mechanisms in Glioblastoma and Tumor-Associated Epilepsy. Cells. 2021;10(5). doi: 10.3390/cells10051226
74. Ishiuchi S, Tsuzuki K, Yoshida Y, Yamada N, Hagimura N, Okado H, et al. Blockage of Ca(2+)-permeable AMPA receptors suppresses migration and induces apoptosis in human glioblastoma cells. Nat Med. 2002;8(9):971-8. doi: 10.1038/nm746
75. Uxa S, Castillo-Binder P, Kohler R, Stangner K, Müller GA, Engeland K. Ki-67 gene expression. Cell Death & Differentiation. 2021;28(12):3357-70. Available from: https://doi.org/10.1038/s41418-021-00823-xdoi: 10.1038/s41418-021-00823-x
76. Geng Y, Xie L, Wang Y, Wang Y. Unveiling the oncogenic significance of thymidylate synthase in human cancers. Am J Transl Res. 2024;16(10):5228-47. doi: 10.62347/iruz1011
77. Unrug-Bielawska K, Earnshaw D, Cybulska-Lubak M, Kaniuga E, Sandowska-Markiewicz Z, Statkiewicz M, et al. Therapeutic Responses to Two New SN-38 Derivatives in Colorectal Cancer Patient-Derived Xenografts and Respective 3D In Vitro Cultures. Anticancer Res. 2024;44(10):4219-24. doi: 10.21873/anticanres.17252
78. Jiang CH, Wei M, Zhang C, Shi YS. The amino-terminal domain of GluA1 mediates LTP maintenance via interaction with neuroplastin-65. Proc Natl Acad Sci U S A. 2021;118(9). doi: 10.1073/pnas.2019194118
79. Grossman SA, Ye X, Chamberlain M, Mikkelsen T, Batchelor T, Desideri S, et al. Talampanel with standard radiation and temozolomide in patients with newly diagnosed glioblastoma: a multicenter phase II trial. J Clin Oncol. 2009;27(25):4155-61. doi: 10.1200/jco.2008.21.6895
80. Kudo Y, Ogura A. Glutamate-induced increase in intracellular Ca2+ concentration in isolated hippocampal neurones. Br J Pharmacol. 1986;89(1):191-8. doi: 10.1111/j.1476-5381.1986.tb11135.x
81. Rajdev S, Reynolds IJ. Glutamate-induced intracellular calcium changes and neurotoxicity in cortical neurons in vitro: effect of chemical ischemia. Neuroscience. 1994;62(3):667-79. doi: 10.1016/0306-4522(94)90468-5
82. Cooper D, Dimri M. Biochemistry, Calcium Channels. In: StatPearls. Treasure Island (FL): StatPearls Publishing

Supplementary information:

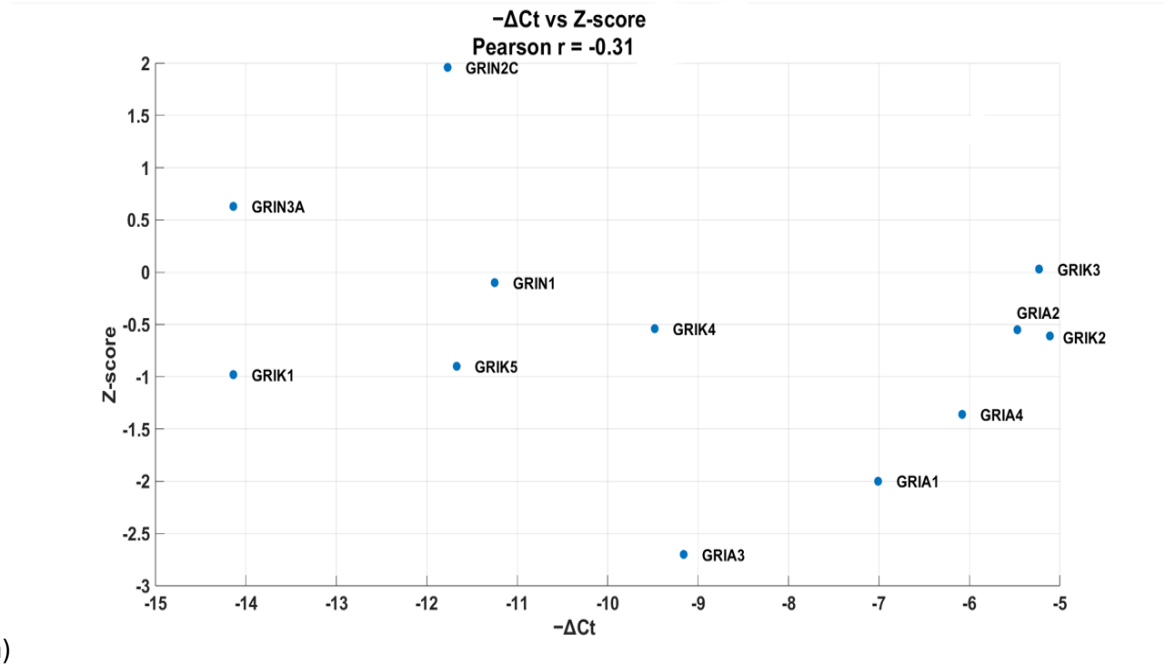

(a)

U3042

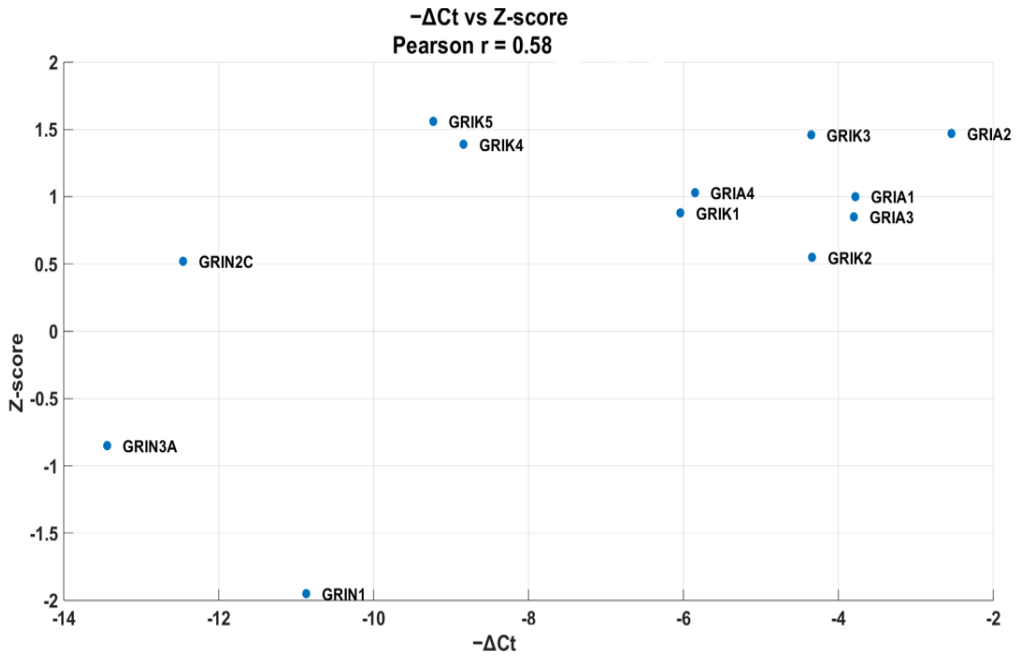

(b)

Supplementary Figure1: The correlation between z-score and -dtCT. A Pearson correlation between the z-score and the mean -dtCT for each receptor subunit was assessed and plotted. (a) the Pearson correlation of U3019 is -0.31, whilst for (b) U3042 it is 0.58